NAVAL POSTGRADUATE SCHOOL
MONTEREY, CALIFORNIA

THESIS

TRANSIENT RESPONSE ANALYSIS OF THE 72 INCH TAC-4 RUGGEDIZED SHIPBOARD RACK SUBJECTED TO AN UNDERWATER EXPLOSION EVENT

by

Mark H. Oesterreich

June 1998

Thesis Advisor: Y.S. Shin

Approved for public release; distribution is unlimited.

REPRODUCTION QUALITY NOTICE

This document is the best quality available. The copy furnished to DTIC contained pages that may have the following quality problems:

- Pages smaller or larger than normal.
- Pages with background color or light colored printing.
- Pages with small type or poor printing; and or
- Pages with continuous tone material or color photographs.

Due to various output media available these conditions may or may not cause poor legibility in the microfiche or hardcopy output you receive.

☒ If this block is checked, the copy furnished to DTIC contained pages with color printing, that when reproduced in Black and White, may change detail of the original copy.

REPORT DOCUMENTATION PAGE

Form Approved OMB No. 0704-0188

1. AGENCY USE ONLY *(Leave blank)*	2. REPORT DATE	3. REPORT TYPE AND DATES COVERED
	June 1998.	Engineer's and Master's Thesis

4. TITLE AND SUBTITLE: Transient Response Analysis of the 72 Inch TAC-4 Ruggedized Shipboard Rack Subjected to an Underwater Explosion Event

5. FUNDING NUMBERS

6. AUTHOR(S) Mark H. Oesterreich

7. PERFORMING ORGANIZATION NAME(S) AND ADDRESS(ES)
Naval Postgraduate School
Monterey CA 93943-5000

8. PERFORMING ORGANIZATION REPORT NUMBER

9. SPONSORING/MONITORING AGENCY NAME(S) AND ADDRESS(ES)
NCCOSC, RDT&E Division, TAC Project Office,
49184 Transmitter Rd, San Diego, CA 92152-7346

10. SPONSORING/MONITORING AGENCY REPORT NUMBER

11. SUPPLEMENTARY NOTES The views expressed here are those of the authors and do not reflect the official policy or position of the Department of Defense or the U.S. Government.

12a. DISTRIBUTION/AVAILABILITY STATEMENT
Approved for public release; distribution is unlimited.

12b. DISTRIBUTION CODE

13. ABSTRACT *(maximum 200 words)*

The finite element modeling and subsequent transient analysis of the 72 Inch TAC-4 Rugged Rack computer system (configurations 0001AA and 0003AA only), currently employed in U.S. Navy shipboard applications, has been performed to determine the system's response to simulated shock inputs. This rack is designed to allow incorporation of commercial-off-the-shelf (COTS) computer systems for naval tactical computing requirements while still meeting MIL-STD-901D, the applicable shock specification. By showing the viability of this computer simulation of the shock response of the current TAC-4 rack system, an argument for a lessening of the actual physical testing requirements for acceptance of future TAC systems can be made.

14. SUBJECT TERMS TAC-4, Transient Analysis, Finite Element Method, COTS, Shock Analysis, UNDEX			15. NUMBER OF PAGES 119
			16. PRICE CODE
17. SECURITY CLASSIFICATION OF REPORT Unclassified	18. SECURITY CLASSIFICATION OF THIS PAGE Unclassified	19. SECURITY CLASSIFICATION OF ABSTRACT Unclassified	20. LIMITATION OF ABSTRACT SAR

NSN 7540-01-280-5500

Standard Form 298 (Rev. 2-89)
Prescribed by ANSI Std. 239-18 298-102

Approved for public release; distribution is unlimited.

TRANSIENT RESPONSE ANALYSIS OF THE 72 INCH TAC-4 RUGGEDIZED SHIPBOARD RACK SUBJECTED TO AN UNDERWATER EXPLOSION EVENT

Mark H. Oesterreich
Lieutenant, United States Navy
B.S. United States Naval Academy, 1991

Submitted in partial fulfillment of the
requirements for the degree of

MECHANICAL ENGINEER

and

MASTER OF SCIENCE IN MECHANICAL ENGINEERING

from the

NAVAL POSTGRADUATE SCHOOL
JUNE 1998

Author: _____
Mark H. Oesterreich

Approved by: _____
Young S. Shin, Thesis Advisor

_____
Terry R. McNelley, Chairman
Department of Mechanical Engineering

ABSTRACT

The finite element modeling and subsequent transient analysis of the 72 Inch TAC-4 Rugged Rack computer system (configurations 0001AA and 0003AA only), currently employed in U.S. Navy shipboard applications, has been performed to determine the system's response to simulated shock inputs. This rack is designed to allow incorporation of commercial-off-the-shelf (COTS) computer systems for naval tactical computing requirements while still meeting MIL-STD-901D, the applicable shock specification. By showing the viability of this computer simulation of the shock response of the current TAC-4 rack system, an argument for a lessening of the actual physical testing requirements for acceptance of future TAC systems can be made.

TABLE OF CONTENTS

LIST OF FIGURES

LIST OF TABLES

ACKNOWLEDGMENT

The author would like to acknowledge the financial support of NCCOSC, RDT&E Division, TAC Project Office (CODE D4103), for allowing the purchase of equipment used in this thesis. Mr. Larry Core and CDR Dave Ready were invaluable to the project's completion.

It is with deep gratitude that I thank Dr. Young Shin for his support and guidance throughout my entire graduate education. His scholarly ambition has increased my confidence in my technical and scholarly abilities, reinforcing the maxim of attention to detail. Special thanks to Tom Christian for his outstanding assistance in ensuring the Vibrations Computer Lab was optimized for this study. His patience is greatly appreciated.

Finally, I dedicate this work to my family and my Lord. The love support that flows from them made all this possible.

I. INTRODUCTION

A. BACKGROUND

Throughout the U.S. Navy's history, warship designers have continually struggled to construct ships that were resistant to damage. Prior to World War II, the primary damage mechanism for these ships was direct impact by shells or torpedoes fired from enemy ships and also the blast wave from firing the ship's own guns. For protection from enemy ordinance, vital equipment was located as far away from the hull as practical and as much armor as possible was carried by the ship. To limit the own-ship gun-blast damage, a limited testing program using rudimentary shock and vibration testing machinery was developed which slowly became more sophisticated as time passed.

During World War II, non-contact ordinance was developed which further complicated the ship designers task. These types of ordinance explode at a distance from the ship hull applying an underwater pressure pulse to a large portion of the hull. Here the primary damage mechanism is not physical damage from the blast itself, but from the violent shaking of the hull produced by this pressure wave. This caused heavy equipment, previously considered safe, to become misaligned and/or inoperative due to mount breakage or casing fracture. Lighter equipment could be damaged due to permanent deformation and internal part interference resulting from the excessive motion. Electronic equipment was also particularly susceptible to damage in this manner. In response to this new type of damage, a more formalized ship shock testing requirement was developed using a variety of more sophisticated testing machines and specifications.

The current evolution of this testing program is contained in MIL-STD-901D [Ref. 1]. This military specification outlines all the shock testing requirements for shipboard machinery, equipment, systems and structures which are required to resist the effects of mechanical shock. The purpose of these requirements is to verify the ability of

these shipboard installations to withstand shock loading which might be incurred during wartime service.

B. MILITARY SHOCK SPECIFICATION (MIL-STD-901D)

MIL-STD-901D breaks the testing requirements down by classifying the equipment to be tested using different criteria and then specifying the types of tests required based on these criteria. These criteria are:

- Shock Grade - vital or non-vital to ship safety or combat capability.
- Equipment Class - uses resilient mounts or not.
- Test Type - principle unit, subsidiary component, or subassembly.
- Mounting Location - surface ship or submarine , hull/deck/plating mounted.
- Mounting Orientation - bulkhead/base/overhead/CG mounted and mounting axis.

In addition to these criteria, the equipment's weight, size and center of gravity are considered.

All of these criteria are used to determine the required test category and the amount of damage allowed for a passing grade. The three test categories are Lightweight, Mediumweight, and Heavyweight. The allowable damage criteria varies significantly based on equipment classification, but essentially ensures that the equipment continues to function and does not become a safety hazard itself. Both Lightweight and Mediumweight testing are performed on a specific laboratory machines, while Heavyweight testing is performed on a specific floating shock platform.

For each type of testing, the number, type, and manner of shock application are specified, and again vary, based on equipment classification. This includes specifying the test fixture, how the equipment is mounted to the test fixture, and the magnitude and direction of the shock force application. More specific information is found in MIL-STD-901D and a general explanation of the testing is found in NRL Report 7396 [Ref. 2].

C. DESCRIPTION OF THE TAC-4 SYSTEM

The TAC-4 ruggedized rack system, as designed by Science Applications International Corporation (SAIC) [Ref. 3], utilizes different ruggedized rack configurations of Commercial Off-the-Shelf (COTS) computer equipment. It is the fourth generation of the Tactical Advanced Computer system developed for United States military use. The system is designed to be flexible enough to provide for many varied equipment configurations mounted within each rack type. Each rugged rack houses and provides conditioned power to user specified COTS console, server, and workstation type installed equipment. The types of installed equipment can include: Central Processing Units, Disk Drives, Monitors, and Power Supplies.

Currently there are three different rack types, a 72 inch, 60 inch and 42 inch variant. Each rack type is designed to provide a shock-mounted housing for the electronic equipment and also provides for air cooling of the installed equipment. Each rack type is also designed to provide for easy replacement and upgrading of installed components.

D. PROBLEM DEFINITION

The rapid pace of current electronic and computer modernization coupled with the slow turnaround and life-cycle outlook of traditional naval contracting has precipitated a situation where the navy can not keep pace with current technology. As a further difficulty in the equipment contracting process, all military-specifications (mil-specs) must be met by the manufacturer. This adds significant cost and design and manufacturing delays to any computer system required for naval tactical use. These design, manufacture, and contracting delays result in a product which is obsolete well before it can be placed into service.

To remedy this situation, the U.S. Navy has changed its contracting procedures, but more importantly the type of computer hardware used for tactical computing.

Previously, each tactical computer was a stand-alone unit specifically designed for its requisite task, or relied upon a standard chassis which was modified to perform the required task (e.g., AN-UYK-7,-43). This approach was satisfactory until the advent of the computer revolution which heralds a new technical innovation or increase in computing capacity about every six months. This time period is far too short for the industry to design mil-spec computers at the same rate as which commercial computers improve.

By using commercial computers, which are not necessarily designed to comply with mil-specs, the military can keep up with the computer revolution. The largest issue remaining, however, is to ensure that these computers actually meet the required mil-specs because of their employment in vital warship systems. With respect to the shock mil-spec (MIL-STD-901D), the assurance involves prescribed physical shock testing as discussed in a previous section.

As written, MIL-STD-901D requires that all shipboard equipment be tested. Due to the myriad of different possible rack configurations, this testing rapidly becomes prohibitively expensive and time consuming. This introduces additional delays to the introduction of current computing technology to the fleet almost defeating the purpose of using COTS technology.

One possible way to solve this problem is to generate a computer model of a general rack system and simulate its response to the shock inputs provided from the shock testing equipment. These simulated results can then be compared to actual physical testing results and the model adjusted to ensure the simulation provides a conservative analysis (Model Verification). Now, the computer model can be adjusted to represent any possible rack equipment configuration and be subjected to the shock simulation. This, along with baseline acceptable g factors provided by the COTS manufactures, can provide for a judge of the shock acceptability of each rack configuration without the need for excessive physical testing. This will definitely drive down system acquisition costs and time, providing a better product to the fleet.

E. SCOPE OF RESEARCH

This work will concentrate specifically on two versions of the 72 inch rack. The first, designated CLIN 0003AA by SAIC, is the single monitor workstation model. Figure 1 is an illustration of the layout of this rack. The second, designated CLIN 0001AA by SAIC, is the dual monitor workstation model, whose layout is illustrated in Figure 2. For each of these rack configurations, a finite element model will be constructed for subsequent computer simulation analysis. Both static and modal analyses will be performed to ensure proper modeling of the racks and to get a generalized idea of their dynamic characteristics. Finally, two separate transient analyses will be performed. The first is a high g impulse load, simulating a single hammer-type blow. The second transient simulation represents a sustained low frequency content shock train representing the type of shaking experienced from an underwater explosion. These two different shock types will allow for a characterization of the system response to most shock inputs.

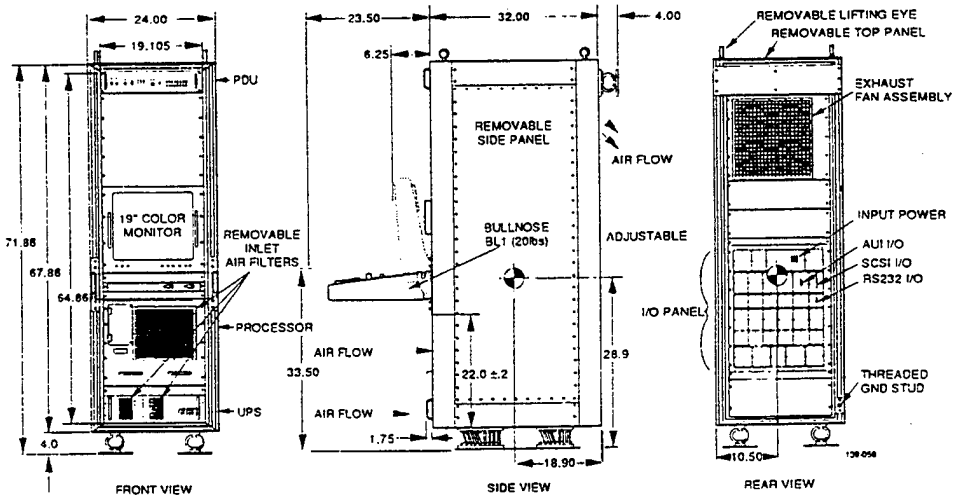

Figure 1: Layout of the Single Monitor Variant of 72" Shipboard Rack (CLIN0003AA), from Ref. 3.

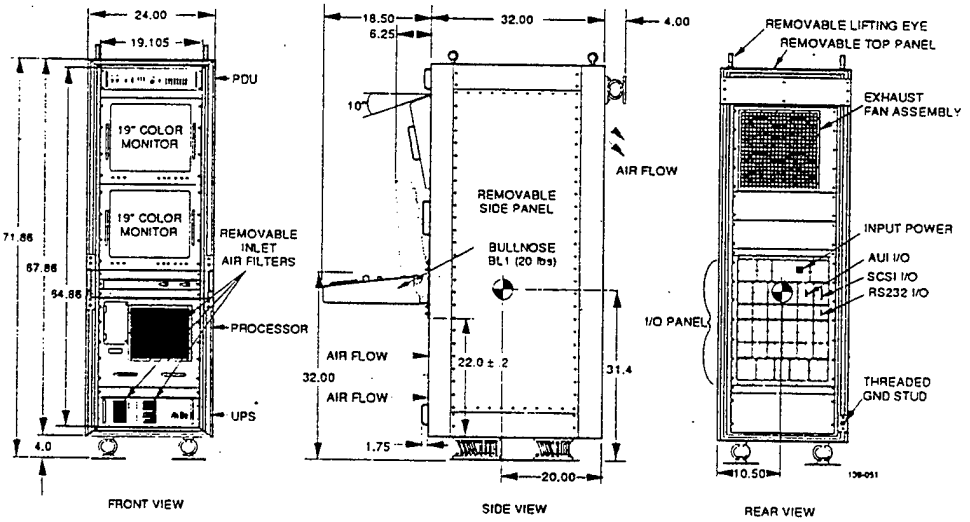

Figure 2: Layout of the Dual Monitor Variant of 72" Shipboard Rack (CLIN0001AA), from Ref. 3

II. THEORETICAL BACKGROUND

A. FINITE ELEMENT METHOD

The analysis of any engineering problem begins with the development of a mathematical description of the system. This description usually consists of coupled differential equations which are difficult to solve analytically. The finite element method is a numerical procedure for approximating the solution to these complex problems. This method divides the system into discrete regions where approximate solutions to the model's behavior are obtained at specific points called nodes. Nodes are the points which connect the discretized regions, or elements, together. The accuracy of any finite element solution depends on the way the finite element model is generated, specifically the number and types of elements used in the model.

The origins of the finite element method began in the 1950s, but only became practical within the last ten years with the advent of modern digital computers. Every node in the model has six degrees of freedom, and the equations developed to describe the system must be applied at every node. For large models, based on number of nodes, this becomes cumbersome and requires a large computing and data storage capacity to solve the engineering problem. The key to an efficient solution, is to balance accuracy requirements, or number of nodes, with the requisite computing time.

Discretization in the finite element method for structural analysis is accomplished by first breaking the structure into nodes and elements. From these nodes and elements, mass, stiffness and damping matrices are produced based on the dimensions and physical properties of the modeled materials and the type of element used. These matrices are then used in the appropriate equations to solve the problem.

B. NORMAL MODE ANALYSIS

Free vibration analysis (Normal Mode Analysis) is a method for predicting the undamped vibration characteristics of a structure. This type of vibration analysis occurs in the absence of external excitation, but provides an excellent understanding of the system's nature in responding to dynamic excitation. The equation of motion of a discrete system is written in matrix form as,

$$[M]\{\ddot{d}\} + [K]\{d\} = \{0\} \tag{1}$$

where, [M] is the nxn structural mass matrix, $\{\ddot{d}\}$ is the nx1 nodal acceleration vector, [K] is the nxn structural stiffness matrix and $\{d\}$ is the 1xn nodal displacement vector. Equation (1) is a system of coupled linear differential equation with n-independent unknowns, where n is the total number of degrees-of-freedom in the structure. By assuming a solution of the form,

$$\{d\} = C\{\phi\}e^{j\omega t} \tag{2}$$

an n^{th} order homogenous eigenvalue problem is generated as,

$$\left[-\omega^2[M] + [K]\right]Ce^{j\omega t} = 0 \tag{3}$$

where, C is a complex constant and $\{\phi\}$ is a nx1 spatial vector. The non-trivial solution to Equation (3) requires that,

$$\det\left[-\omega^2[M] + [K]\right] = 0 \tag{4}$$

This is the characteristic equation of the system. The roots of this equation are the eigenvalues, $\lambda_i = \omega_i^2$, where each ω_i is a natural frequency of vibration. For each natural frequency, there is a corresponding eigenvector $\{\phi\}$ which is the mode shape associated with that frequency. Thus, the solution to the free vibration problem is n eigenpairs, consisting of ω_n and $\{\phi^n\}$. These eigenpairs have interesting properties which make them very useful in simplifying the equations used to mathematically model the system.

C. MODAL TRANSIENT RESPONSE ANALYSIS

The following discussion is for the generalized case of transient response analysis. This study is strictly a base excitation problem which requires a slight modification to this discussion, specifically in the description of the excitation force vector $\{F\}$. This modification will be discussed further in the following section, entitled The Large Mass Method.

The previous discussion of Modal Analysis resulted in n eigenpairs of ω_n (eigenvalue) and $\{\phi^n\}$ (eigenvector or mode shape) which will be subsequently used to decouple the system differential equations. This decoupling drastically simplifies the response calculations for the system. Because each eigenvector is orthogonal to every other eigenvector it allows vibration response to be described as a linear combination of these mode shapes. By constructing a square transformation matrix whose columns consist of the n mode shapes, $\left[\phi^1\phi^2...\phi^n\right]$ or $[\Phi]$, it can be used to change the physical system coordinates into a different coordinate system (modal coordinates) by substituting for $\{d(t)\}$, the physical coordinate vector, in

$$[M]\{\ddot{d}\}+[C]\{\dot{d}\}+[K]\{d\}=\{F\} \tag{5}$$

with

$$\{d(t)\}=[\Phi]\{\eta(t)\} \tag{6}$$

where $\{\eta(t)\}$ is the modal coordinate vector (Note that Equation 5 introduces the damping matrix [C]):

$$[M][\Phi]\{\ddot{\eta}\}+[C][\Phi]\{\eta\}+[K][\Phi]\{\eta\}=\{F\} \tag{7}$$

Premultiplying each term in Equation 7 with $[\Phi]^T$ produces:

$$[M]\{\ddot{\eta}\}+[C]\{\dot{\eta}\}+[K]\{\eta\}=\{F\} \tag{8}$$

where $[M]$ is the diagonalized mass matrix, $[C]$ is the diagonalized damping matrix, $[K]$ is the diagonalized stiffness matrix and $\{F\}$ is the modal Force vector. It is important here to state that [C] must be diagonalizable by $[\Phi]$. To ensure this, the system damping

matrix in physical coordinates can be defined as a linear combination of [M] and [K] or specified in modal coordinates, already diagonalized, using a percent format.

This process of diagonalizing these matrices is known as modal decomposition and results in n independent equations, one for each modal degree of freedom (DOF). The i^{th} DOF's equation corresponds to the ith row of Equation (3) and may be written as:

$$M_{ii}\ddot{\eta}_i + C_{ii}\dot{\eta}_i + K_{ii}\eta_i = F_i \tag{9}$$

Premultiplying Equation (8) through by $\frac{1}{[M]}$ results in:

$$\{\ddot{\eta}\} + [2\zeta_i\omega_i]\{\dot{\eta}\} + [\omega_i{}^2]\{\eta\} = \{a\} \tag{10}$$

where ζ_i is the i^{th} modal damping factor (percent damping), ω_i is the i^{th} natural frequency and $\{a\}$ is the time varying acceleration vector produced by the forcing function. The i^{th} row of the uncoupled system of equations (with time dependence added for emphasis) is now:

$$\ddot{\eta}_i(t) + 2\zeta_i\dot{\eta}_i(t) + \omega_i{}^2\eta_i(t) = a_i(t) \tag{11}$$

The solution to Equation (5) requires two initial conditions of the form:

$$\{d\}_{t=0} = \{d_0\} \tag{12}$$

and

$$\{\dot{d}\}_{t=0} = \{\dot{d}_0\} \tag{13}$$

These equations must also be transformed into modal coordinates. This is accomplished in a similar manner as the equations of motion for the system resulting in:

$$\{\eta_0\} = [M]^{-1}[\Phi]^T[M]\{d_0\} \tag{14}$$

and

$$\{\dot{\eta}_0\} = [M]^{-1}[\Phi]^T[M]\{\dot{d}_0\} \tag{15}$$

By applying these transformed initial conditions to Equation (11), a solution for the modal displacements is obtained of the form:

$$\eta_i(t) = \eta_{0i}\cos(\omega_i t) + \frac{1}{\omega_i}\dot{\eta}_{0i}\sin(\omega_i t) + \frac{1}{\omega_i}\int_0^t a_i(t)\sin\omega_i(t-\tau)d\tau \tag{16}$$

Each modal coordinate has a solution of this form. All of these are then combined into vector form $\{\eta\}$. The physical displacements are then obtained using Equation (6):

$$\{d(t)\} = [\Phi]\{\eta(t)\}$$

This method as shown here works well for models with up to a few hundred DOF. It becomes extremely cumbersome and time consuming for larger models, but requires only a slight modification to remedy this situation. Most of the system transient response is contained in the lower frequency mode shapes, therefore a very accurate approximation of the system response can be made using a relatively small proportion of the total mode shapes. This is known as modal truncation and is done by modifying Equation (6) as follows:

$$\{d(t)\} = [\Phi]\{\eta(t)\} \cong \sum_{i=1}^{NDOF} \{\phi_i\}\eta_i(t) \qquad (17)$$

Here, NDOF is the total number of mode shapes selected to be used in the approximation. Further information on both Normal Mode Analysis and Transient Response Analysis is contained in Reference 4.

D. THE LARGE MASS METHOD

Equation (5) requires that the base excitation be defined as a force vector. It is however much easier to physically measure a displacement, velocity, or acceleration of a base than a transmitted force. Now the excitation force can be defined as simply a base acceleration multiplied by the base mass (the appropriate derivatives are taken if the actual input is defined as a displacement or velocity time history). In many structural analyses, the actual physical base mass is unknown or unmeasurable, so it is assumed as a very large value. This ensures that any errors in calculations remain insignificant.

The Large Mass Method is implemented by placing large point masses (m_0) at all enforced degrees of freedom. These masses should be several orders of magnitude larger than the structural mass (typically 10^6 times larger) which ensures sufficient numerical

accuracy. Now the appropriate acceleration time histories are applied via the large masses. The converted force is now simply $F(t)=m_0a(t)$ at each enforced node.

One drawback to the Large Mass Method is that it can remove the static determinancy of the model, introducing rigid body modes into the solution. Rigid body modes are undeformed gross translations and rotations of the entire model which are not physically present in the real system. This is easily avoided by excluding these rigid body modes while using modal truncation. A second difficulty arises because you have added mass to the system which is not physically there. Because of this, care must be taken to ensure that this does not affect the calculated results. This entails using the proper scale factors within the NASTRAN input deck to ensure proper force application. See Reference 5 for further explanation of the Large Mass Method.

III. MODEL DEVELOPMENT

The entire modeling process was accomplished using the computer code MSC/PATRAN (Version 6). This pre-processor program allows the user to use a simple graphical and menu interface to create both the model geometry and finite element mesh. Additionally, it will construct the required computer input file for various finite element codes for the required model analyses. Due to the similarity in both of the rack systems analyzed in this study, only the single monitor was modeled initially modeled and then it was modified into the dual monitor model.

A. GEOMETRIC MODELING

The first step in any finite element structural analysis is to create a geometric model of the structure. This was accomplished using the drawings provided in Reference 3 as a guide. Certain features of the solid model such as bolt holes, electrical connections, and fasteners were not modeled because this level of detail was not required in the study. Also, certain complicated geometric features of the model, such as drawer slides and flanges, were simplified (while retaining appropriate physical dimensions and properties) for the same reason.

The geometric model was made by constructing and joining appropriate points, curves, surfaces, and solids in proper relation to each other. Due to the complicated internal structure of the rack, it was initially divided into several manageable portions which were later combined to form the entire structure. The following paragraphs describe how each individual portion of the rack was modeled. The rack was broken down into the following sections and will be referred to with the following names: tubular frame, rack frame, shell, and equipment drawers and bullnose. From the outset, the goal of the modeling process was to minimize the number of elements in order to minimize the computational requirements, but to still ensure an accurate model response.

A large portion of this strategy is to simplify the actual structural shapes into idealized structures, thus keeping the mathematical model as small as possible with minimal impact on solution accuracy.

The tubular frame is the portion of the rack which is the gross load bearing structure in the rack. Because the various channels and mini-flanges on this structure would severely complicate the modeling of it, this structure was simplified to a rectangular box of similar dimensions. This will provide for a similar dynamic model response. The large flange on the tubing, however, was modeled because of its comparatively large dimensions. Figure 3 shows the critical dimensions of the 72" Rack midsection (Plane View), clearly indicating the complexity of the tubular sections.

The rack frame is the portion of the rack which the drawers are connected to using sliding rail mounts. Due to the fact that the large numbers of small bolt holes in this portion of the model would severely complicate the model, all bolt holes were ignored. Although holes in any solid material significantly affect that piece's structural properties (e.g. bending, torsion), the effects can easily be compensated for by later changing the material's other properties (Young's Modulus, thickness) to account for this. This portion of the model also includes the drawers' sliding rail mounts. These pieces are a very complicated nesting of steel channels, rollers, and cam locks. Since this would be difficult to model, these pieces were modeled as solid metal bars. Again, material properties can easily be varied later to account for the actual behavior of these rails.

The shell consists of all the cover plates in the rack system: top, bottom, sides, front, and back. These were very simple to model because they are flat plates.

The equipment drawers and bullnose, due to their complicated internal structure, also had to be simplified during the modeling process. The drawers were modeled as solid blocks of the appropriate size with a corresponding density so they had the correct weight. Other material properties were approximated in order to give the appropriate dynamic response.

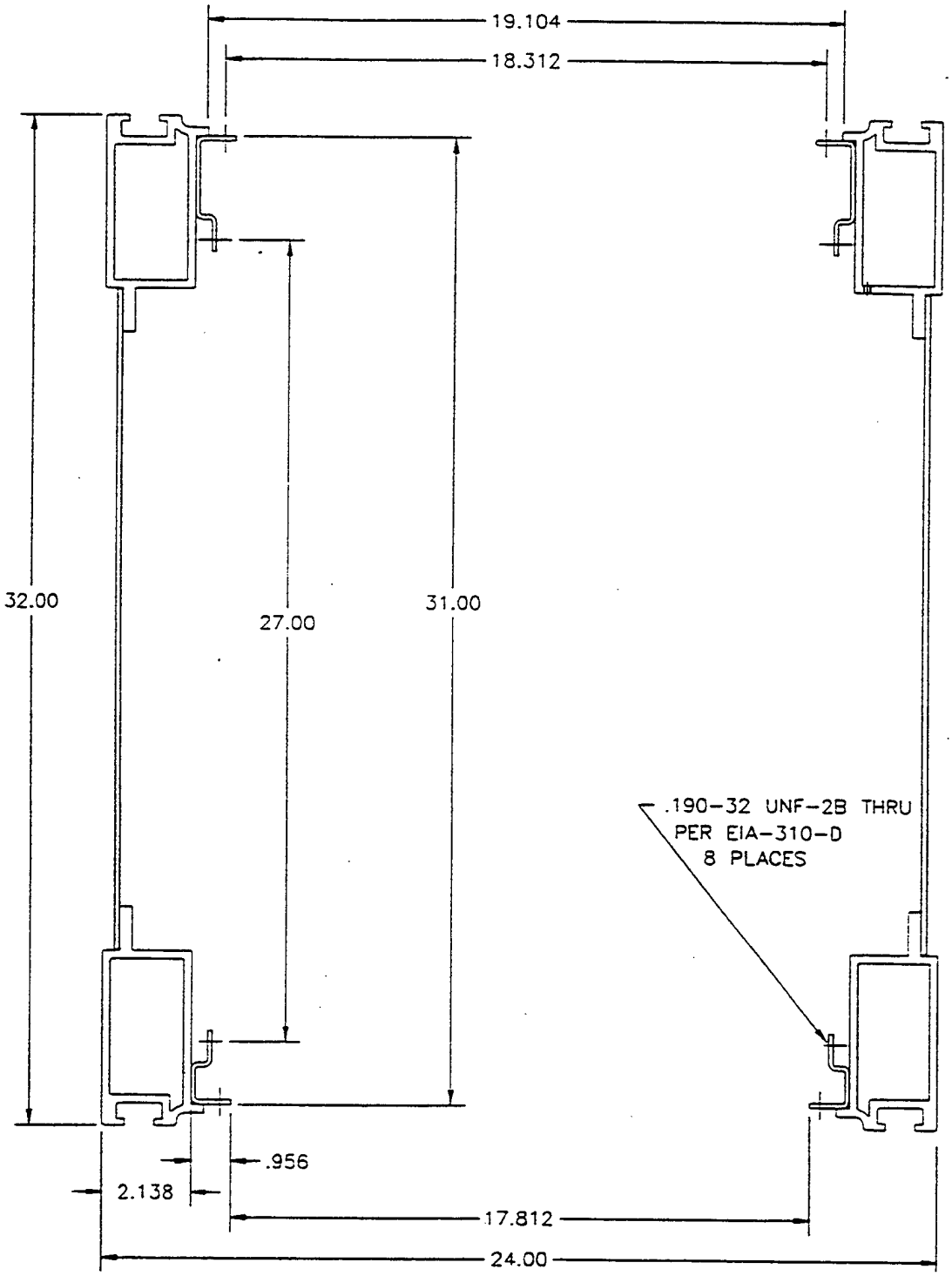

Figure 3: Critical Dimensions of 72" Rack Midsection (Plane View)

B. FINITE ELEMENT MODELING

Once each portion of the model was modeled geometrically, it is ready to be discretized into finite elements. This was done to each separate portion of the rack. Here, the next most important part of the modeling strategy is to make the individual elements as large as possible. This serves to minimize the mathematical model size and to maintain the accuracy of calculated responses.

Two types of finite elements were used to model the rack. The first type are called quadrilateral plate elements, while the second are called hexagonal, or brick, elements. The plate elements were used everywhere except in the electronics components and the bullnose where brick elements were used. Plate elements were chosen because they model structures whose thicknesses are much smaller than their other dimensions well, as most of the rack parts resemble this. Brick elements were used to model the electronic components to maintain the spatial representation of these components in the model and because their physical properties are easy to modify.

All metal structures in the rack were modeled using plate elements of appropriate thickness using the physical properties of 18-8 stainless steel. Plate elements were chosen over beam elements for the tubular frame to ease the modeling process with respect to connectivity of overlapping parts and the resulting varying thicknesses. The electronic components used brick elements whose density was adjusted to produce the appropriate weight. Also, the stiffness of the brick elements was modified to introduce more flexibility than that of steel to more closely mimic the true drawer response.

The last portion of the rack requiring modeling is the shock mounts. The system shock mounts were also idealized. This consisted of connecting the appropriate nodes on the cabinet using rigid beam elements, maintaining the correct geometric offsets, to the coincident nodes used for the linear spring elements. Each mount model uses three springs one in each translational direction. The manufacturer supplied mount force-displacement curves [Ref. 6] were then used to obtain linearized approximations of the spring constant values for each of these springs. Because no rotational data was available,

rotational spring stiffness was not modeled. Figures 4 through 6 shows the finite element discretization of each portion of the rack system for the single monitor model.

Once each portion of the rack system was discretized, they were appended to each other to form the entire rack system assembly. Figures 7 and 8 show the appended models for the single and dual monitor models respectively. Now that the model portions are joined, all possible model continuity checks were performed. All elements were checked to ensure that their dimensions and shapes were well within acceptable mathematical standards to ensure the accuracy of all ensuing model calculations. Also, checks for duplicate nodes and elements, as well as missing nodes and elements were performed. If the model is properly constructed, the free edges will show the actual model boundaries. If not, a free edge will appear to indicate either a crack or a hole in the model. Finally, a static analysis was performed on the model Using MSC/NASTRAN (Version 69) as a gross model integrity check. This serves as a final common sense check of the model prior to performing the more elaborate dynamic calculations. This is accomplished by comparing the calculated static deflection of a component with normal gravity applied, for example - the center of a drawer rail, with what you would expect for the given loading condition.

The process of creating the finite elements, joining them, and applying the appropriate physical properties is the most important part of the entire simulation process. Mistakes made during this process can easily invalidate all calculations made using the model. Because of this, this process is the most time consuming of them all. Once a good, basic model is constructed it can easily be modified as required to different rack configurations for simulation testing. Reference 7 contains further information on the finite element modeling process.

Appendix A contains a listing of the important physical characteristics (including major dimensions, weights, and mount characteristics) used to model both the single and dual monitor rack variants.

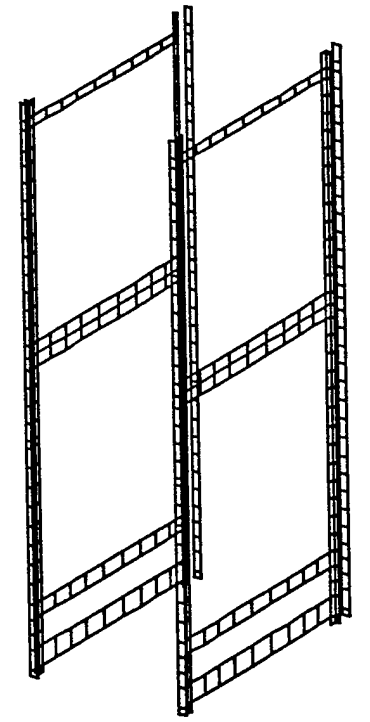

(a)

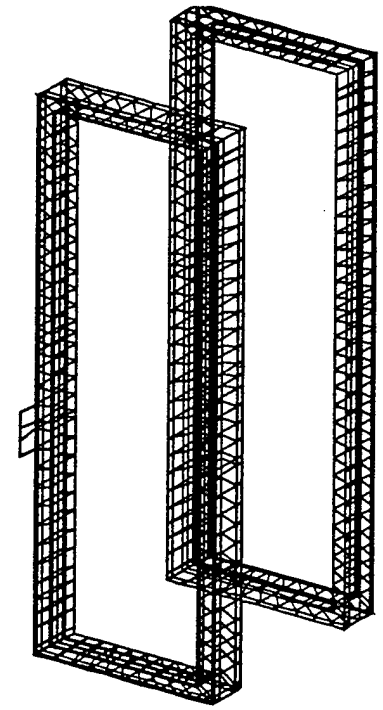

(b)

Figure 4: Finite Element Models Showing Discretization of the: a) Internal Rack Frame and b) Tubular Support Frame.

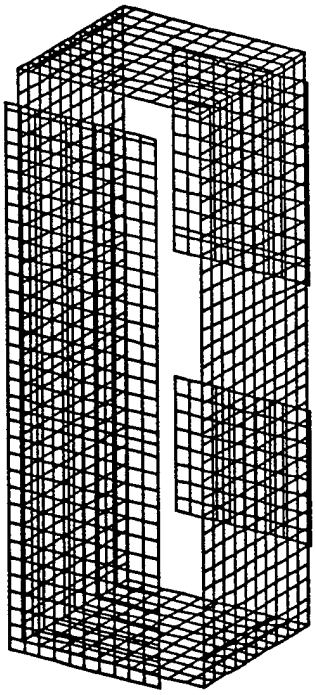

(a)

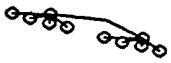

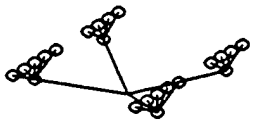

(b)

Figure 5: Finite Element Models Showing Discretization of the: a) Shell Plating and b) Isolation Mounts.

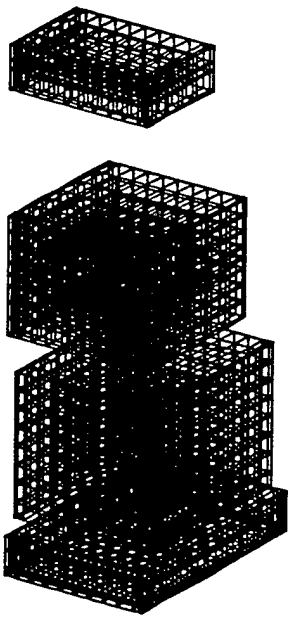

(a)

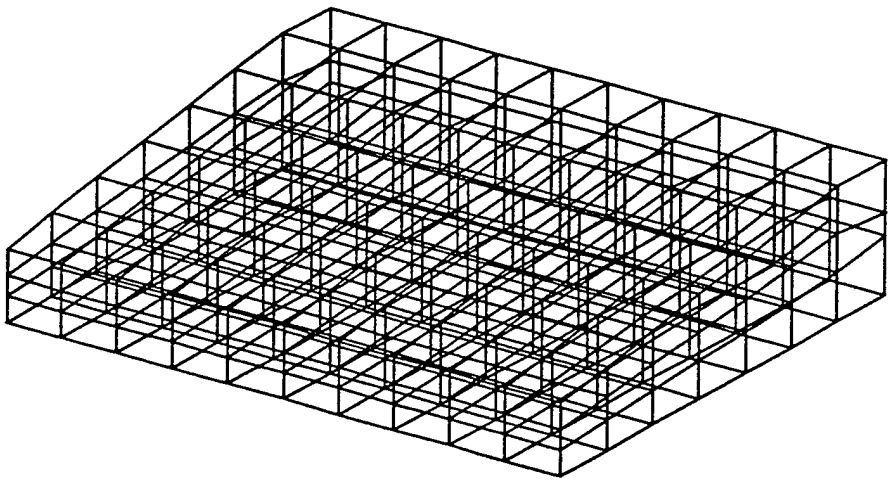

(b)

Figure 6: Finite Element Models Showing Discretization of the: a) Electronic Components and b) Rack Bullnose.

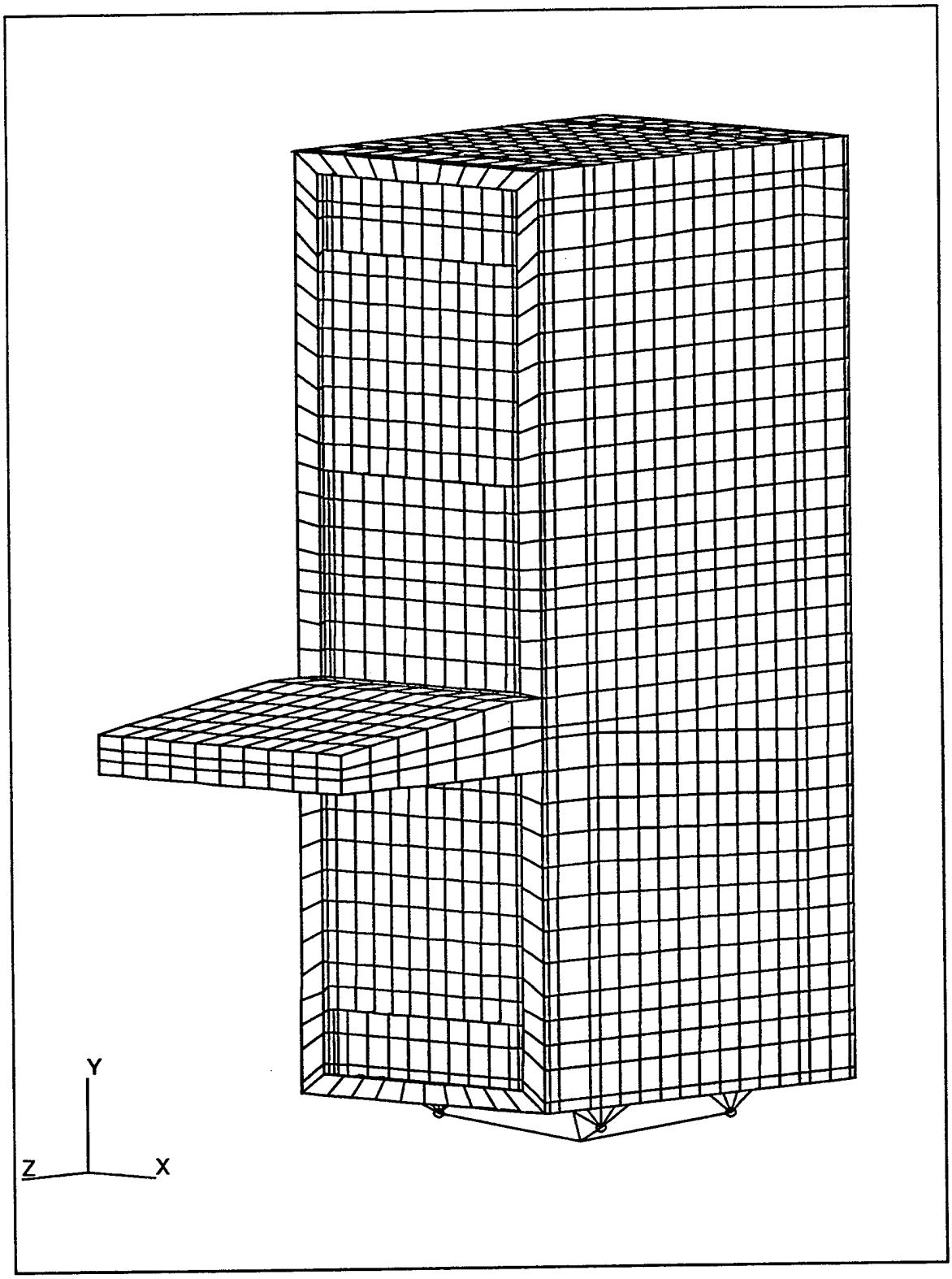

Figure 7: Overview of Single Monitor Rack Variant Discretization into Finite Elements.

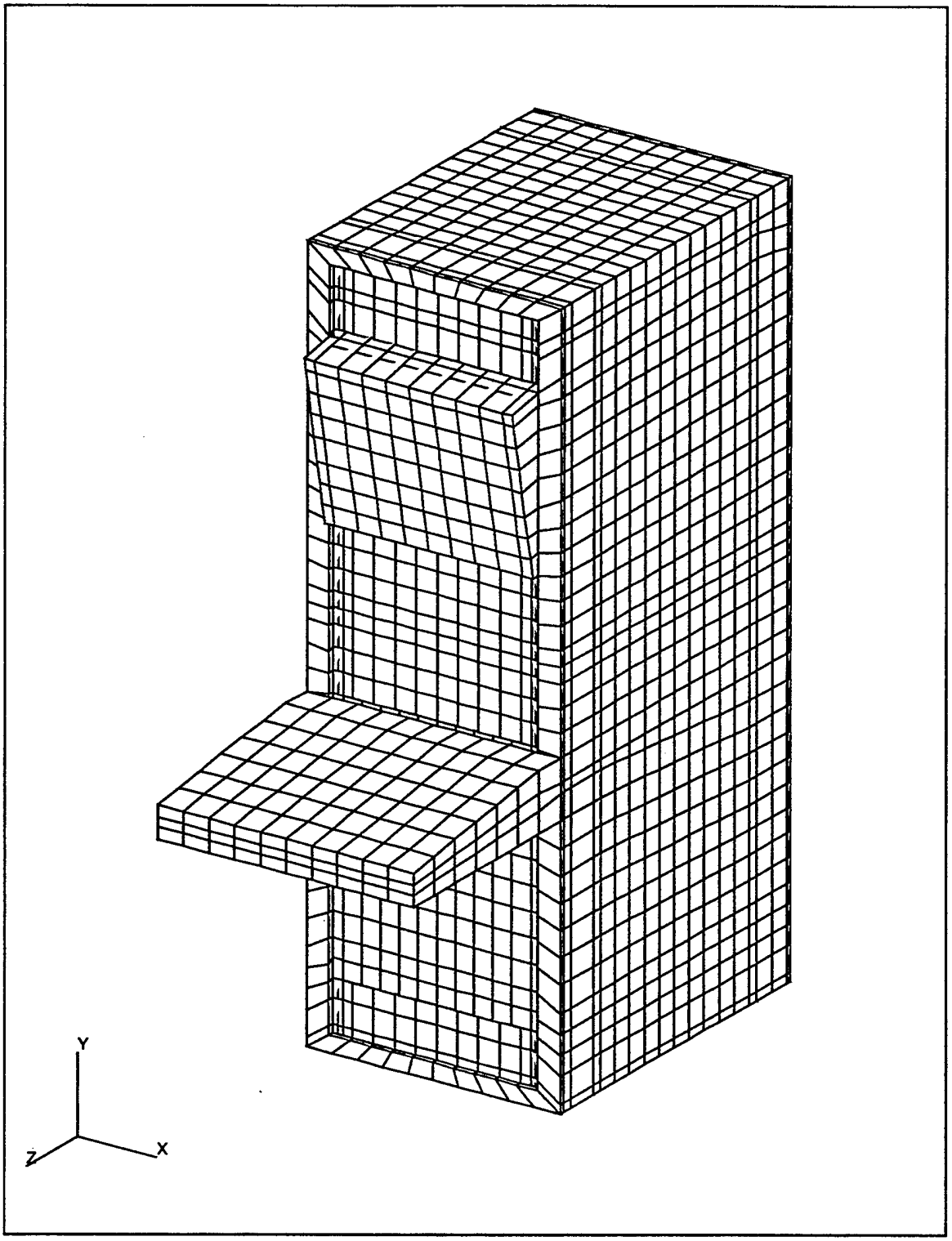

Figure 8: Overview of Dual Monitor Rack Variant Discretization into Finite Elements.

IV. NORMAL MODE ANALYSIS

The normal modes of vibration for both models were solved for using MSC/NASTRAN (Version 69) finite element structural code. From the theory previously discussed, a full normal mode analysis will produce a normal mode for every degree of freedom. For large models, as in this case (over 30,000 DOF), this level of computation becomes tedious and is generally unnecessary. MSC/NASTRAN has several methods to choose from in order to determine the normal modes. The Lanczos Method [Ref. 8] was used because it is the most efficient method for large problems and is also very accurate. The following two sections will discuss the most important modes, from a dynamic response perspective.

Physically, a mode represents the shape of vibration an object takes if the object is vibrated at its corresponding natural frequency. From this description, it is easy to understand why they can be useful in transient response analysis, providing a base understanding of dynamic response characteristics.

In order to facilitate the description of the mode shapes, the directions of motion must be defined. Vertical motions occur along the Y-axis, transverse motions along the X-axis, and fore-aft motions occur along the Z-axis. Because mode shapes (eigenvectors) are scaleable, the deformations shown in all figures are not to scale with the rack itself but are exaggerated for visual display purposes. The number associated with the deformation is the mass normalized value for the eigenvector. This establishes the modal mass at unity for the subsequent decoupling of the equations of motion.

A. SINGLE MONITOR VARIANT (CLIN 0003AA)

The model of this rack configuration contains 83 separate modes below 100 Hz. This group of modes can be divided into two general categories, gross and localized modes. Gross modes occur when the entire rack essentially moves as a unit with some twisting of the entire structure (this is not a rigid body mode, which indicates unrestrained

motion). The first six modes can be characterized as gross modes. A description of these modes follows. Appendix B lists the characteristics of the local modes 7 through 25.

Mode 1 at 3.50 Hz , shown in Figure 9, depicts a gross mode consisting of a complicated rocking motion. This motion consists of a combination of pivoting about two separate axis parallel to the Z-axis and the Y-axis. This is indicated by the annular shaped deflection zones shown on the figure.

Mode 2, which occurs at 5.34 Hz, consists of a rocking motion about an axis parallel to the X-axis. This is shown in Figure 10.

The 3rd Mode at 7.37 Hz indicates an almost pure rocking motion about an axis parallel to the X-axis. Figure 11 again shows the annular deflection zones which indicates this.

Figure 12 shows Mode 4 which occurs at 7.44 Hz. The deflection pattern here indicates that this mode is a rocking motion about an axis which goes from the middle-front to the middle-top of the rack (white zones).

Next is Figure 13 which is Mode 5 at 9.13 Hz. This mode is a pure rocking motion about an axis which occurs where the bullnose is attached to the rack (white zone).

Mode 6, which occurs at 9.87 Hz, indicates another rocking mode. This occurs around an axis from the middle-front extending to the back-bottom edge of the rack. This is shown in Figure 14.

Modes 7 through 83 consist of localized modes. These occur when the rack, as a whole, remains relatively stationary while individual parts on the rack vibrate separately. Figures 15 and 16 show two examples of localized modes. Figure 15 shows the 8th mode at 24.65 Hz and Figure 16 shows the 21st mode at 29.58 Hz.

Mode 8 is characterized by two separate localized plate bending modes. The first is the cabinet's top panel which exhibits a minimal first bending mode. The other is the cabinet side panels which also exhibit a strong first bending mode, while vibrating in opposite phase to each other. The 21st Mode is also characterized by localized plate bending modes. Here, the 1st plate bending mode of the top panel is still present, but

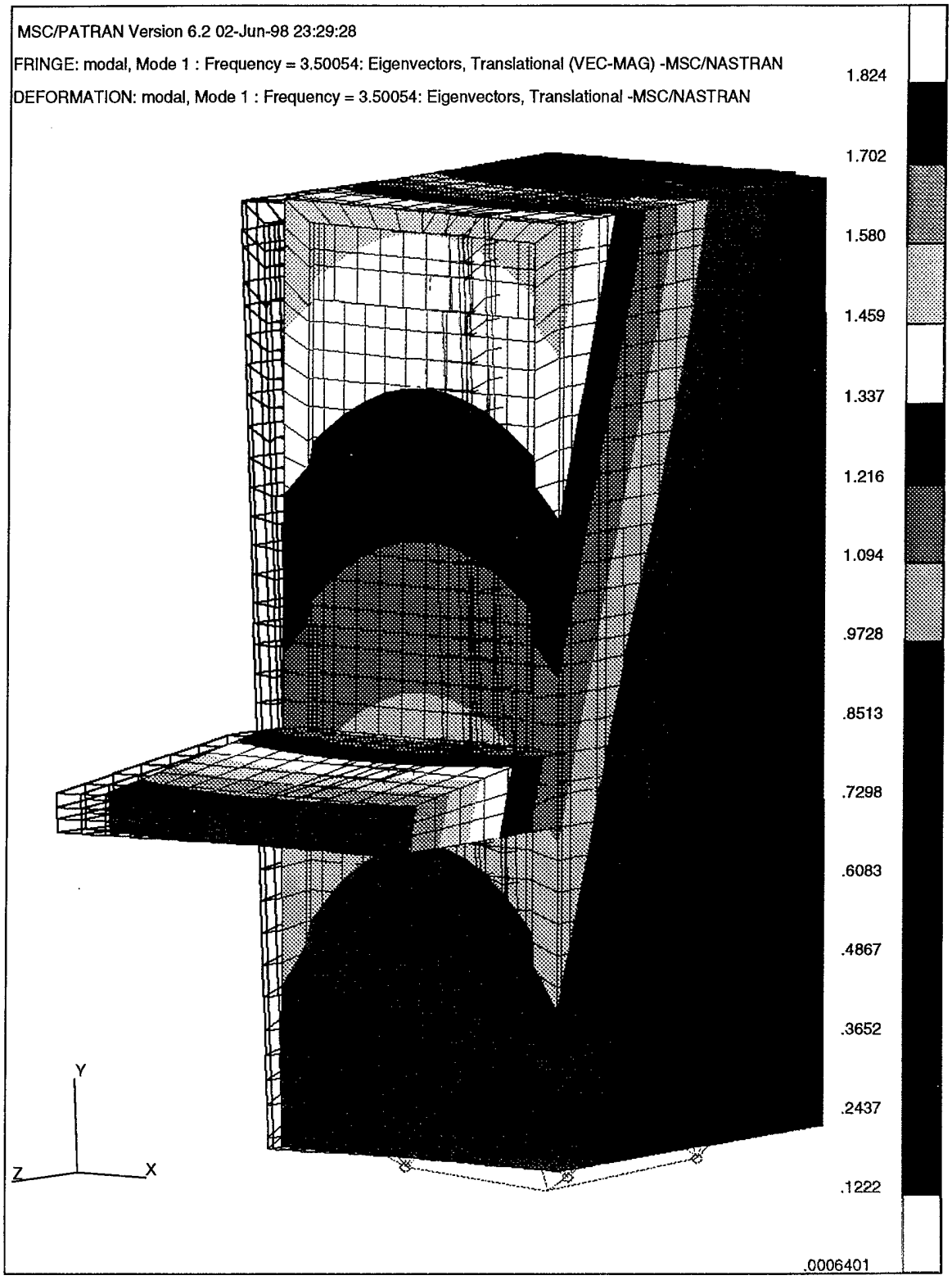

Figure 9: Single Monitor Variant, Mode 1, 3.50 Hz.

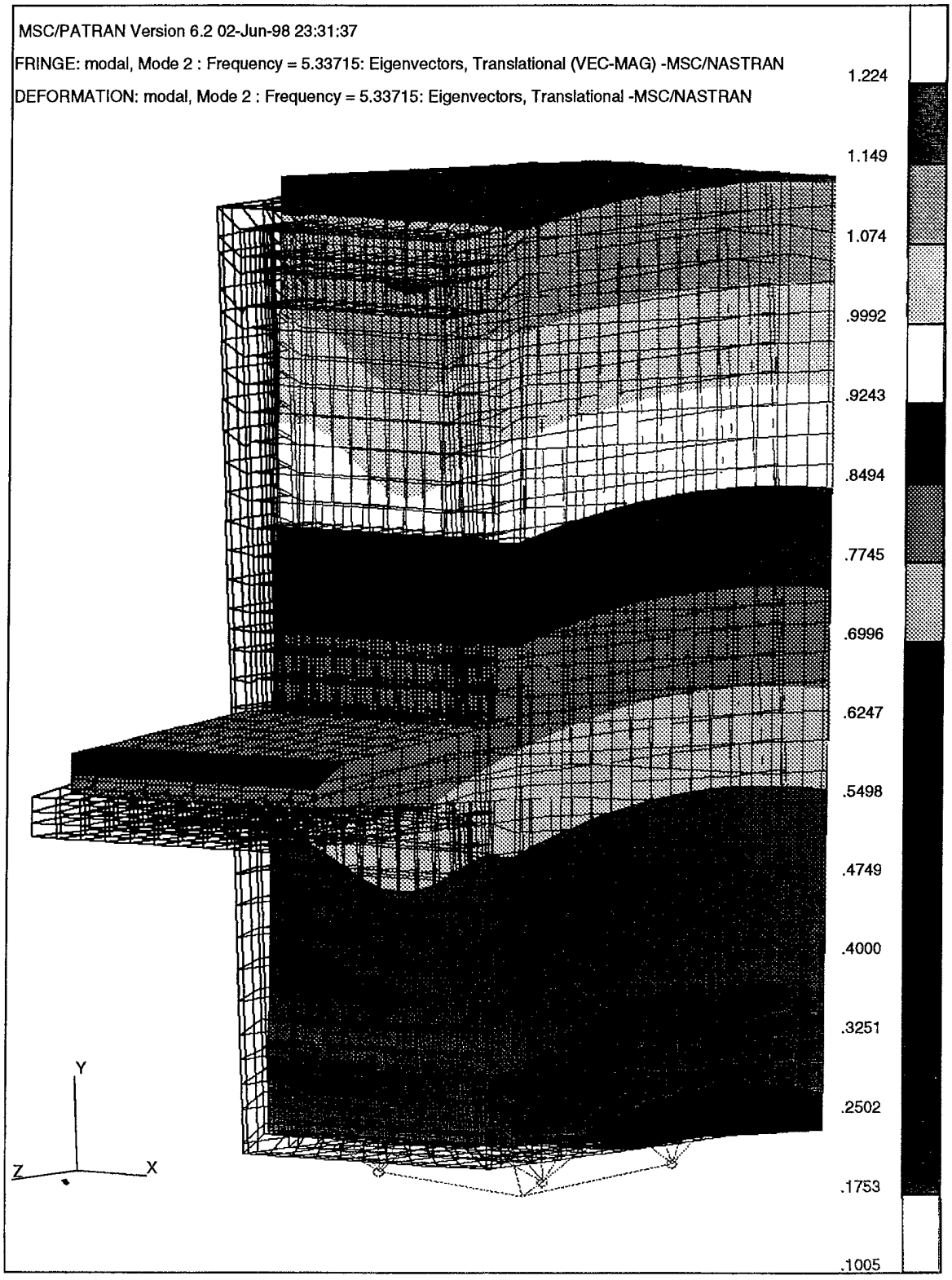

Figure 10: Single Monitor Variant, Mode 2, 5.34 Hz.

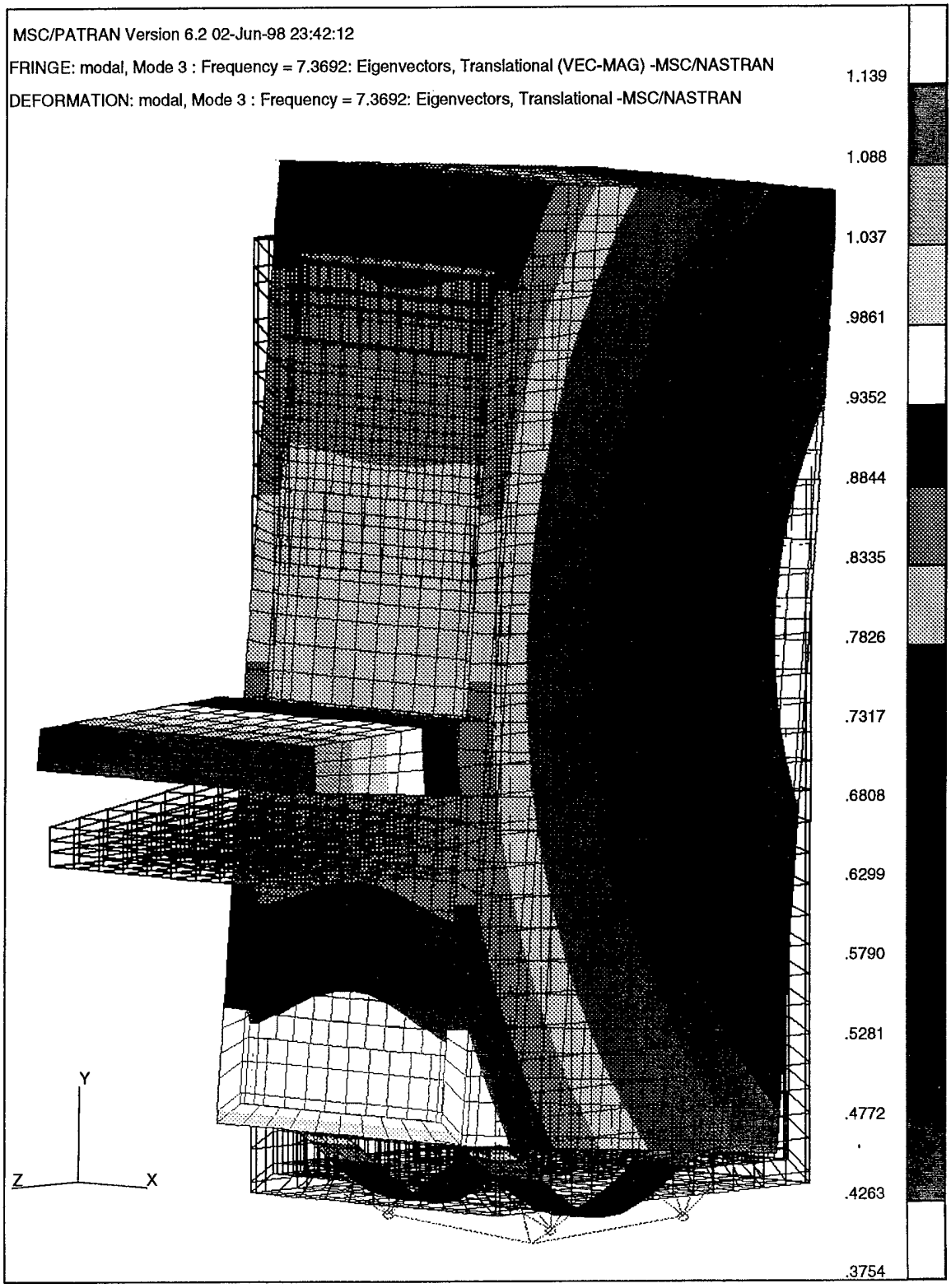

Figure 11: Single Monitor Variant, Mode 3, 7.37 Hz.

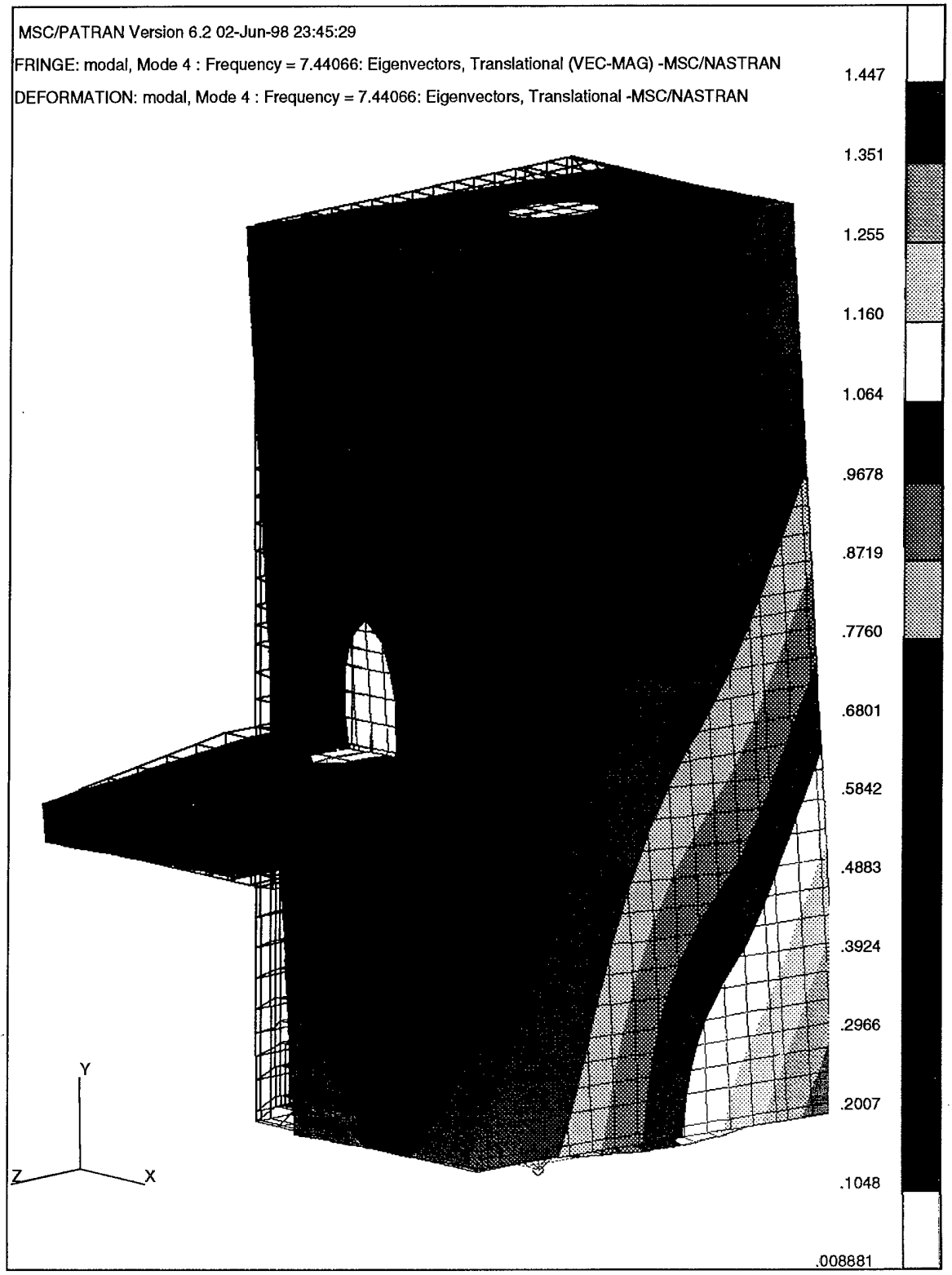

Figure 12: Single Monitor Variant, Mode 4, 7.44 Hz.

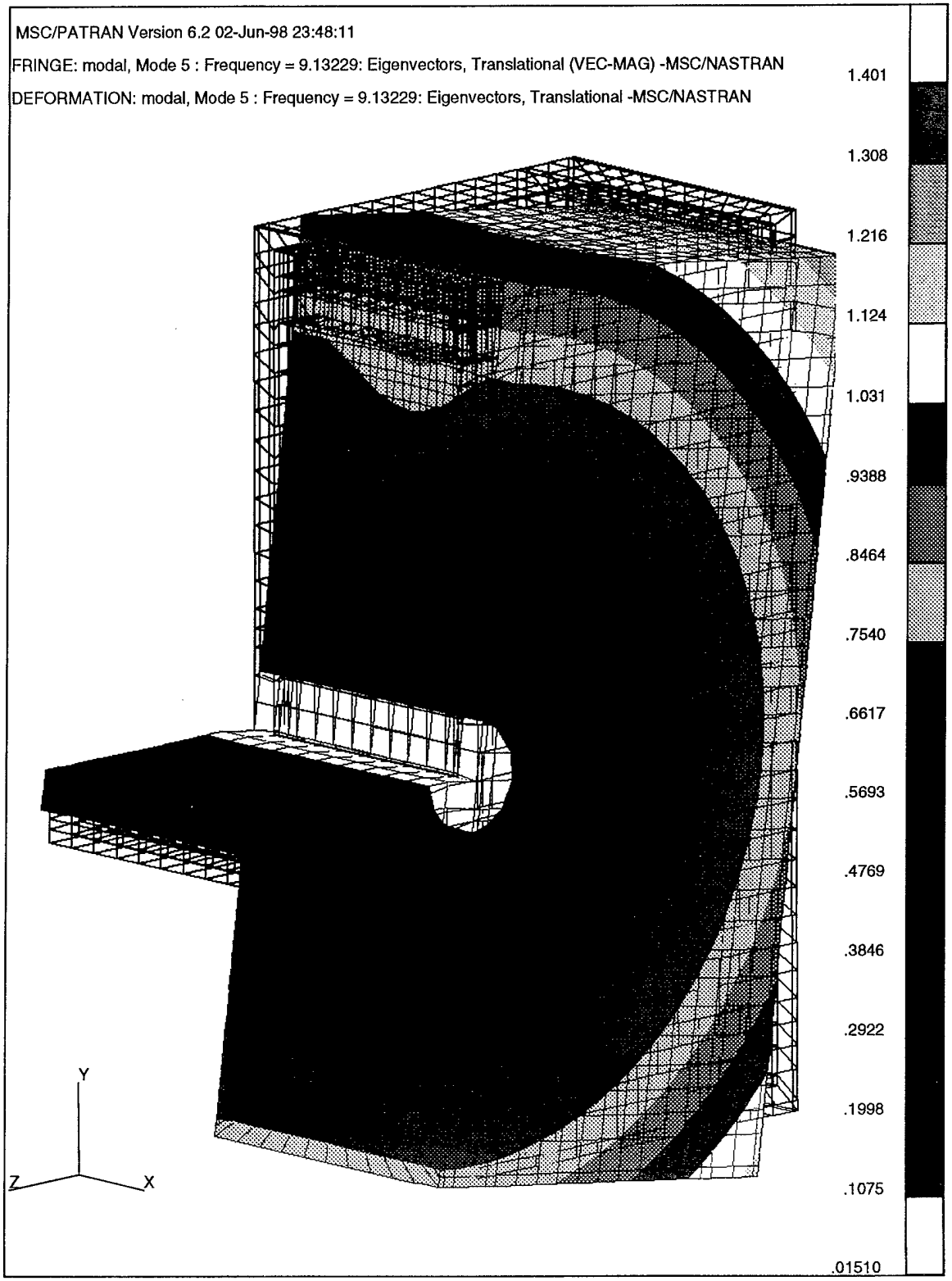

Figure 13: Single Monitor Variant, Mode 5, 9.13 Hz.

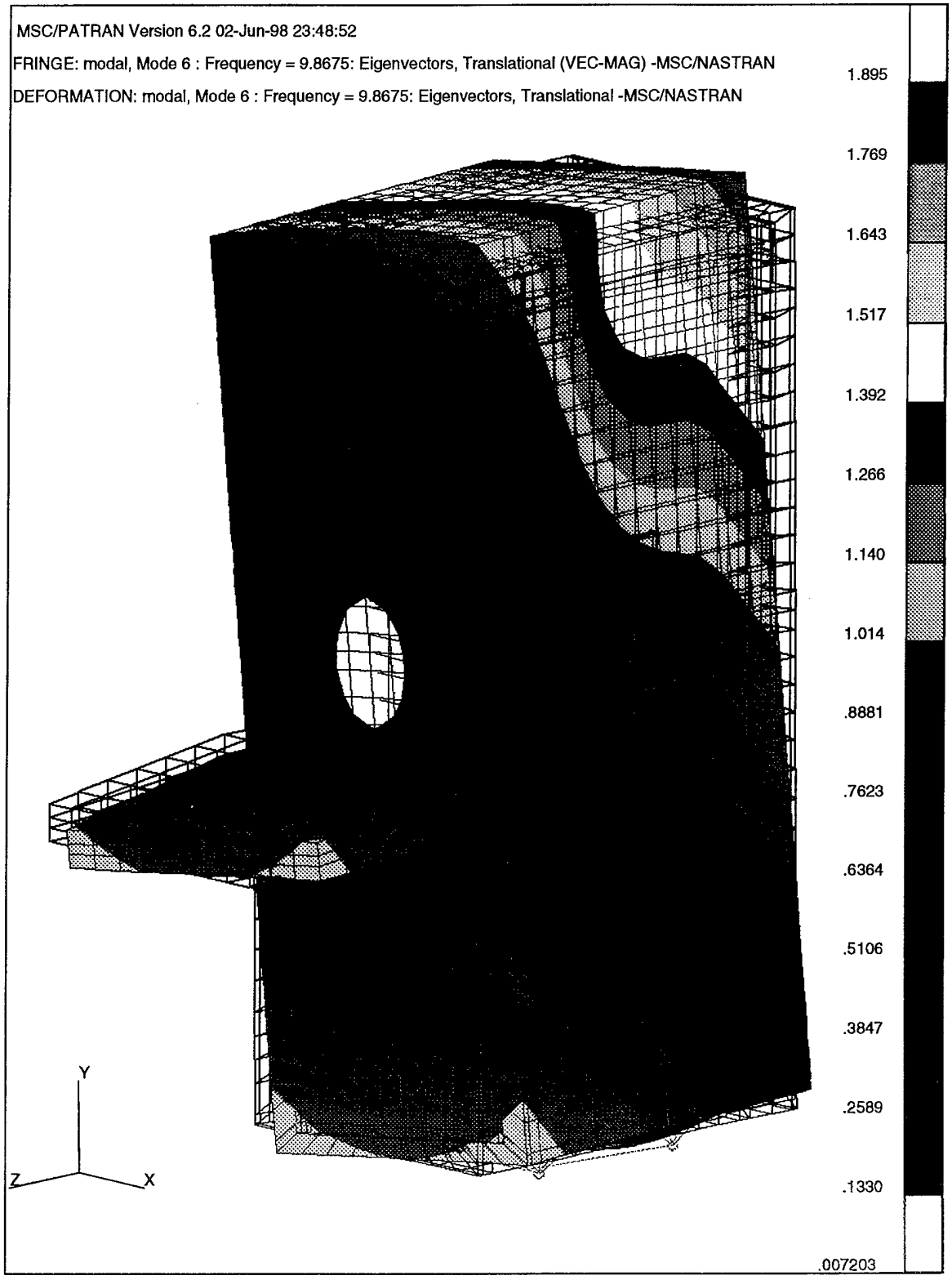

Figure 14: Single Monitor Variant, Mode 6, 9.87 Hz.

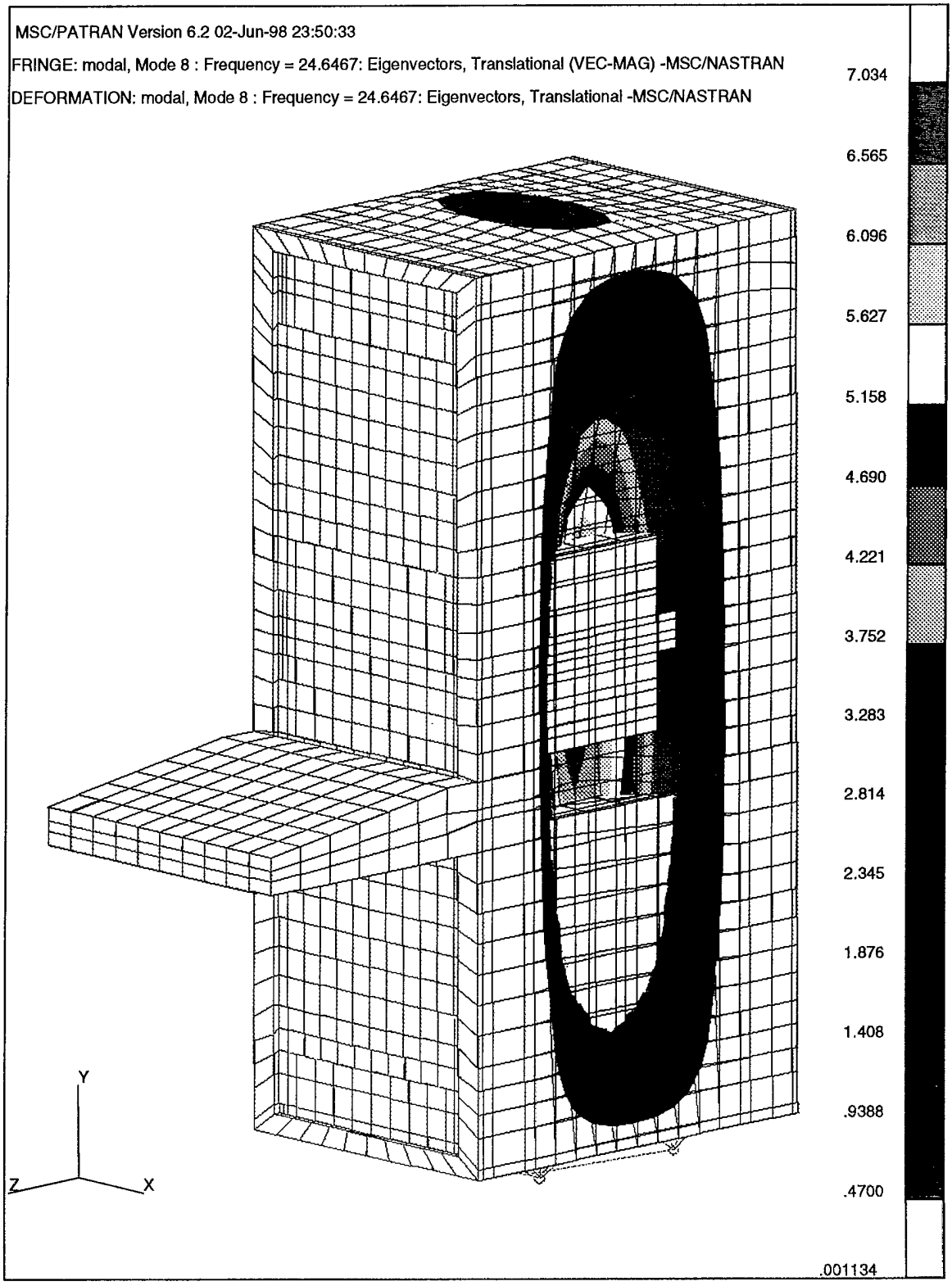

Figure 15: Single Monitor Variant, Mode 8, 24.65 Hz.

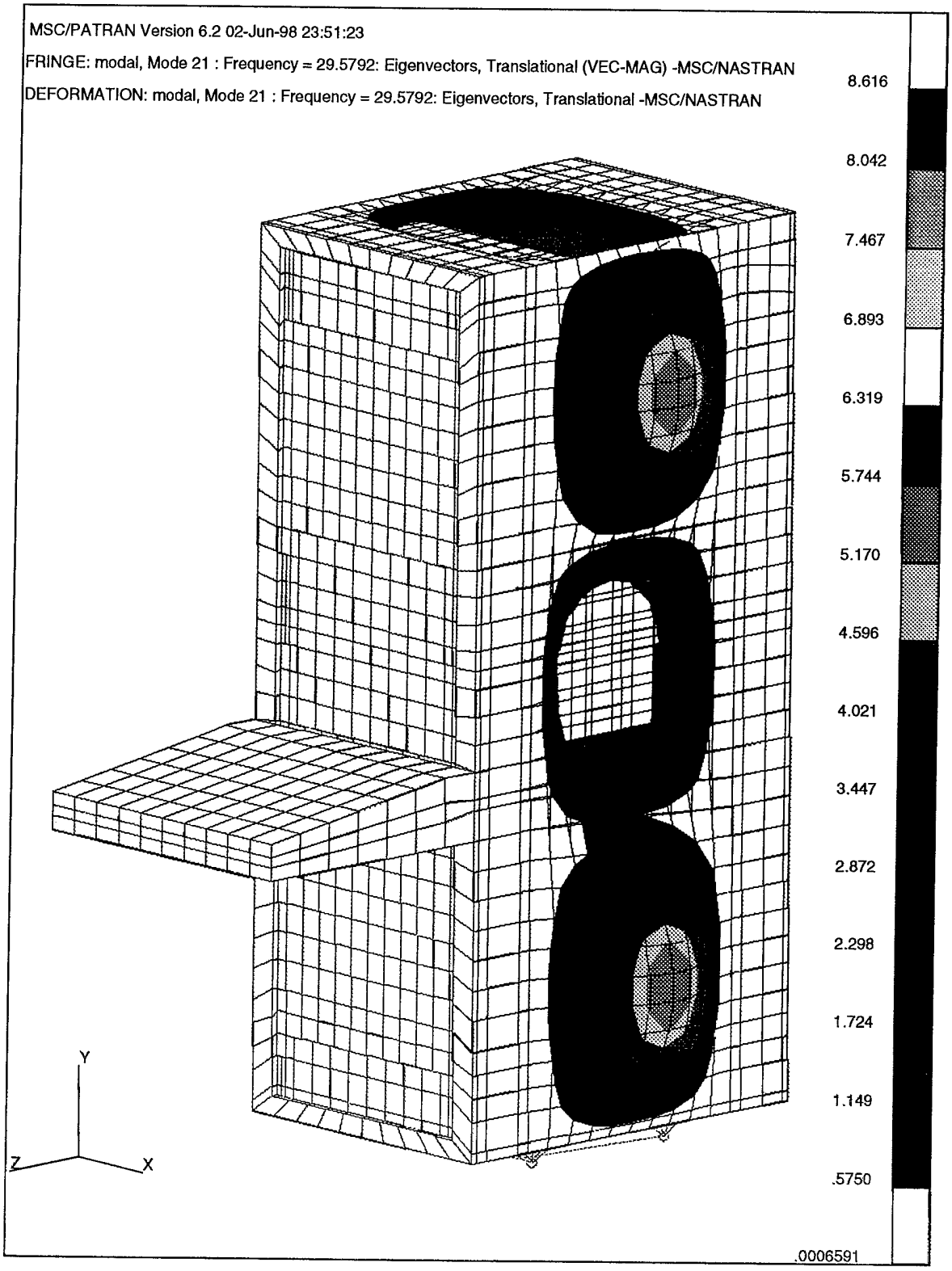

Figure 16: Single Monitor Variant, Mode 21, 29.58 Hz.

stronger. The side panels have shifted into their 3rd plate bending mode, while vibrating in opposite phase to each other. The other localized modes consist of higher order modes for the top and side panels, as well as localized modes in other locations on the rack. Appendix B lists the characteristics of the first 25 modes for this rack variant.

B. DUAL MONITOR VARIANT (CLIN 0001AA)

The model of this rack configuration also contains 83 separate modes below 100 Hz. This group of modes is also divisible into the same two general categories, gross and localized modes. As expected, these modes are very similar to the modes for the single monitor variant. Table 1 lists the first 30 natural frequencies for each rack variant. Note that the 7th through the 30th modes have essentially the same frequency between the two rack variants.

The first six modes of this rack variant are characterized as gross modes and are very similar in shape to the first six modes of the single monitor rack variant. The only difference is a shifting in the natural frequency at which these modes occur. This is mainly due to the difference in weights between the two racks. Figures 17 through 22 show the modes for the dual rack variant. Comparing them to Figures 9 through 13 readily shows the similarities.

As with the other model, the rest of the modes are localized vibration modes. The local modes in the dual monitor variant are exactly the same as in the single monitor rack variant (between parts common to both models). This is expected because local modes are only dependent on the physical properties of the local part. Figures 23 and 24 show Modes 8 and 20 which correspond to Modes 8 and 21 in the single monitor variant (Figures 15 and 16) . These modes are exactly the same in both models. Other common modes are discernible from Table 1. Appendix B lists the characteristics of the 7th through 25th modes which are the same as for the single monitor rack variant.

The modal analysis of both of these models has revealed that the first six modes are the most important to consider for transient response and probably account for 80 to 90 percent of the dynamic response characteristic. These modes are most heavily influenced by the weight of the rack (including its distribution) and the mount spring characteristics. Changes to any of these will certainly change the mode frequencies and shapes.

Local modes account for the other 10 to 20 percent of the dynamic response. Note that by theory, the lower the frequency of the mode, the more it contributes to this response. Eventually, the higher modes can be ignored and still obtain a very accurate solution to any dynamic problem. This will be discussed further in the next chapter.

Mode	Single Monitor Variant Natural Frequency (Hz)	Dual Monitor Variant Natural Frequency (Hz)
1	3.50	3.09
2	5.34	4.77
3	7.37	6.96
4	7.44	7.37
5	9.13	8.77
6	9.87	9.32
7	23.98	23.98
8	24.65	24.65
9	25.08	25.01
10	26.20	26.19
11	26.31	26.31
12	26.34	26.35
13	26.48	26.47
14	26.54	26.53
15	26.55	26.54
16	26.77	26.77
17	26.87	26.80
18	27.44	27.92
19	27.94	29.52
20	29.52	29.58
21	29.58	30.11
22	31.13	30.18
23	30.18	31.42
24	31.43	31.61
25	32.83	32.83
26	33.48	33.48
27	34.20	34.07
28	34.50	34.50
29	35.46	35.56
30	35.58	35.89

Table 1: First 30 Natural Frequencies of the Single and Dual Monitor Variants

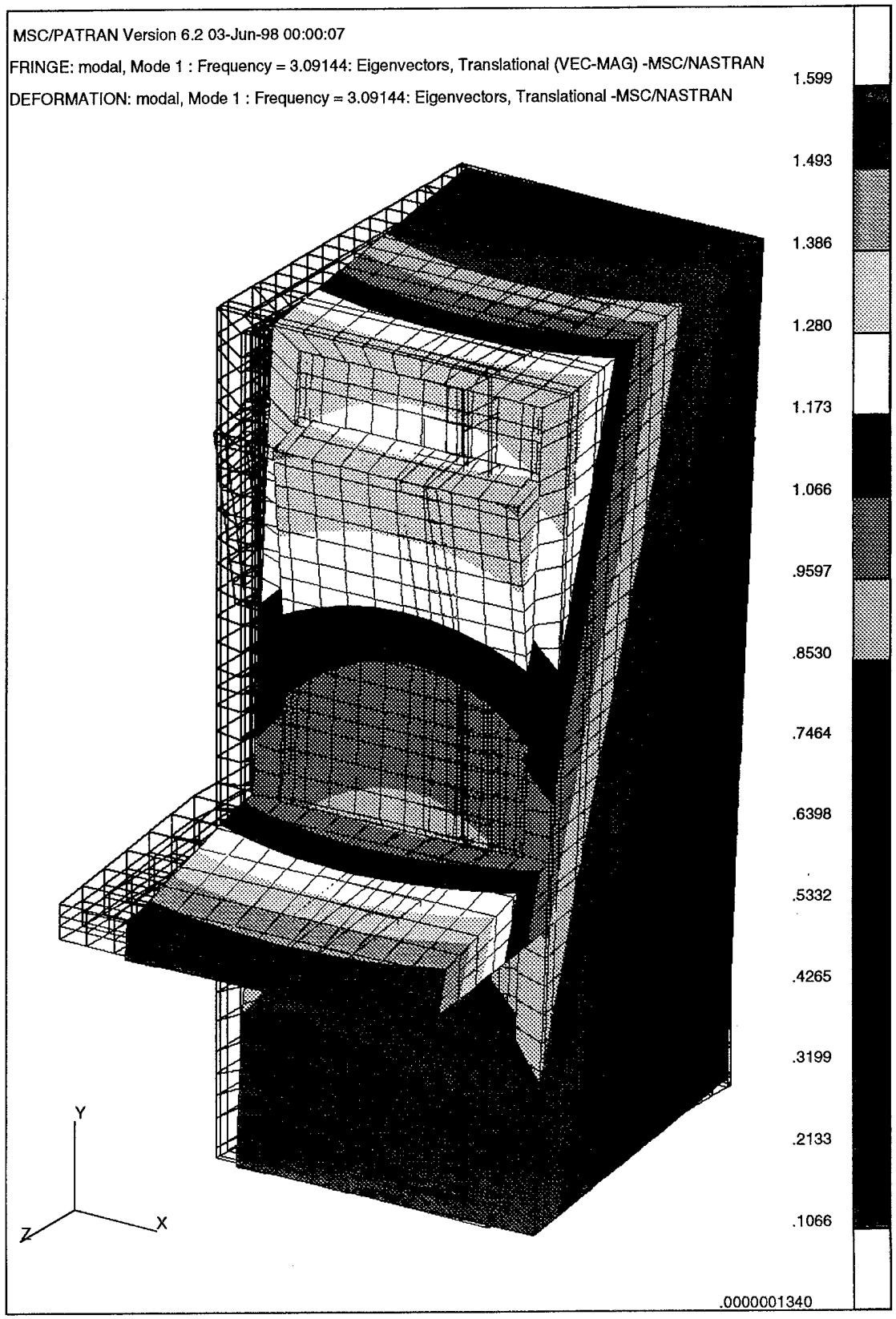

Figure 17: Dual Monitor Variant, Mode 1, 3.09 Hz.

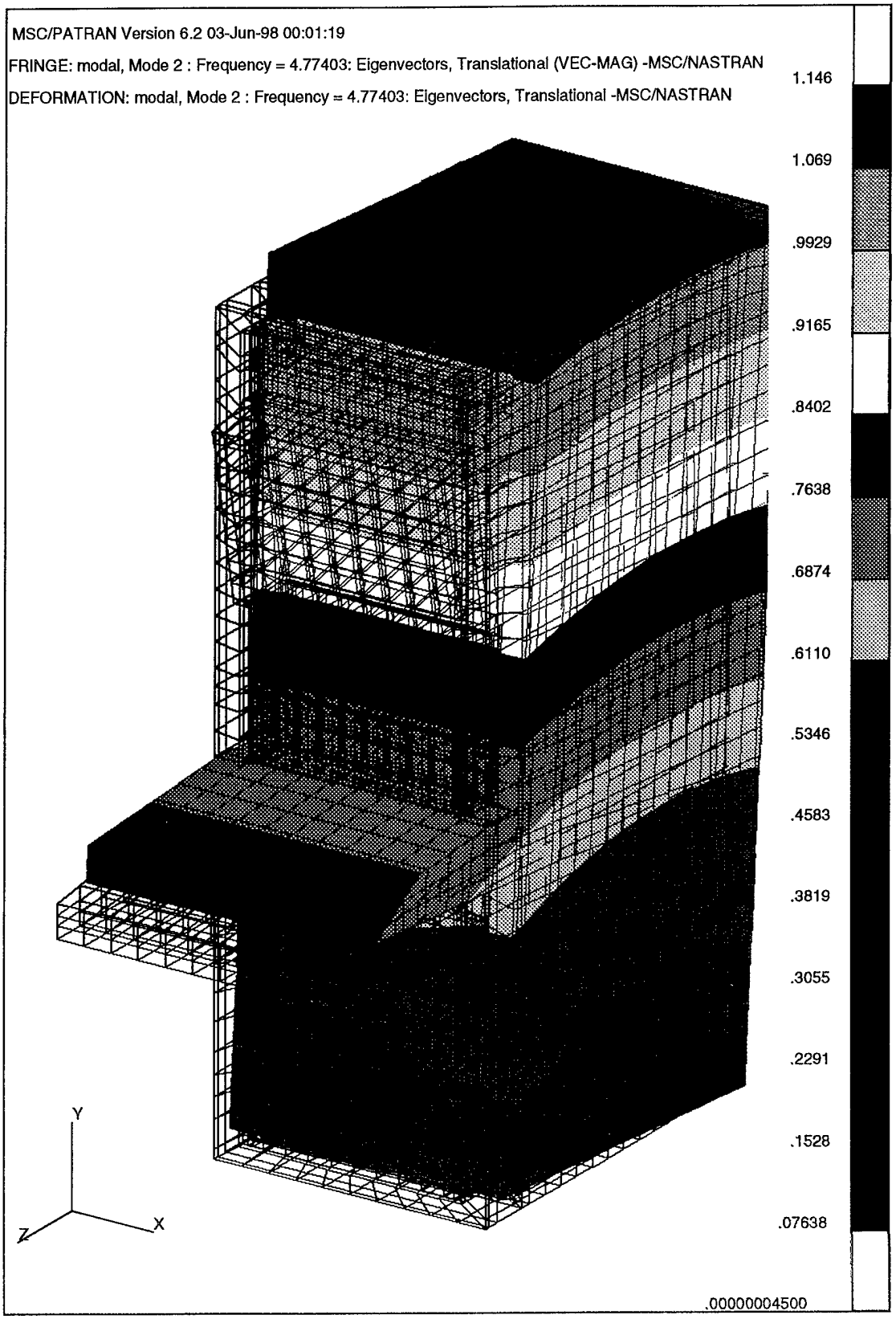

Figure 18: Dual Monitor Variant, Mode 2, 4.77 Hz.

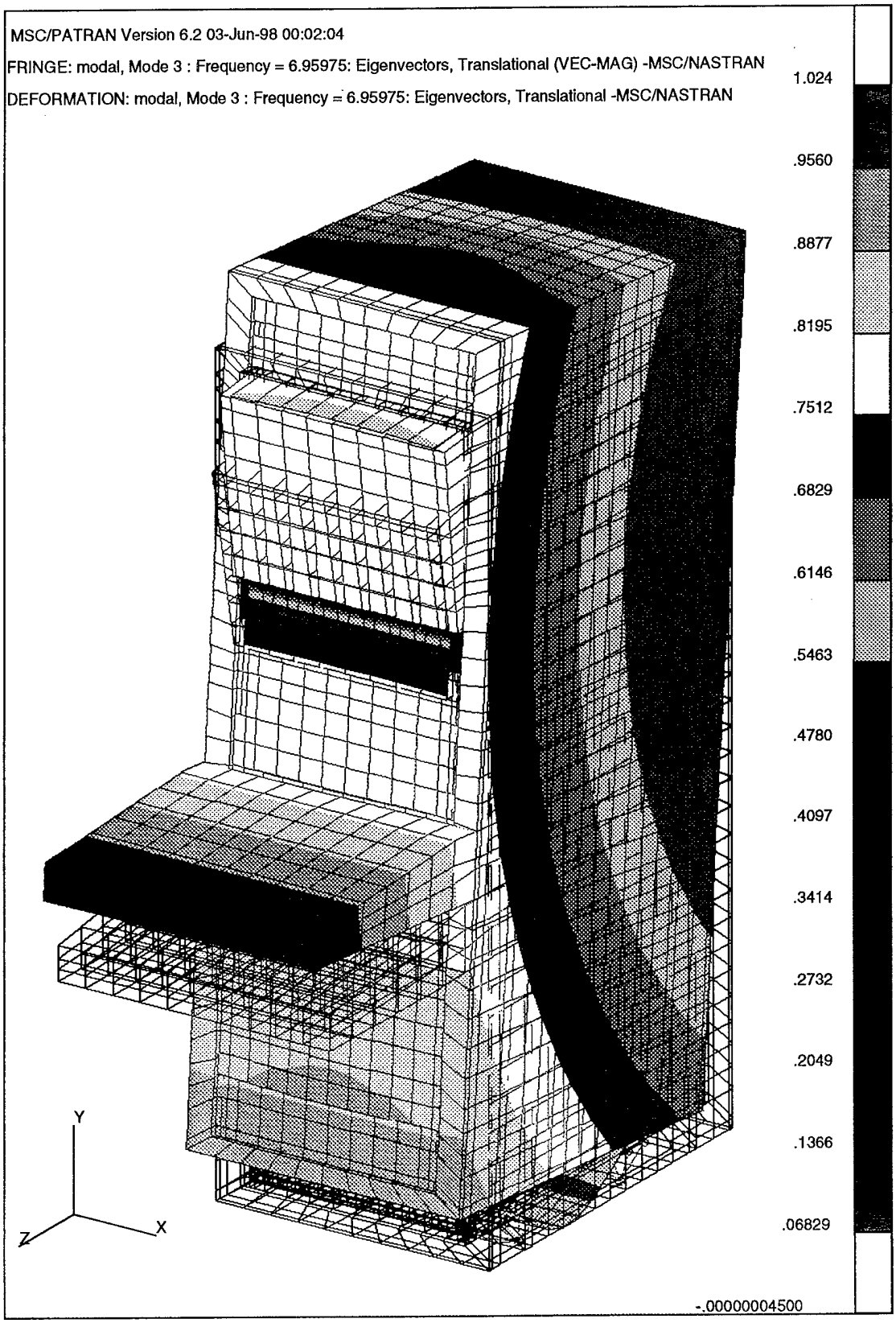

Figure 19: Dual Monitor Variant, Mode 3, 6.96 Hz.

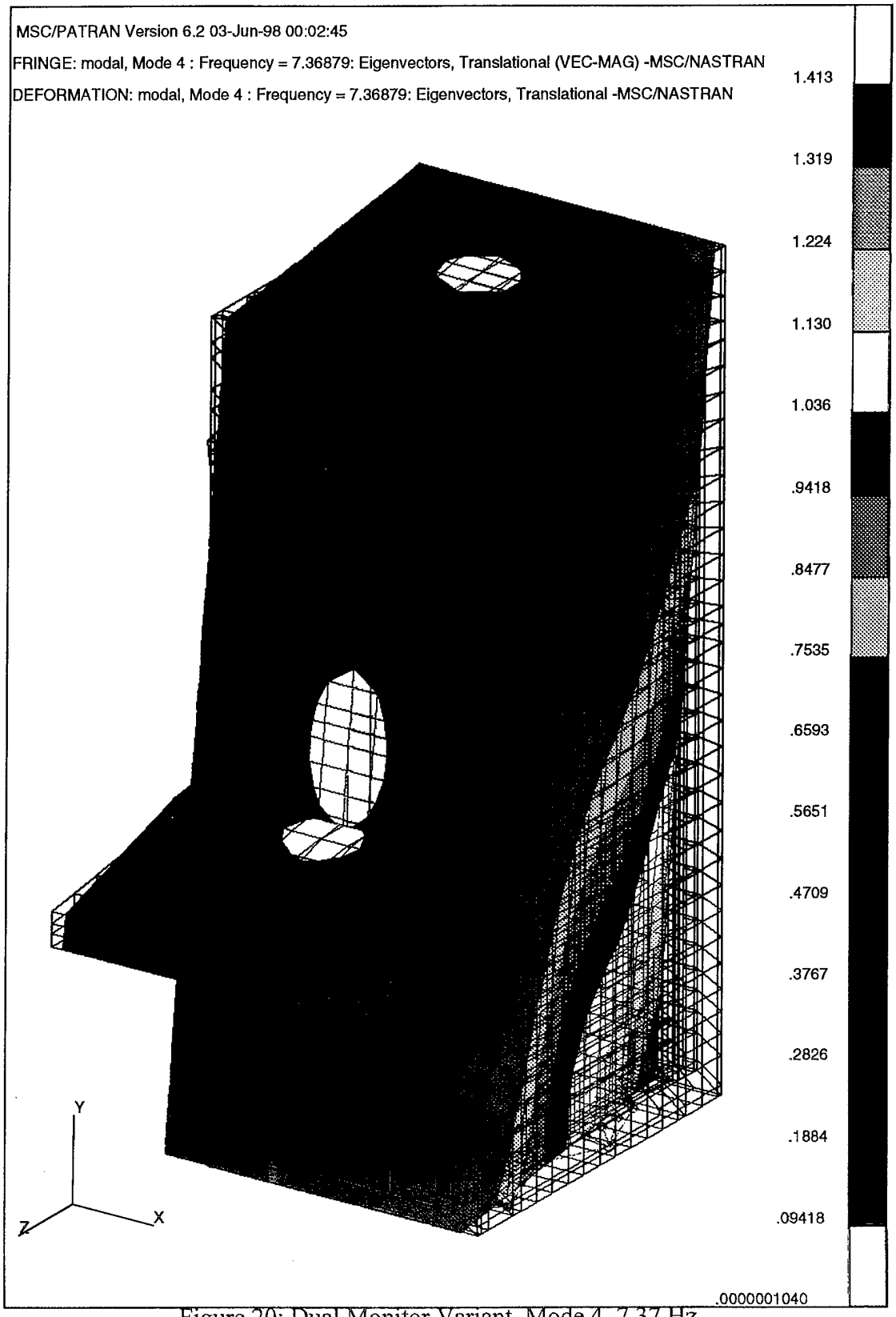

Figure 20: Dual Monitor Variant, Mode 4, 7.37 Hz.

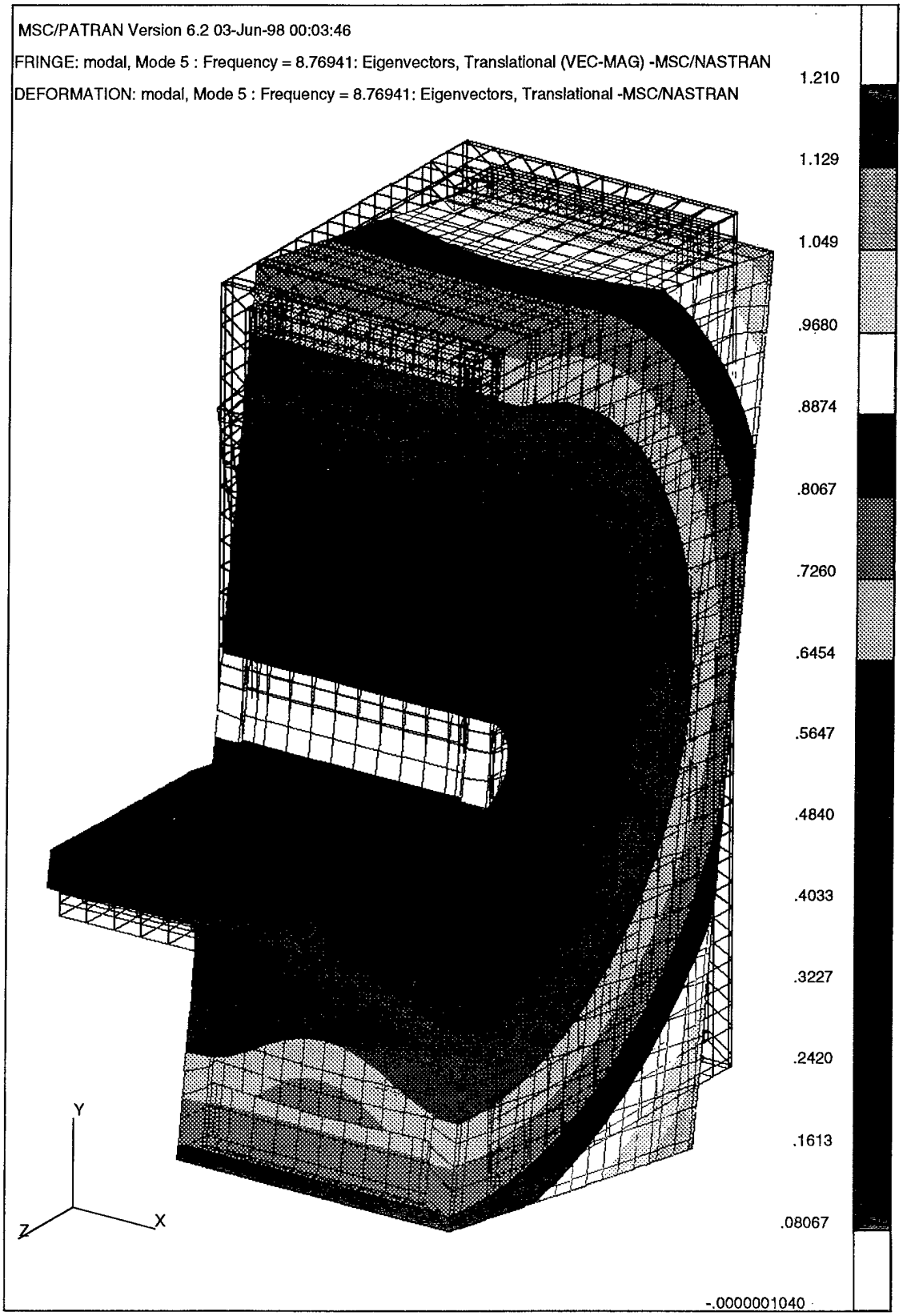

Figure 21: Dual Monitor Variant, Mode 5, 8.77 Hz.

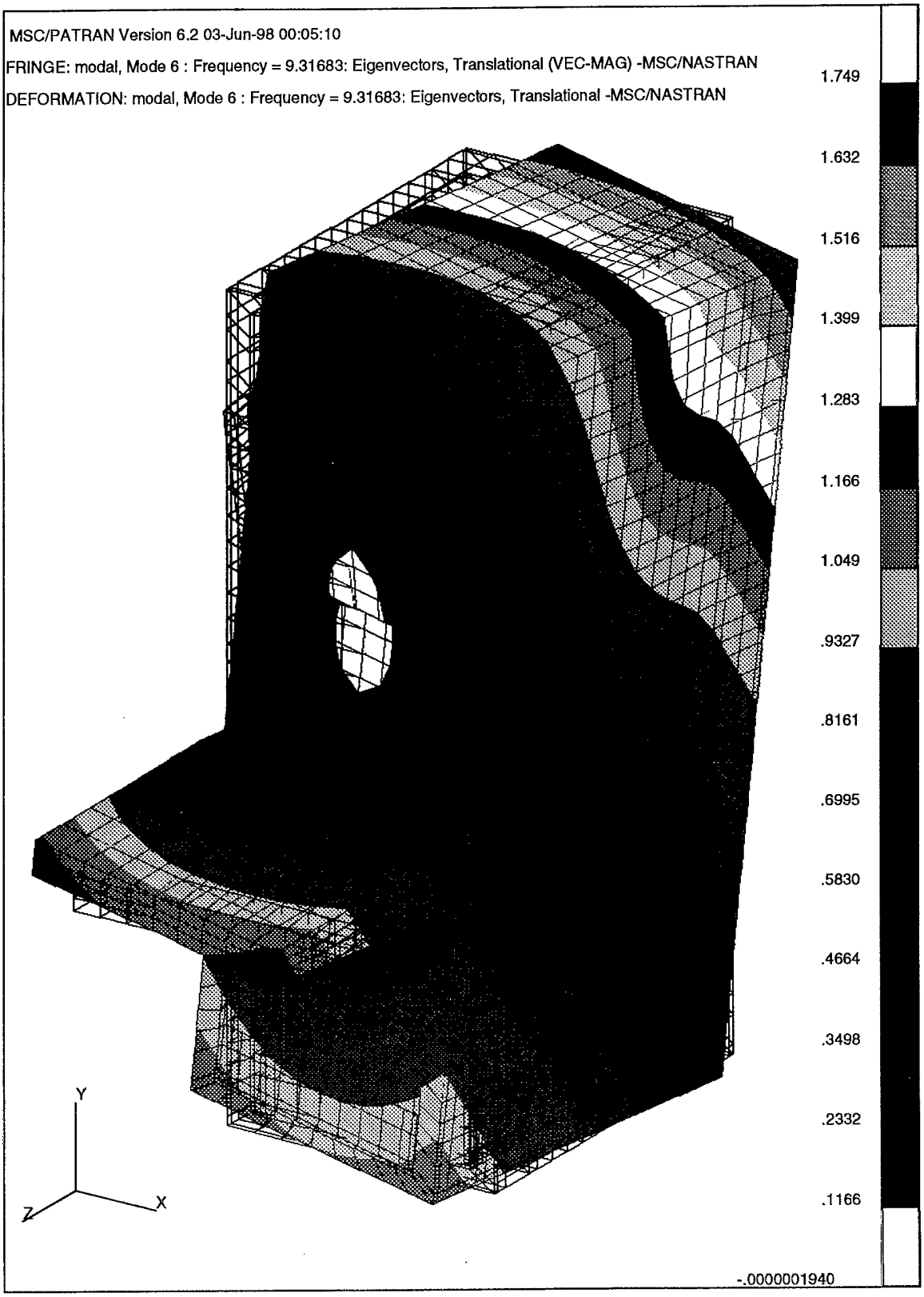

Figure 22: Dual Monitor Variant, Mode 6, 9.32 Hz.

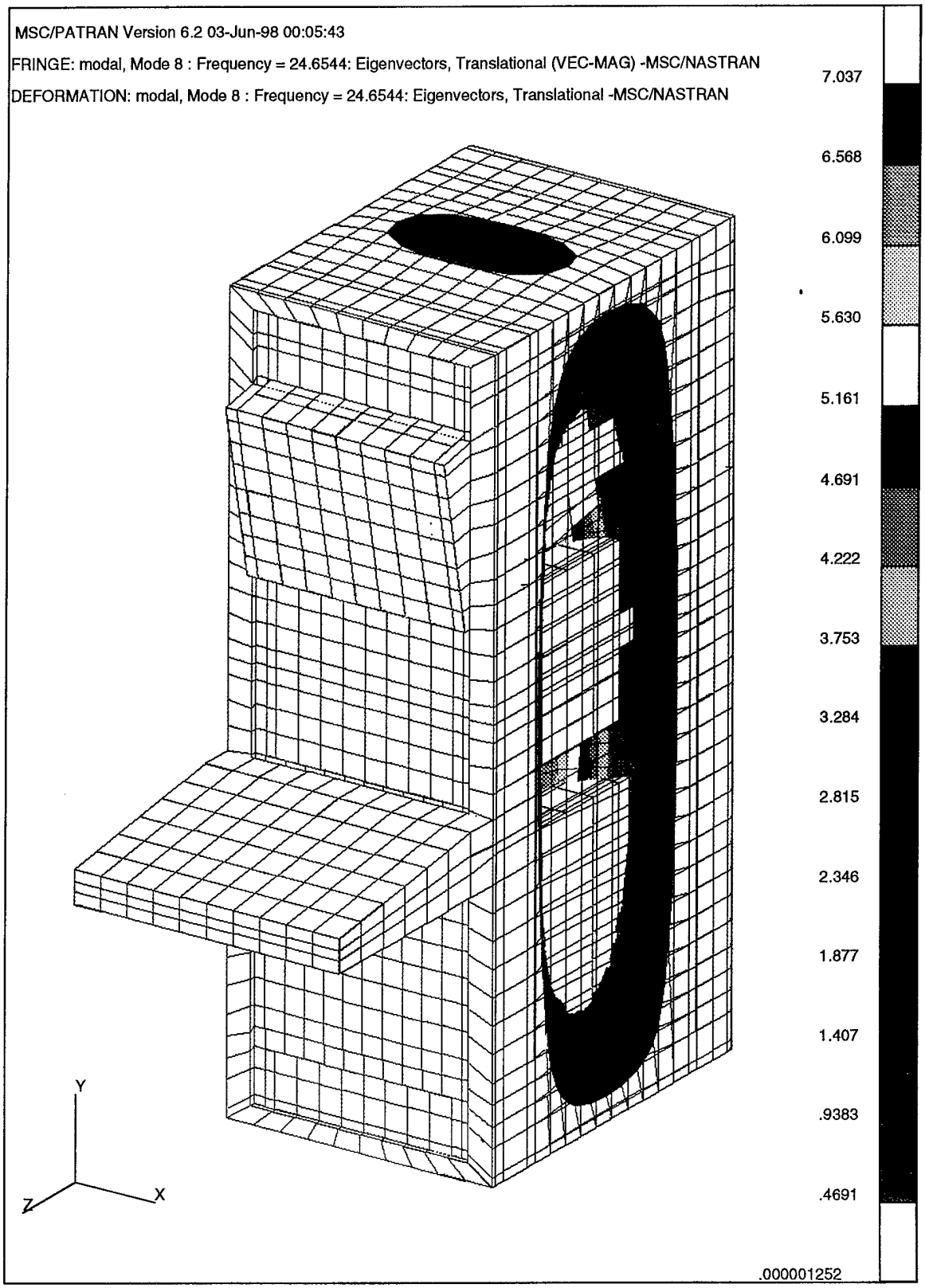

Figure 23: Dual Monitor Variant, Mode 8, 24.65 Hz.

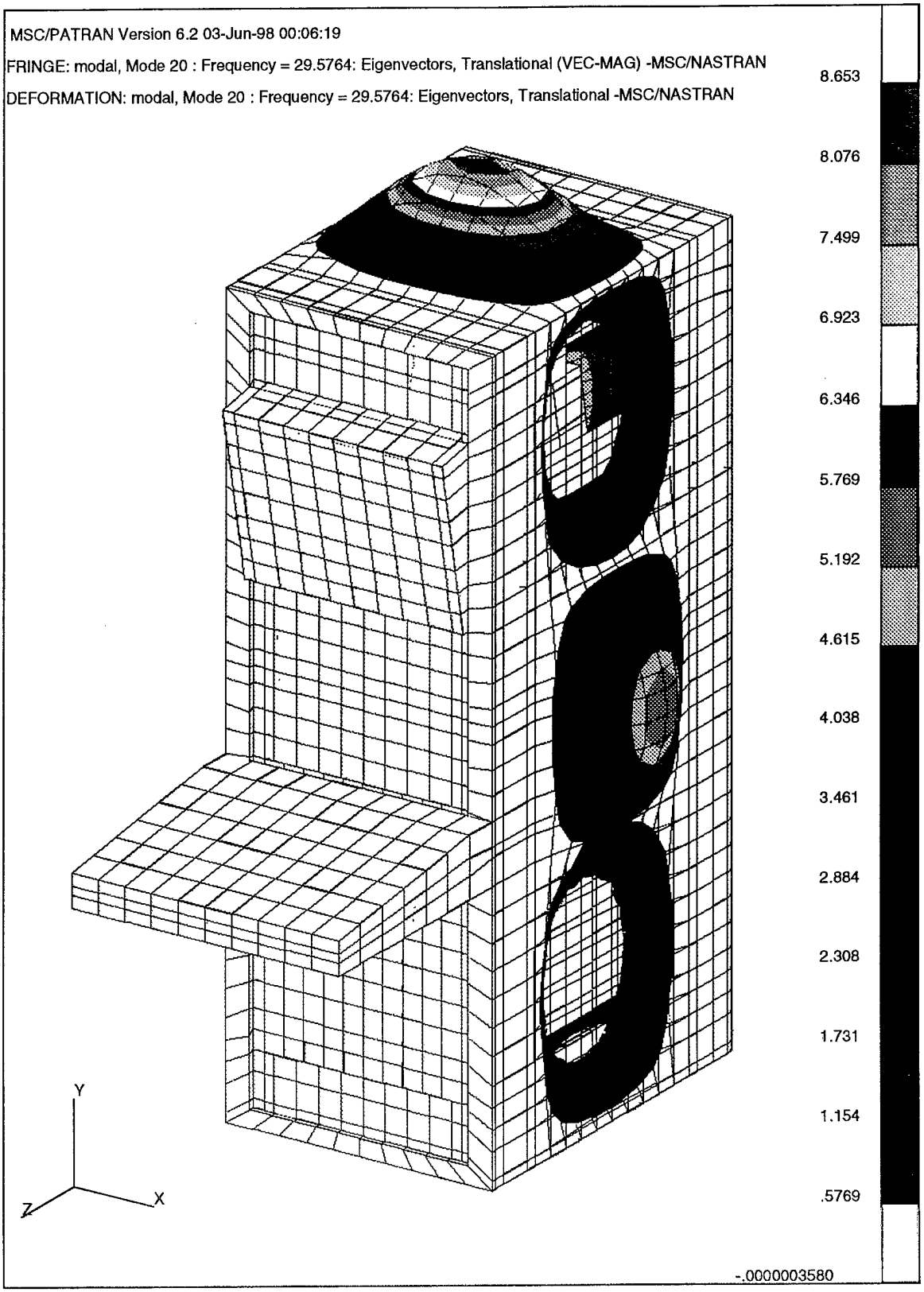

Figure 24: Dual Monitor Variant, Mode 20, 29.58 Hz.

V. TRANSIENT RESPONSE ANALYSIS

Two separate analyses of each model were performed. The first analysis used an idealized input which represents a generic shock pulse designed to get the feel of each rack variant's response. This consisted of a 40G, 2msec half sine wave shock pulse. The second analysis used an actual shock input acceleration obtained from a barge test performed for human response trials.

All transient responses were obtained using MSC/NASTRAN (Version 69) finite element structural code, employing the Modal Transient Response Analysis method (incorporated with the Large Mass Method). The following results show to varying degrees how well the rack system mitigates the shock acceleration of the various portions of the rack. Throughout the discussion it is important to note that in the case of both shock inputs, the results were purposely guided towards theoretical conservatism (worst possible case). Each type of shock input will be described separately as it applies to each rack type, the single and dual monitor variants. Refer to Figure 25 for the location of the nodes for the single monitor variant and to Figure 26 for the dual monitor variant. Table 2 lists the analogous nodes between the two rack variants for comparisons between variant responses.

A. HALFSINE BASE EXCITATION

Figure 27 is a plot of the shock input used for this analysis. All responses were calculated out to 1 second to ensure that the peak responses were captured. The modal cutoff frequency used for these analyses is 200Hz. This ensures that enough mode shapes are used in the solution to maintain mathematical accuracy. The solution time step used for these analyses is 1.25e-4 seconds. This balances the desire for high accuracy with the limitation of computer resources, ensuring that the input acceleration characteristics are captured. All calculations using this input use 2 percent modal damping.

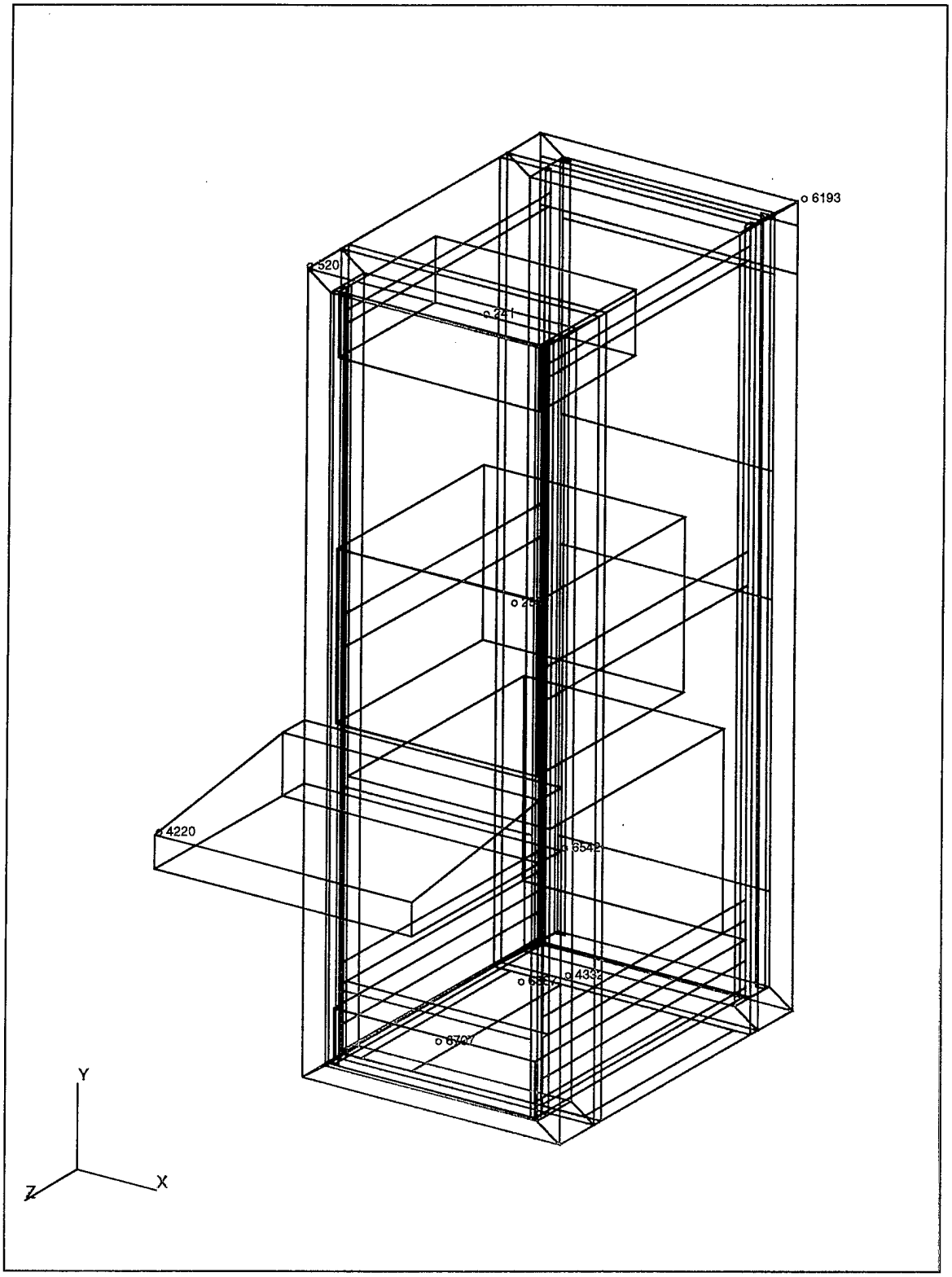

Figure 25: Locations of Nodes in the Single Monitor Rack Variant used for the Transient Analysis.

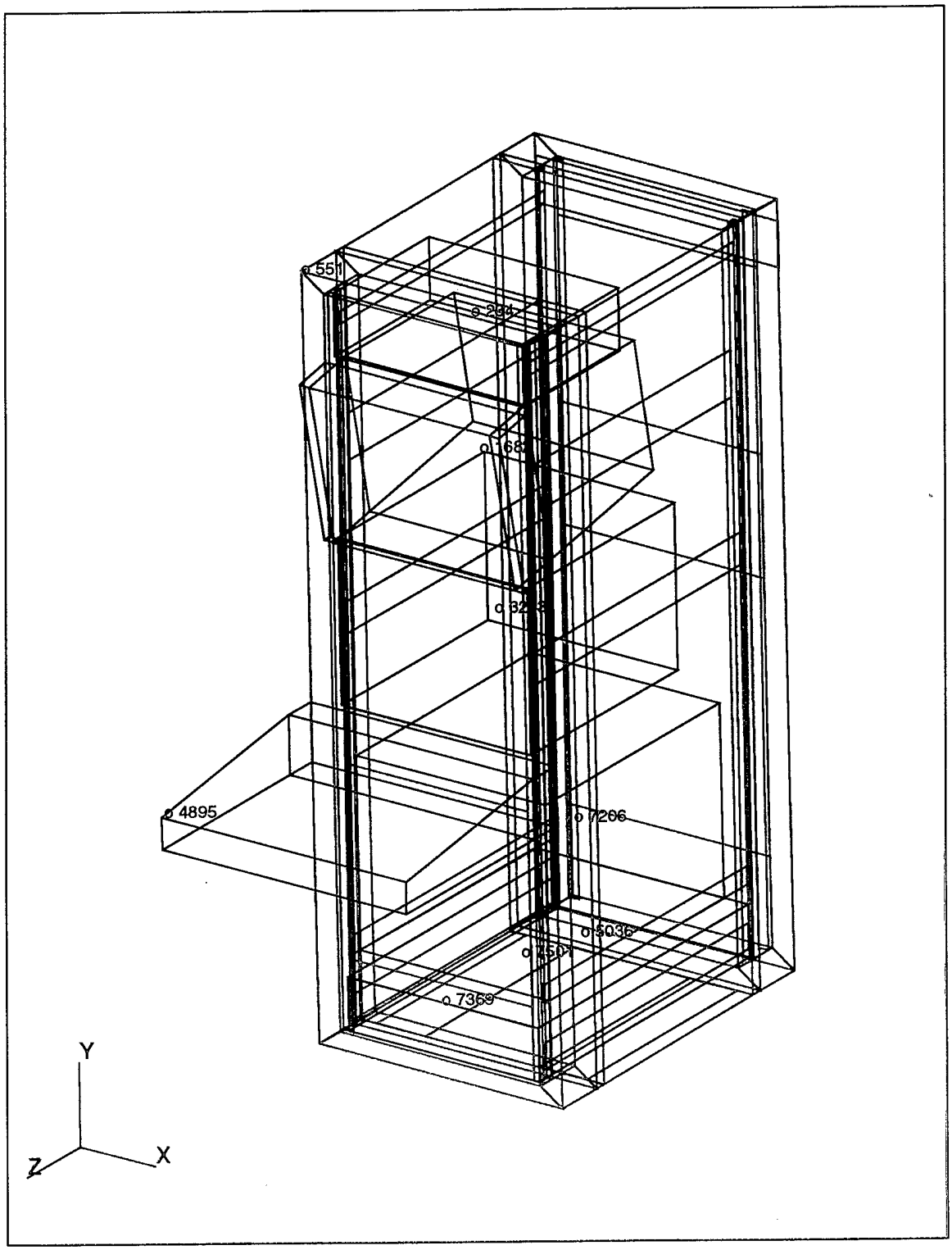

Figure 26: Locations of Nodes in the Dual Monitor Rack Variant used for the Transient Analysis.

	SINGLE MONITOR	DUAL MONITOR
Front Left Bottom Mount (accl)	6707	7369
Rear Left Bottom Mount (accl)	6887	7501
Power Supply	4332	5036
Power Distribution Unit	241	234
Lower Monitor	2531	3233
Upper Monitor	N/A	1682
Central Processing Unit	6542	7206
Bullnose Tip	4220	4895
Front Top Left Cabinet Corner	520	551
Front Left Bottom Mount (disp)	6846	7515
Rear Right Bottom Mount (disp)	6850	7514

Table 2: Analogous Node Locations Between Rack Variants

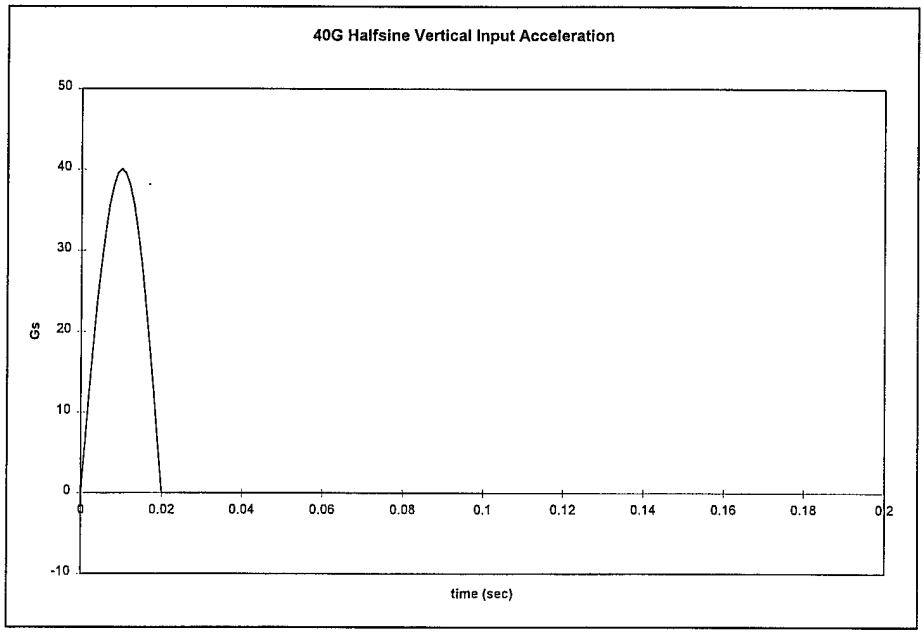

Figure 27: 40G, 2msec Halfsine Shock Base Excitation in the Vertical (Y) Direction.

1. Single Monitor Variant (CLIN 0003AA)

Figures 28 and 29 show the acceleration response transmitted through the top of the base shock mounts with Figure 28 being the front-bottom mount (NODE 6707) and Figure 29 the rear-bottom mount (NODE 6887). For both of these figures, the initial shock input pulse is mitigated somewhat (by approximately 5 Gs), and is then rapidly damped down (with a ring-down effect) to approximately 3G peaks at each node location. This shows that the mounts, are mildly effective for impulse type loads.

The rack system is designed to mitigate shock to the electronic components. Figures 30 through 33 are the acceleration time responses for representative nodes in each of electronic component mounted within the rack, corresponding to the Power Supply, Power Distribution Unit, Monitor, and Central Processing Unit respectively. For all of these components the peak shock value is mitigated by about four or more Gs. Although the peak value is still around 35 G's for each component, this equates to almost a 12% reduction from the input peak. Also as in the case of the mounts, the shock value is quickly mitigated to 2G peaks. Figure 34 shows the acceleration response of NODE 4220 at the tip of the bullnose. Note that the peak value here is the same as the input shock, indicating no mitigation at all. This is because the location of this node is extended out from the system's center of gravity, acting as a cantilever. This node was chosen to represent the largest response in the bullnose. As in the other electronic components, the shock is quickly mitigated down, however these peaks are slightly higher at 3Gs due to this cantilever effect.

Figure 35 shows the acceleration response of the upper-left front corner of the rack. This node was chosen to represent how the cabinet itself responds to the shock loading. The peak response for NODE 520 is mitigated by approximately 4 G's and quickly is mitigated down to 2G peaks as discussed before.

The next major area of concern with the rack is to determine if the shock mounts themselves will exceed design limits or bottom out. Figure 36 shows the magnitude of the displacement response of the front-bottom mount (NODE 6846), while Figure 37

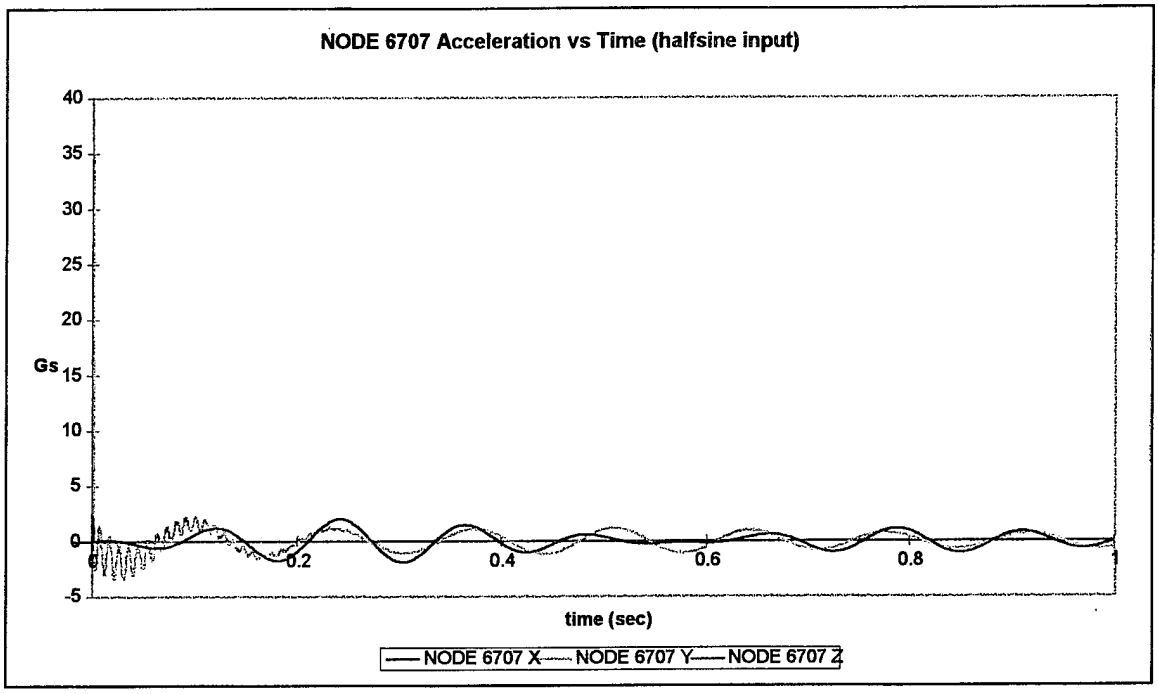

Figure 28: Acceleration Response to Halfsine Input of NODE 6707 (Top of Front Left Bottom Isolation Mount).

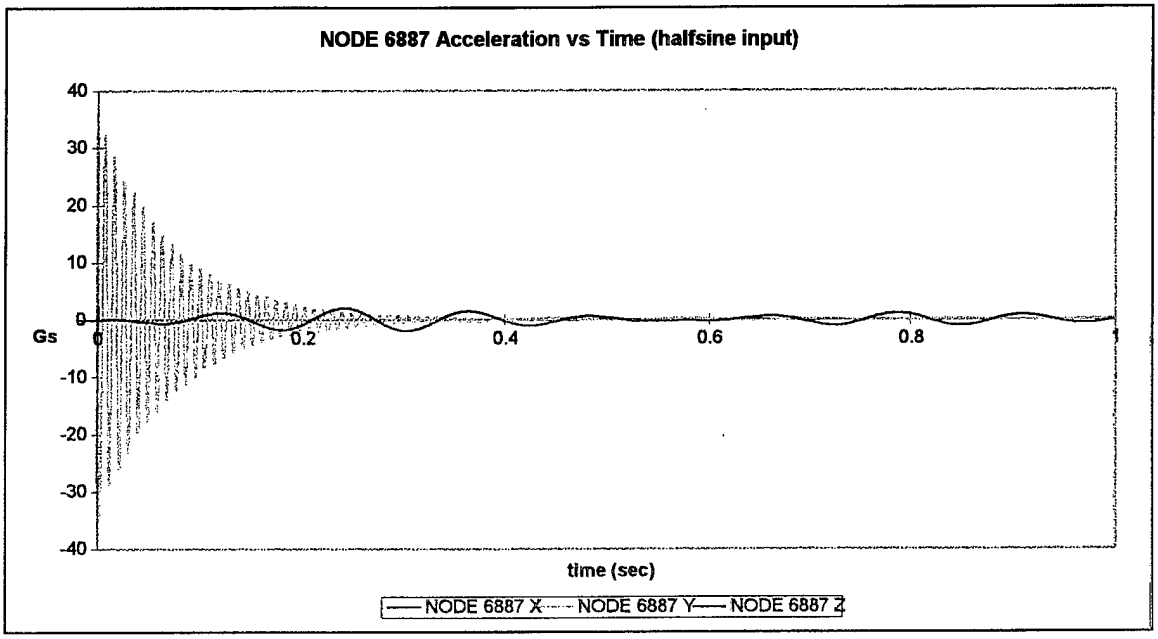

Figure 29: Acceleration Response to Halfsine Input of NODE 6887 (Top of Rear Left Bottom Isolation Mount).

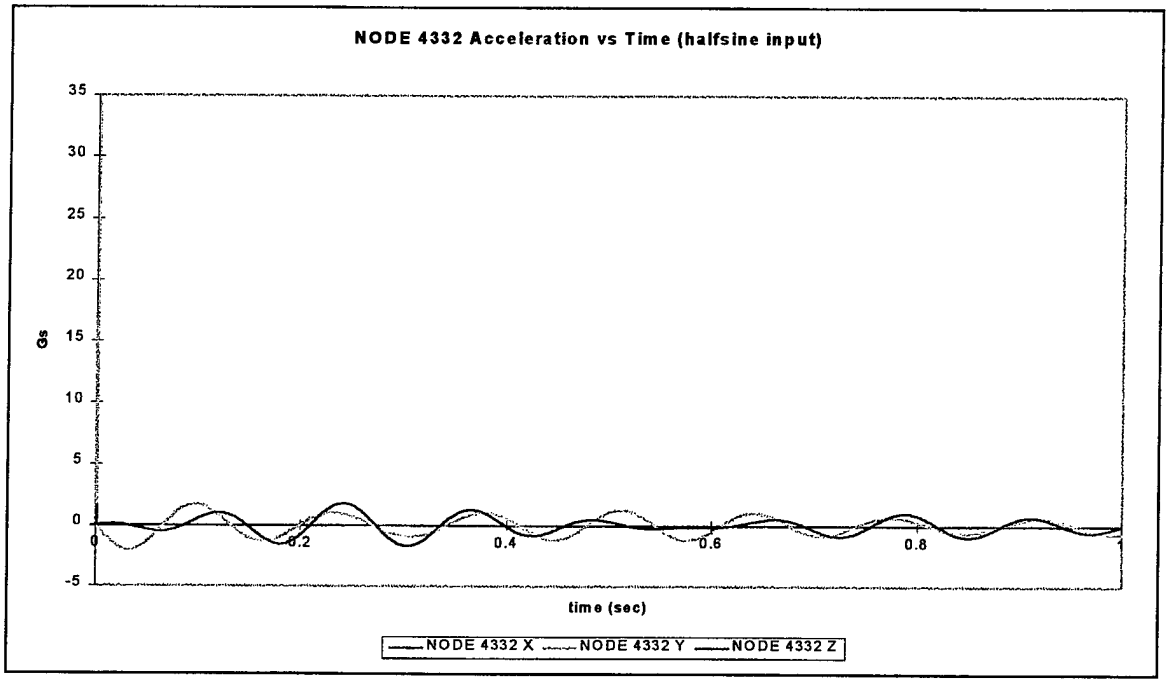

Figure 30: Acceleration Response to Halfsine Input of NODE 4332 (Power Supply).

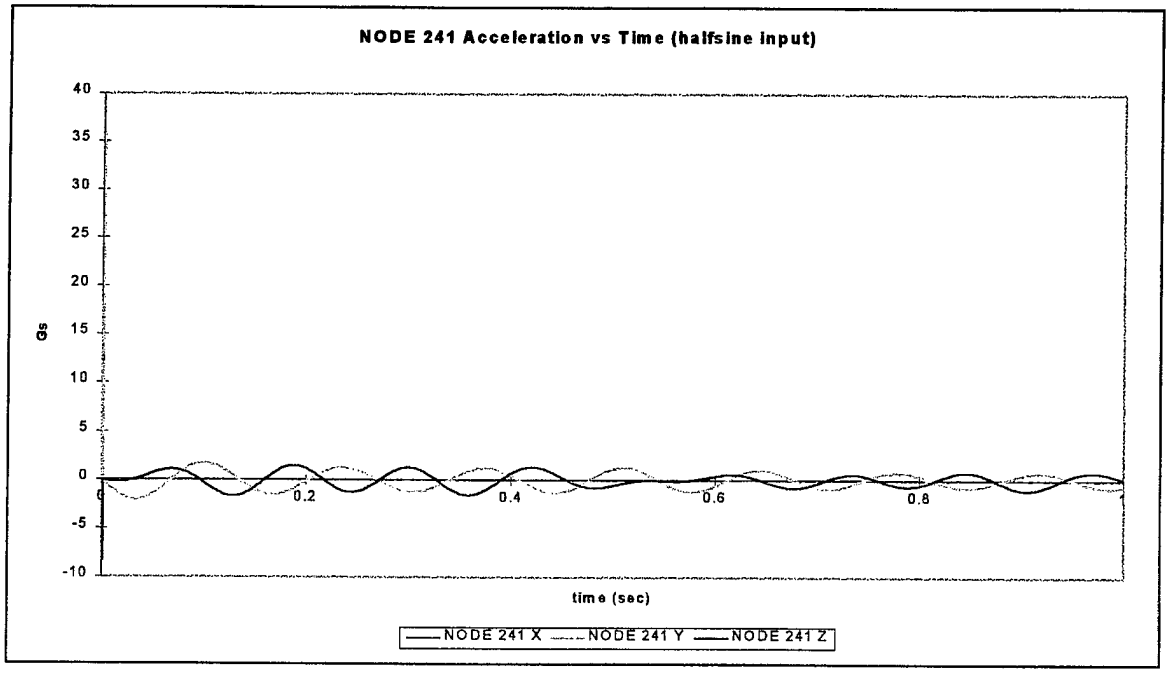

Figure 31: Acceleration Response to Halfsine Input of NODE 241 (Power Distribution Unit).

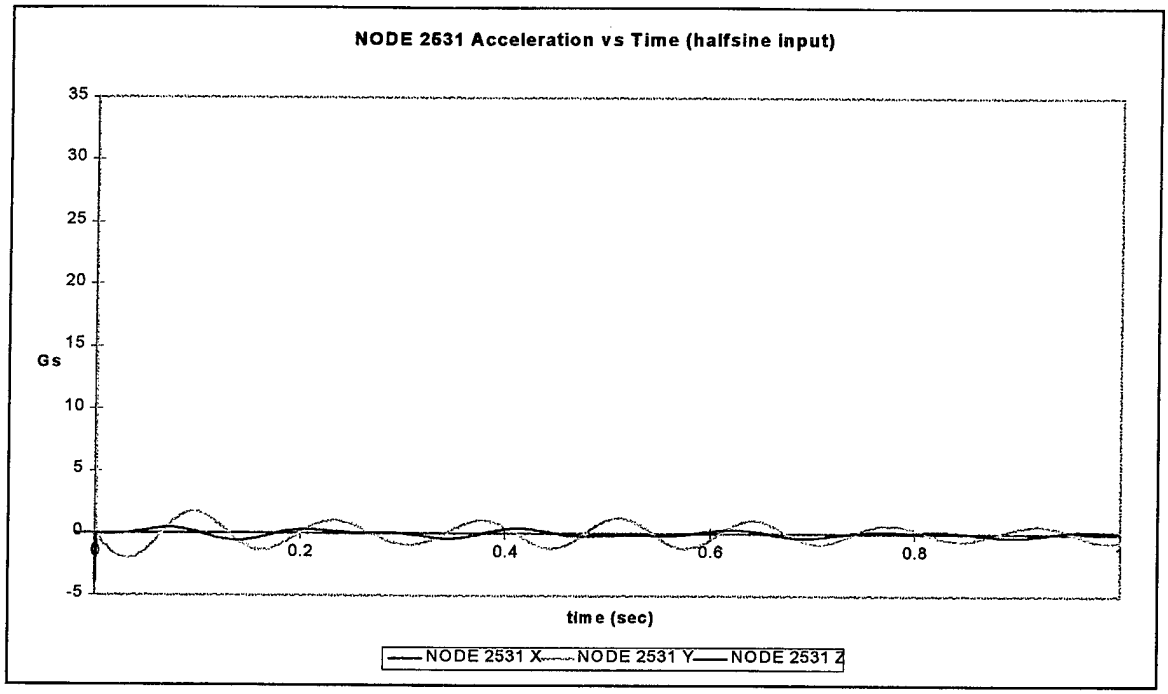

Figure 32: Acceleration Response to Halfsine Input of NODE 2531 (Monitor).

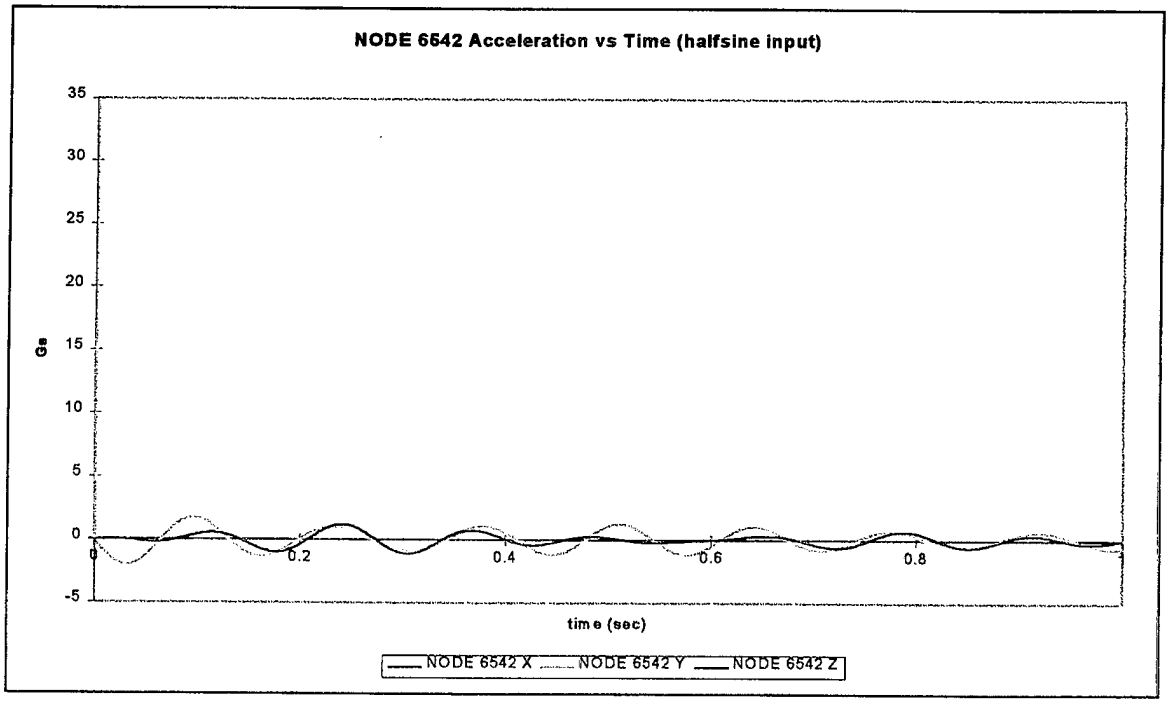

Figure 33: Acceleration Response to Halfsine Input of NODE 6542 (Central Processing Unit).

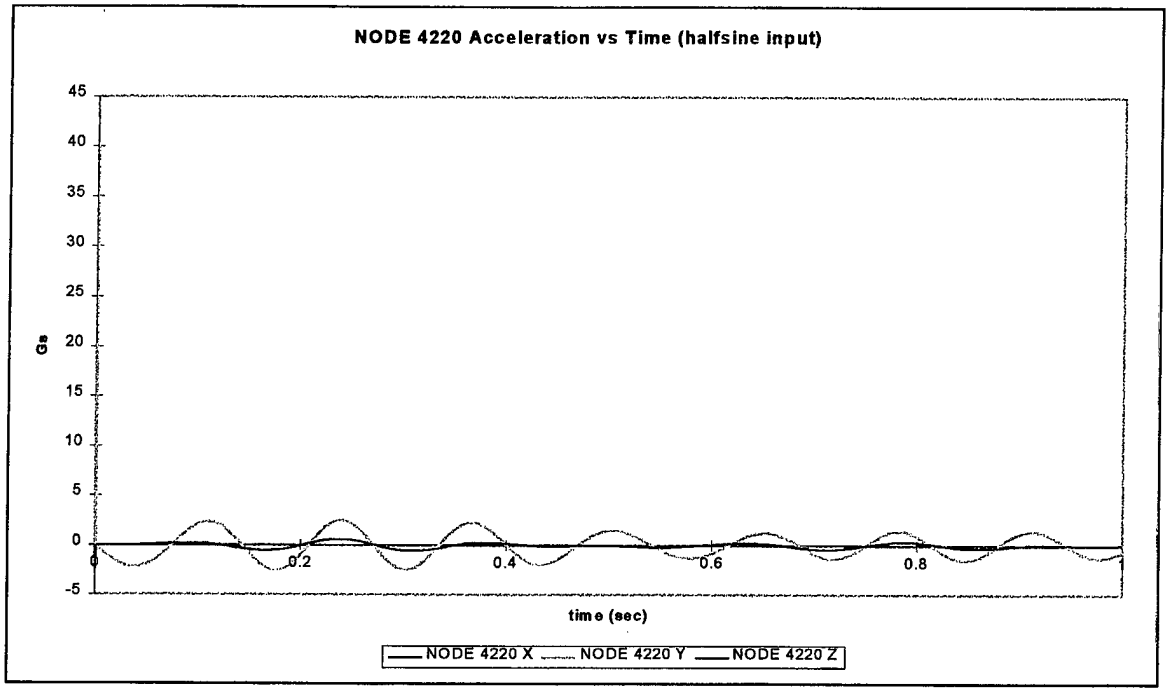

Figure 34: Acceleration Response to Halfsine Input of NODE 4220 (Bullnose Tip).

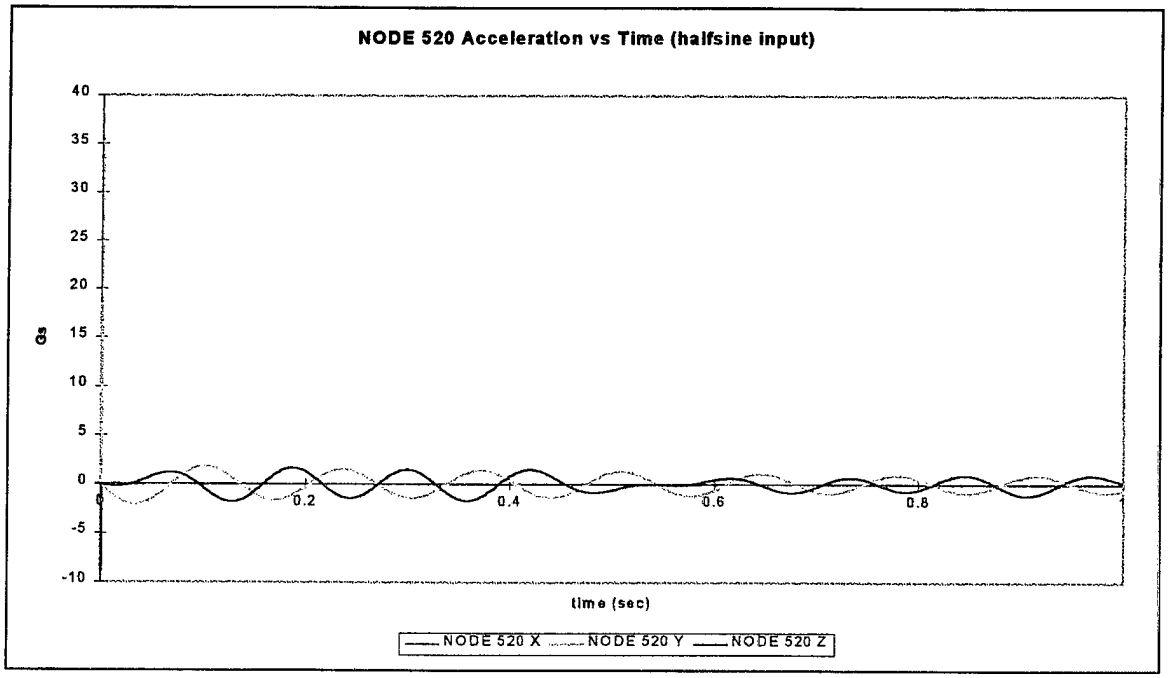

Figure 35: Acceleration Response to Halfsine Input of NODE 520 (Top Front Left Cabinet Corner).

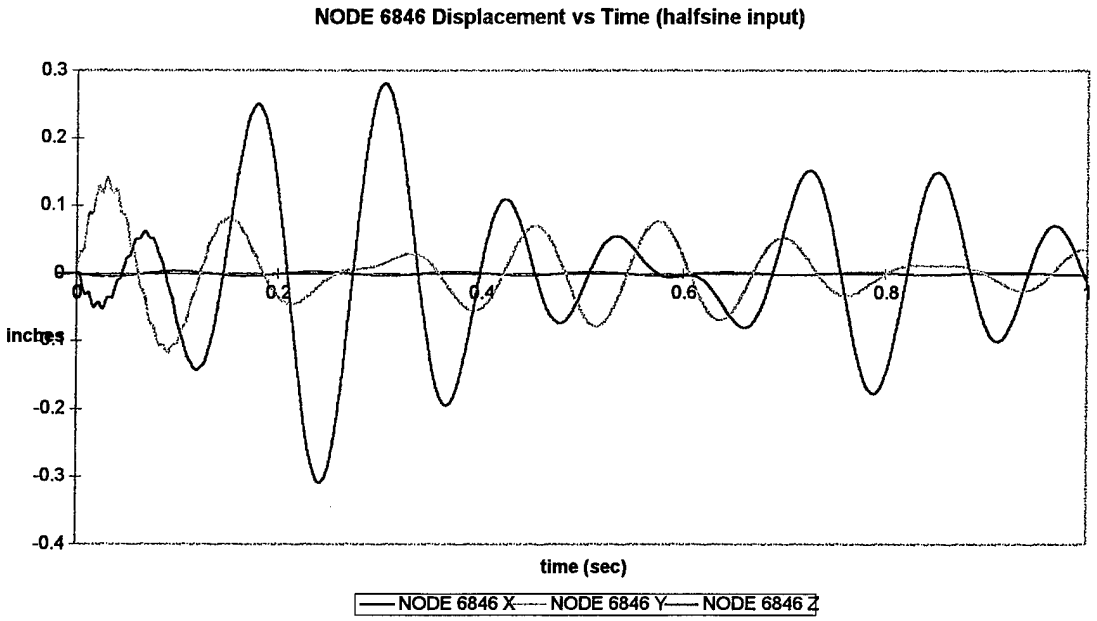

Figure 36: Displacement Response to Halfsine Input of NODE 6846 (Bottom Left Front Mount).

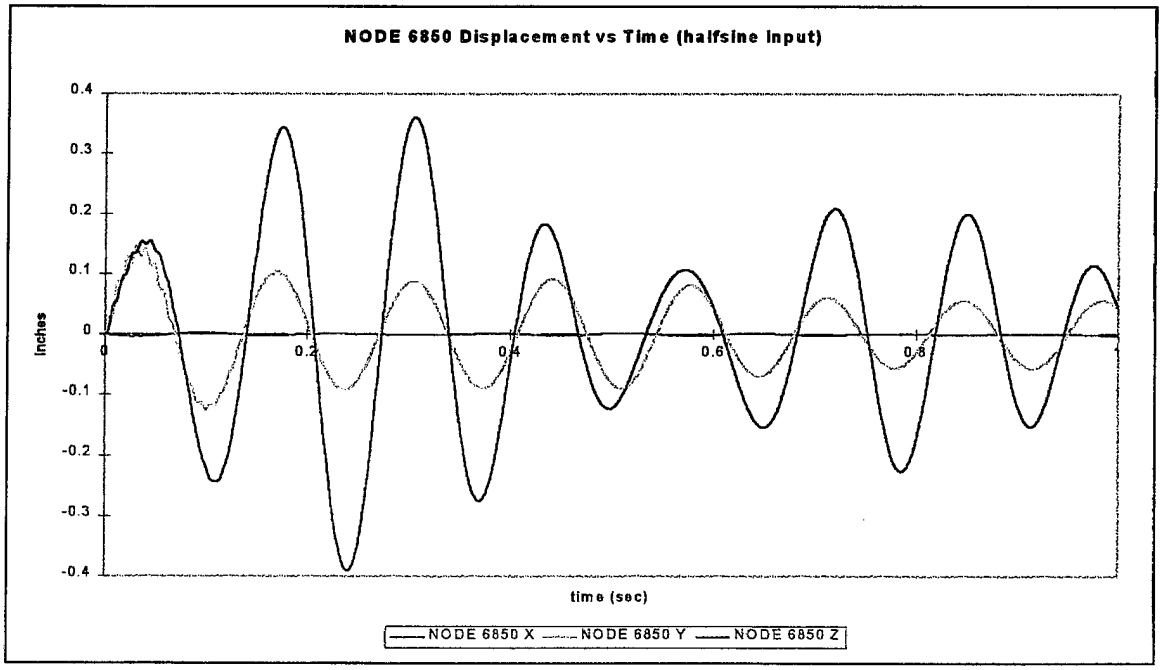

Figure 37: Displacement Response to Halfsine Input of NODE 6850 (Bottom Left Rear Mount).

shows the same for the rear-bottom mount (NODE 6850). All displacements are well within design limitations (2 to 3 inches depending on axis direction), with no bottoming out of the mount either (nominally 3.5 inches). Of concern, however, is the Z Displacement (front/rear direction) whose considerable motion with respect to the other directions indicates a significant transference of energy from the Y to the Z direction.

2. Dual Monitor Variant (CLIN 0001AA)

Many of the general response characteristics for this rack variant are similar to those of the single monitor variant. Figures 38 and 39 show the transmitted acceleration responses for NODES 7369 and 7501, respectively (bottom left mounts). As with the single monitor variant, the initial input pulse is mitigated somewhat to less than 35 Gs with a rapid decrease to 2.5G peaks. Again a ring-down effect is present at these locations.

Figures 40 through 44 are the acceleration time responses for representative nodes within each electronic component mounted within the rack, corresponding to the Power Supply, Power Distribution Unit, Lower Monitor, Upper Monitor, and Central Processing Unit respectively. For all of these components, the initial peak shock level is mitigated by 4 to 5 Gs, which is a minimum of a 10% reduction in peak acceleration. In all of these cases, the acceleration is quickly mitigated down to approximately 2G peaks. Figure 45 shows the acceleration response for NODE 4895 at the tip of the bullnose. As in the case of the single monitor variant, the peak value is the same as the input response. This is again probably due to the cantilever effect previously mentioned. Here, the shock is quickly mitigated to about 3Gs.

The acceleration response of NODE 551 is shown in Figure 46. This generically shows how the cabinet itself responds to the shock input. Here the peak shock is mitigated by about 3Gs and quickly lowers to about a 2G free response.

Finally, the mount displacement time responses are shown in Figures 47 and 48. The front left bottom mount (NODE 7515) and the rear left bottom mount (NODE 7514)

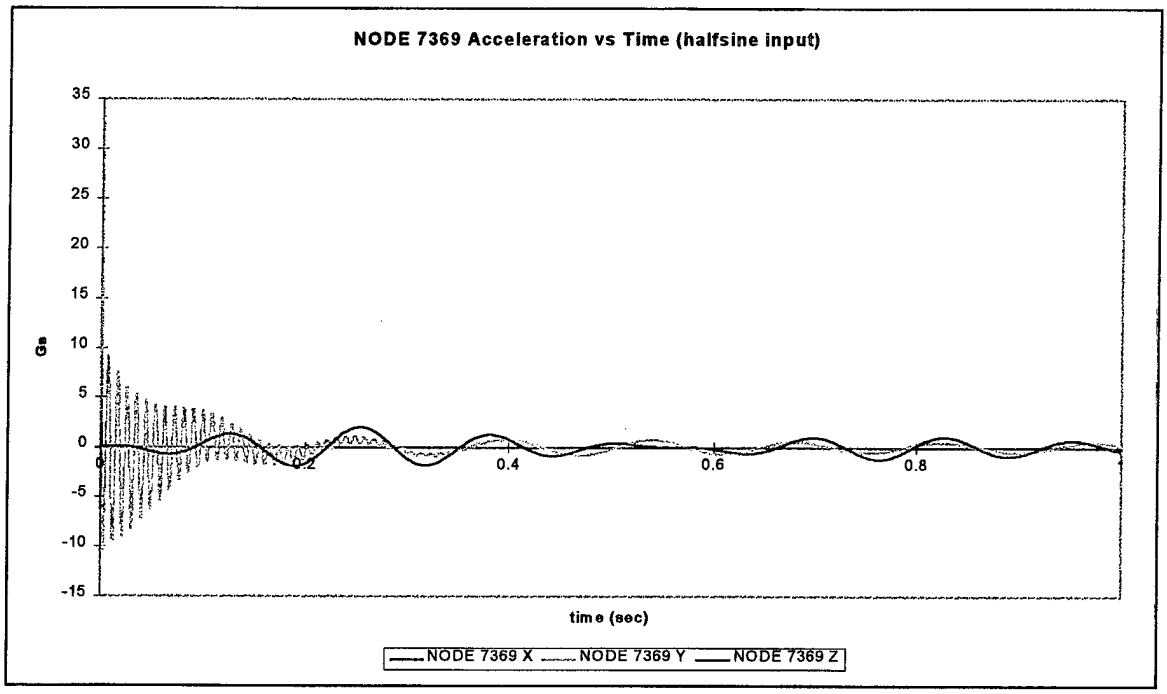

Figure 38: Acceleration Response to Halfsine Input of NODE 7369 (Top of Front Left Bottom Isolation Mount).

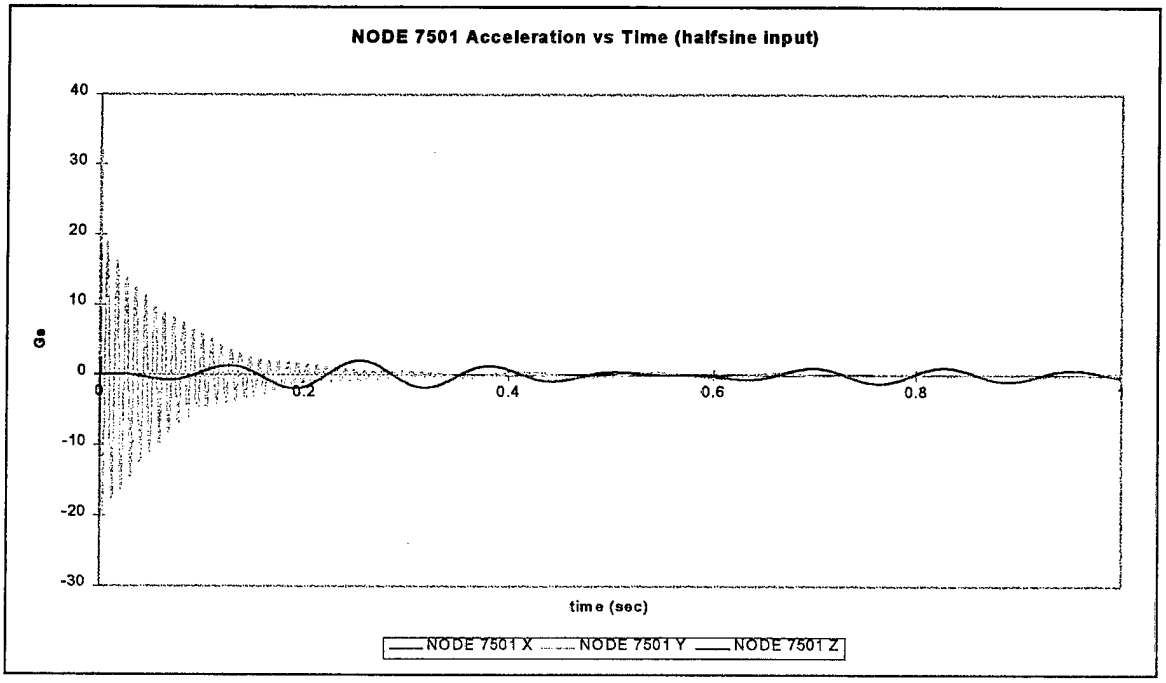

Figure 39: Acceleration Response to Halfsine Input of NODE 7501 (Top of Rear Left Bottom Isolation Mount).

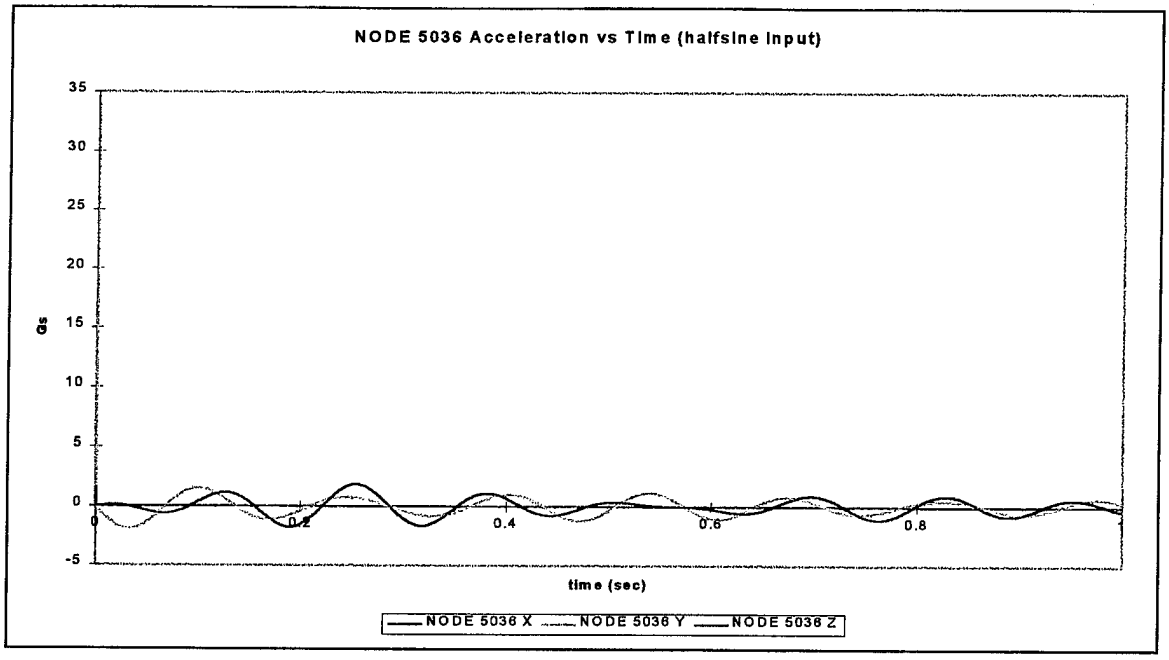

Figure 40: Acceleration Response to Halfsine Input of NODE 5036 (Power Supply).

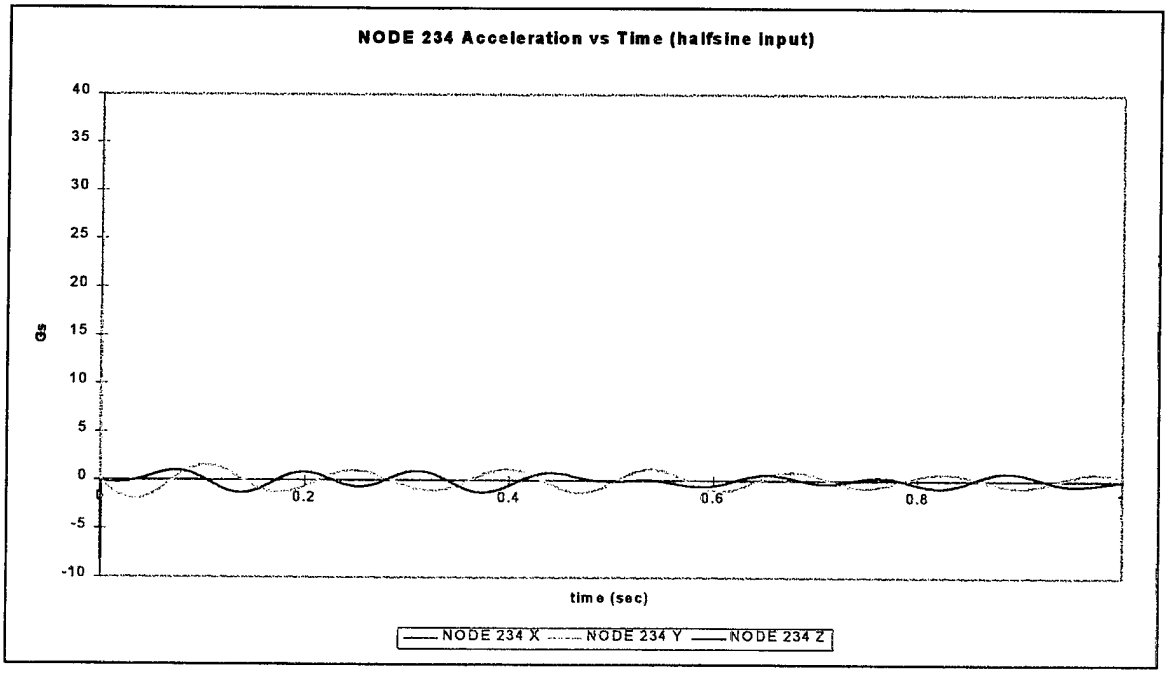

Figure 41: Acceleration Response to Halfsine Input of NODE 234 (Power Distribution Unit).

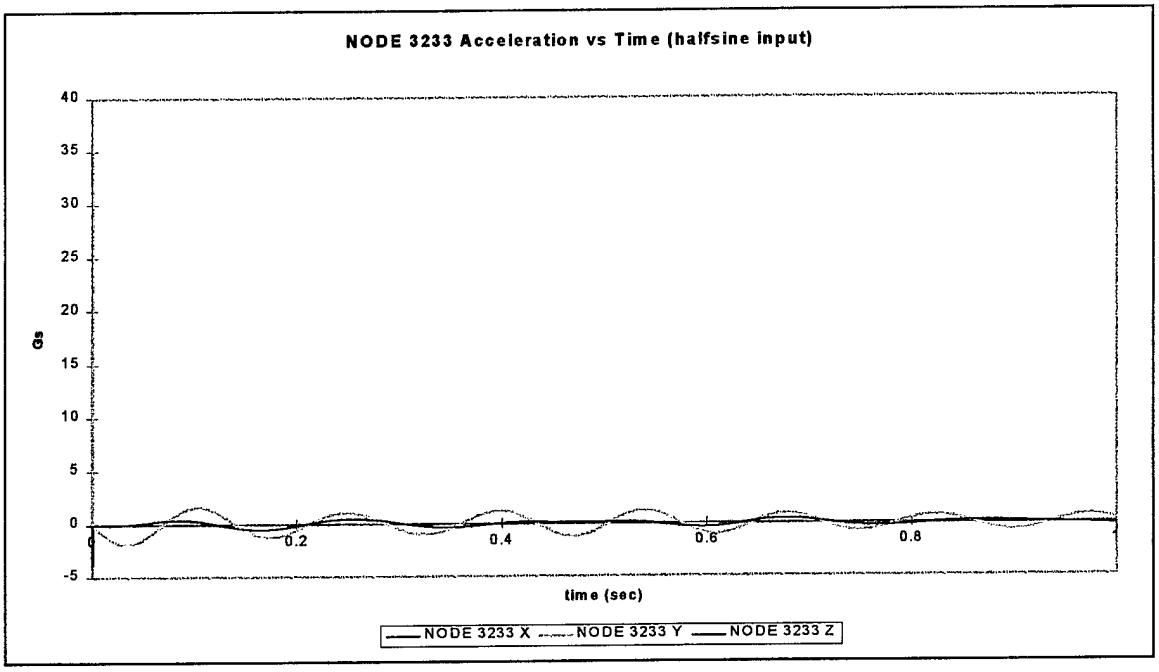

Figure 42: Acceleration Response to Halfsine Input of NODE 3233 (Lower Monitor)

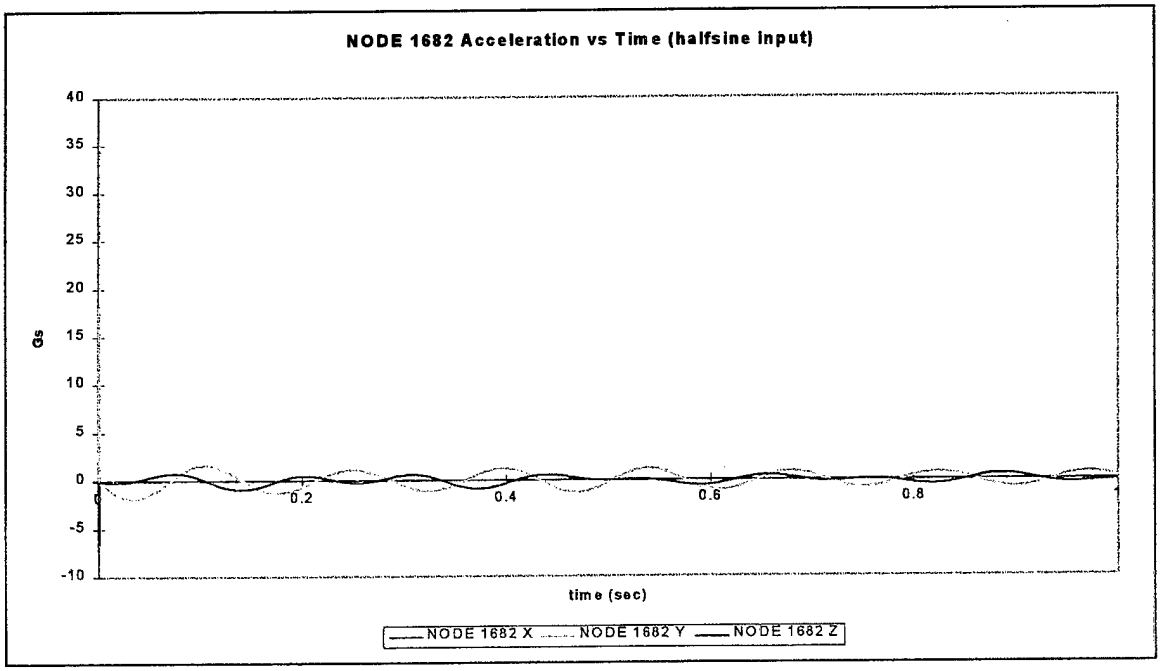

Figure 43: Acceleration Response to Halfsine Input of NODE 1682 (Upper Monitor)

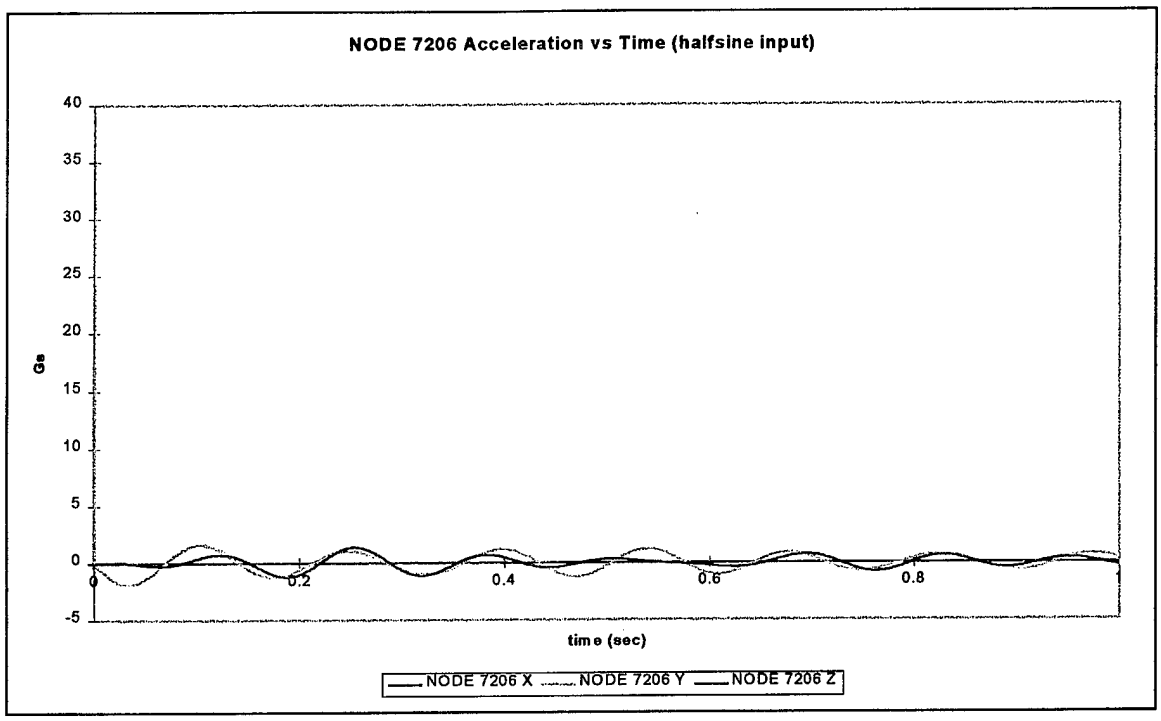

Figure 44: Acceleration Response to Halfsine Input of NODE 7206 (Central Processing Unit).

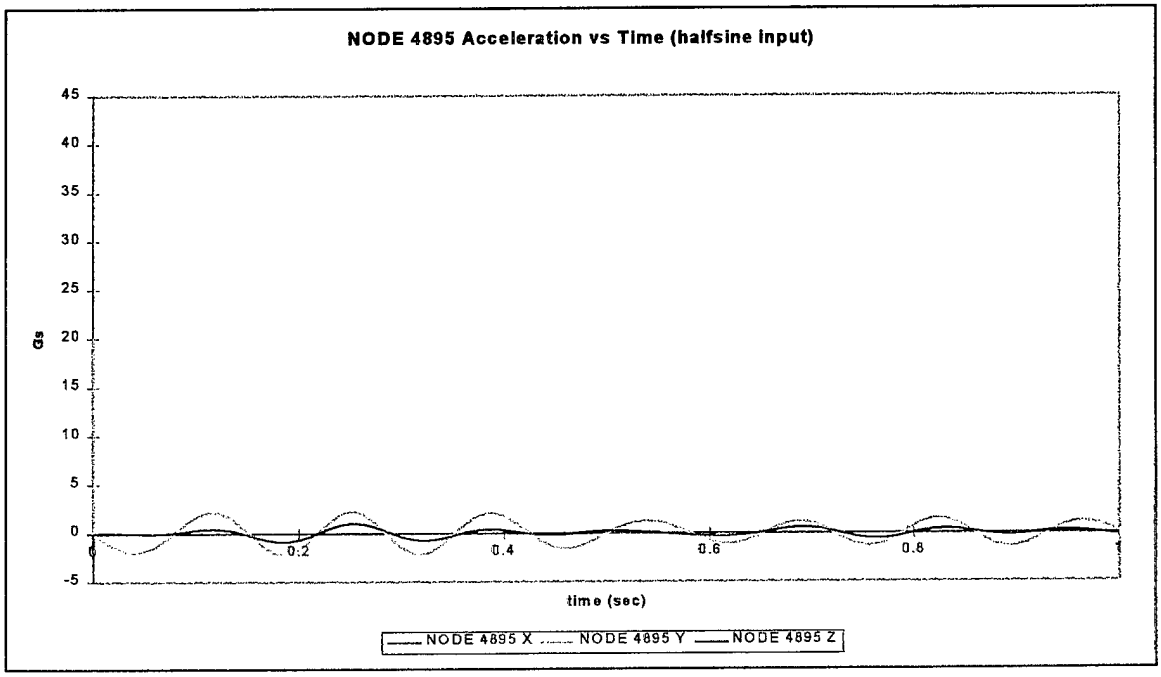

Figure 45: Acceleration Response to Halfsine Input of NODE 4895 (Bullnose Tip).

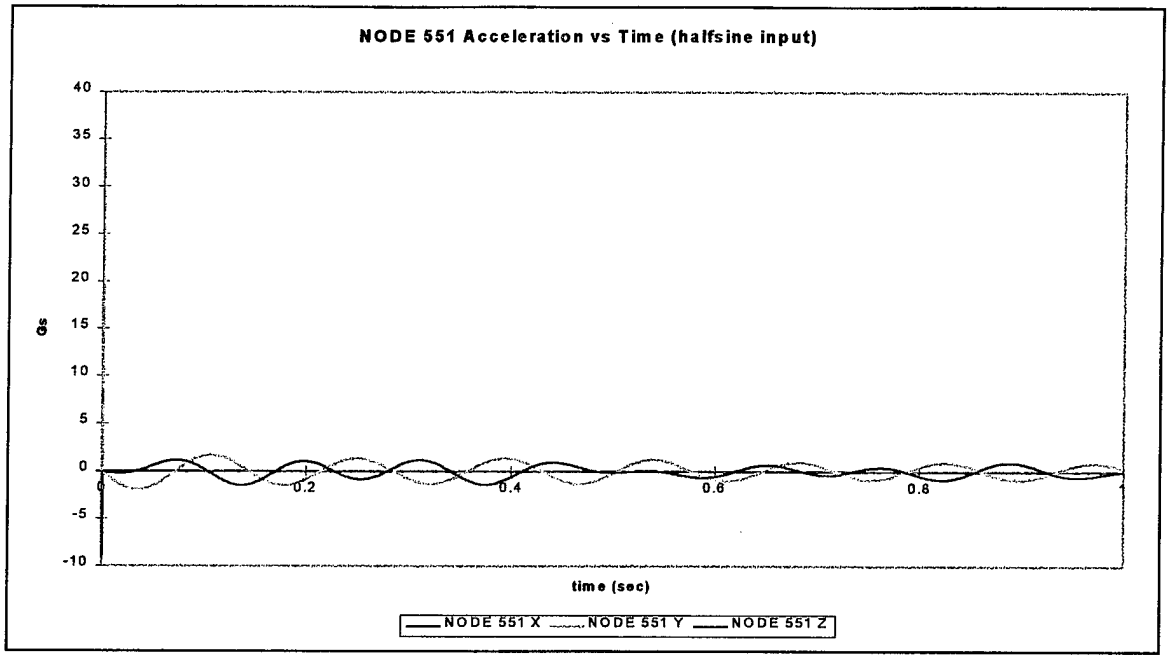

Figure 46: Acceleration Response to Halfsine Input of NODE 551 (Top Front Left Cabinet Corner).

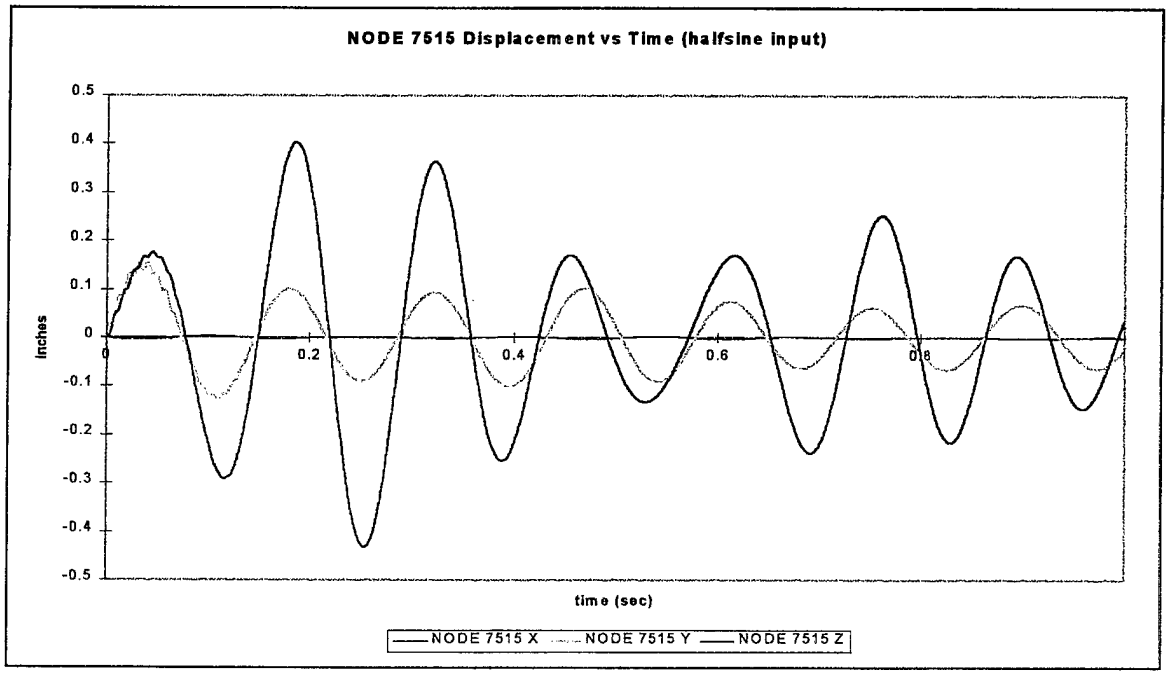

Figure 47: Displacement Response to Halfsine Input of NODE 7515 (Bottom Left Front Mount).

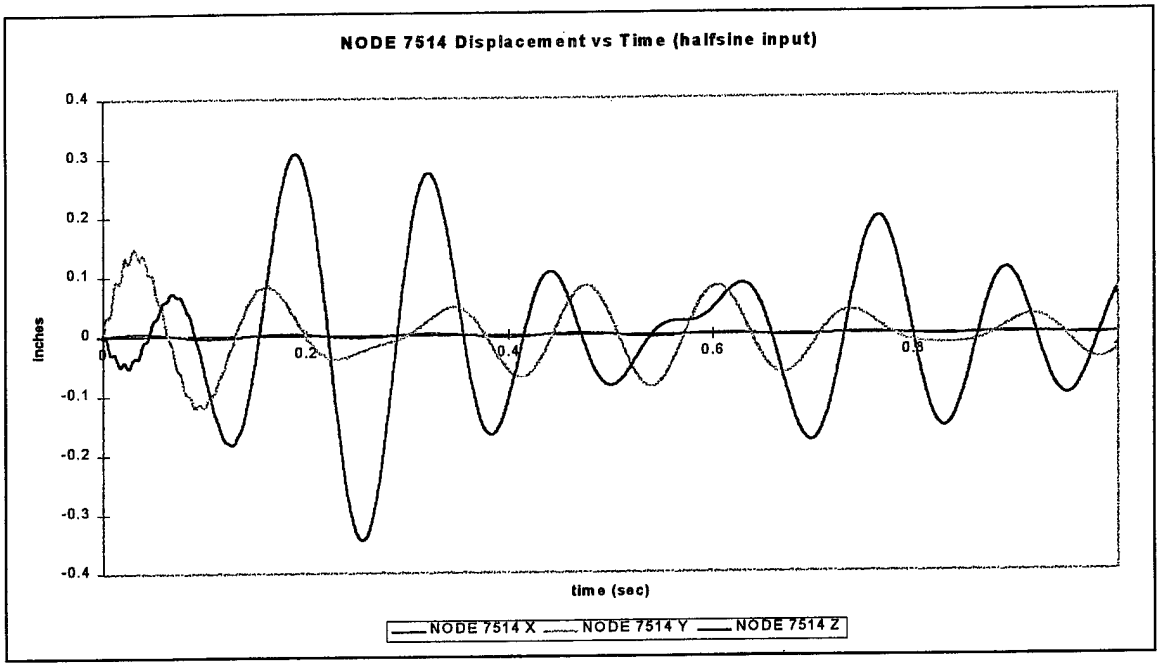

Figure 48: Displacement Response to Halfsine Input of NODE 7515 (Bottom Left Front Mount).

B. REPRESENTATIVE BARGE TEST SHOCK INPUT

Figure 49 shows the shock input time history in both the vertical and horizontal (fore/aft) directions from the human shock response test data [Reference 9]. For this analysis case, responses were calculated out to two seconds because this was the available length of time history for the shock input. The modal cutoff frequency is 200Hz, again to ensure solution accuracy, and the solution time step is .002 seconds in order to maximize computer resource management. This input is significantly different from the previous one because shock energy is added to the rack system over the entire two second time period, corresponding to a sustained shock loading. All calculations using this shock input used 2 percent modal damping.

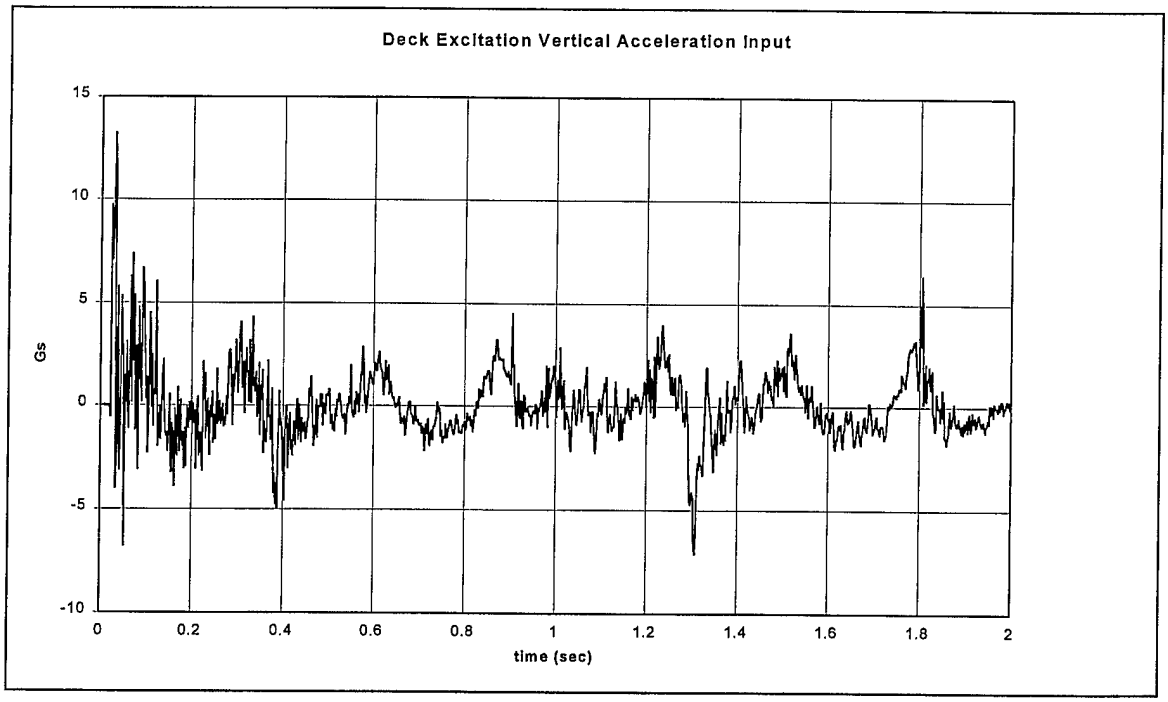

(a)

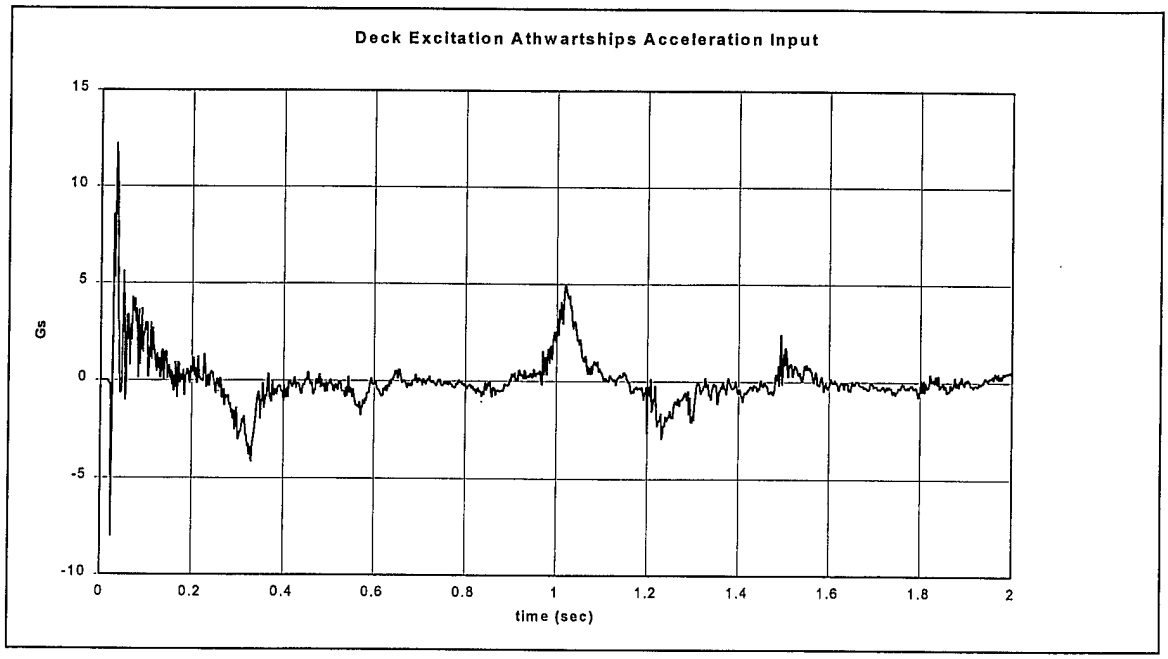

(b)

Figure 49: Sample Barge Test Base Acceleration Input. a) Vertical (Y) Direction b) Athwartships (Z) Direction.

1. Single Monitor Variant (CLIN 0003AA)

Figures 50 and 51 show the acceleration at the tops of the left, bottom mounts, NODES 6707 and 6887 respectively. Note the rather violent motion of the rear mount, Figure 51. Here the peak amplitude (28Gs) in the time history is much higher than the input acceleration peak, indicating a reinforcing of the motion over time. The forward mount, Figure 50, however does not exhibit this reinforced amplitude.

Figures 52 through 55 show the acceleration response time histories for representative nodes for the electronic components mounted with the cabinet, corresponding to the Power Supply, Power Distribution Unit, Monitor, and Central Processing Unit respectively. Figure 56 shows the acceleration response of the tip of the bullnose. The response amplitudes for all of these electronic components generally increase over the entire time history once past the initial peak acceleration. This is due to two factors. The first is due to the addition of shock energy throughout the entire analysis time period instead of an impulsive energy input. The other is simply the compounding of the inertial response of the system. As with the 40G, 2msec Halfsine input case, the bullnose values are higher than the internally mounted components due to the cantilevered position of the bullnose.

Next, Figures 57 shows the acceleration response of the upper left corner of the cabinet (NODE 520). As with the electronic components, the response amplitudes increase throughout the analysis time period due to the previously discussed reasons. Note that the maximum values here are generally, slightly larger than those seen in the electronic components themselves, indicating that the rack is mitigating the shock transmitted to the electronic components somewhat.

Figures 58 and 59 show the displacement time histories of the front left bottom mount and the rear left bottom mounts (NODES 6846 and 6850, respectively). The large transference of energy from the Y to the Z direction, evident in the Halfsine Input, are also evident here to a higher degree. The Z direction deflections (athwartships) are more than twice the Y direction deflections (vertical). Although the mounts did not exceed

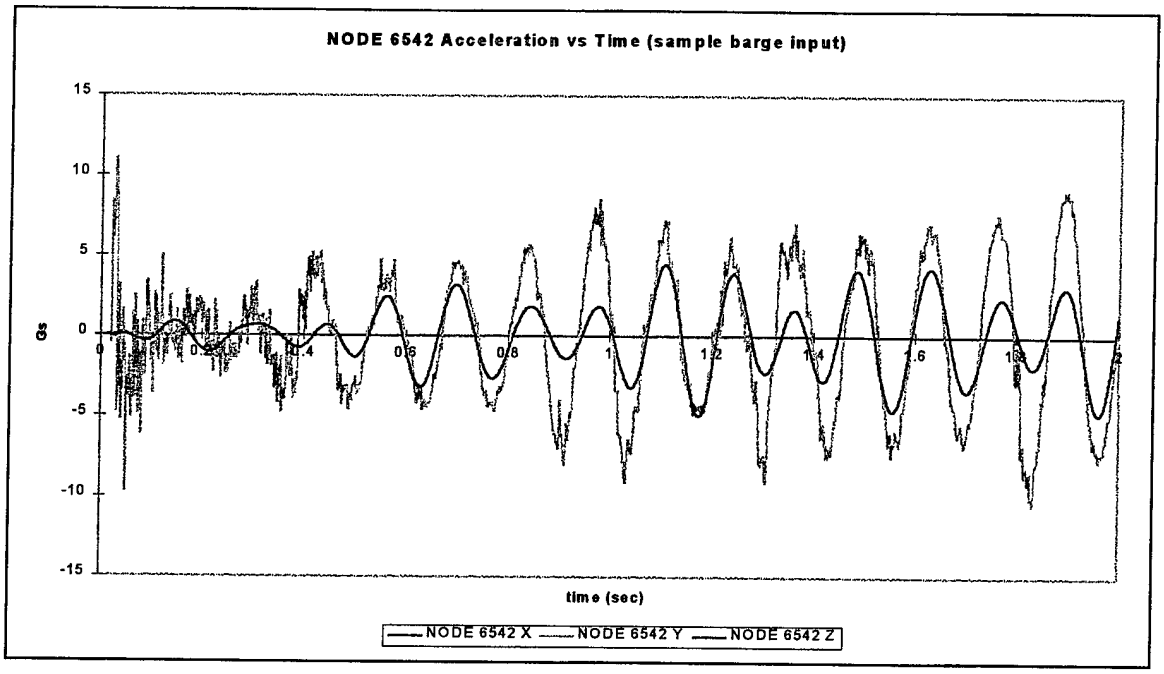

Figure 50: Acceleration Response to Sample Barge Test Input of NODE 6707 (Top of Front Left Bottom Isolation Mount).

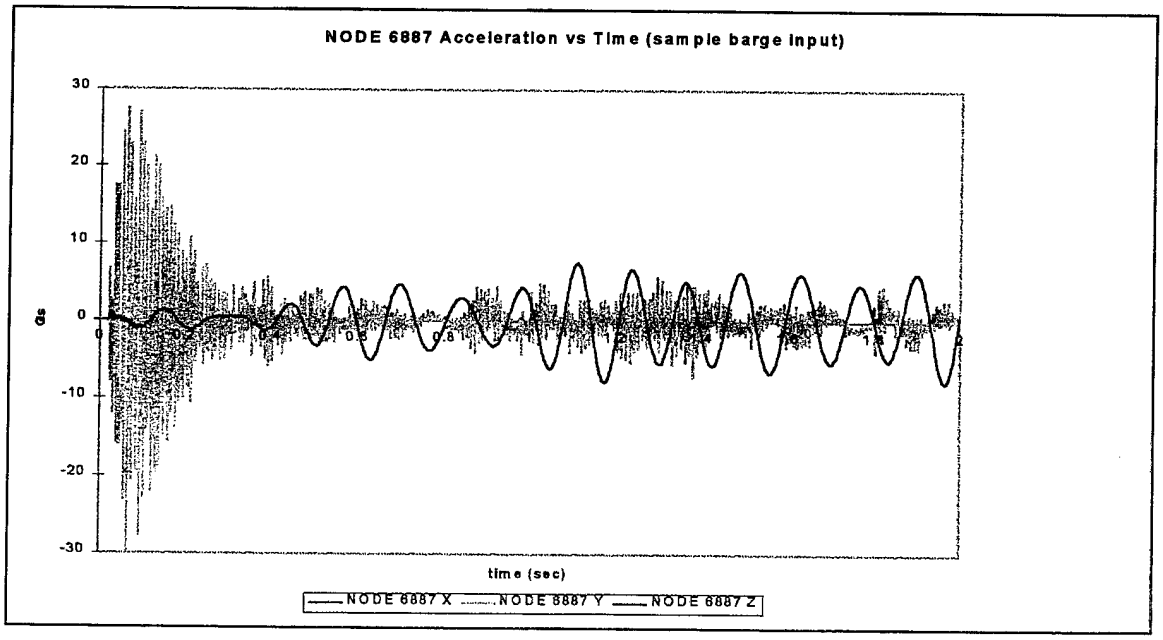

Figure 51: Acceleration Response to Sample Barge Test Input of NODE 6887 (Top of Rear Left Bottom Isolation Mount).

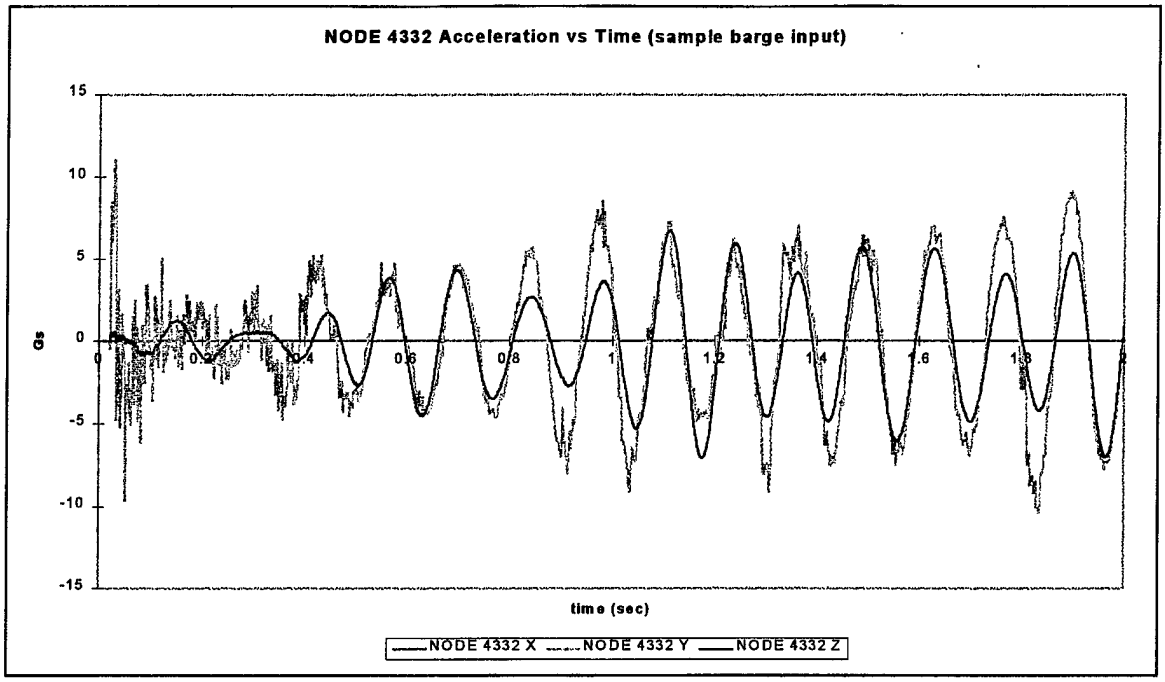

Figure 52: Acceleration Response to Sample Barge Test Input of NODE 4332 (Power Supply).

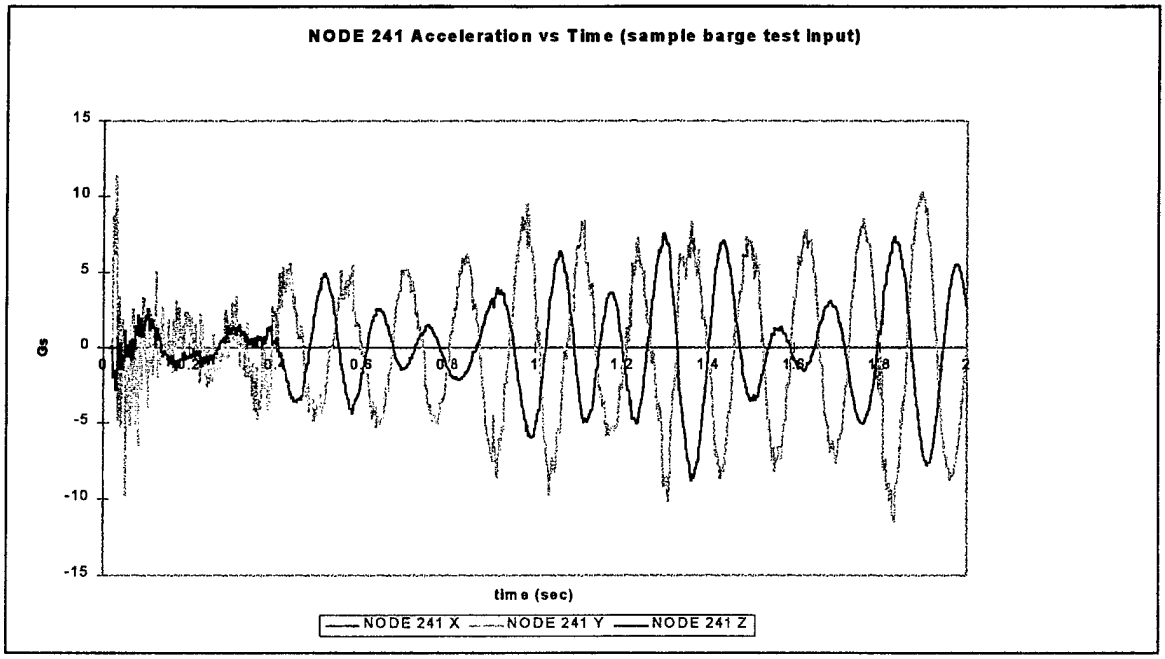

Figure 53: Acceleration Response to Sample Barge Test Input of NODE 241 (Power Distribution Unit).

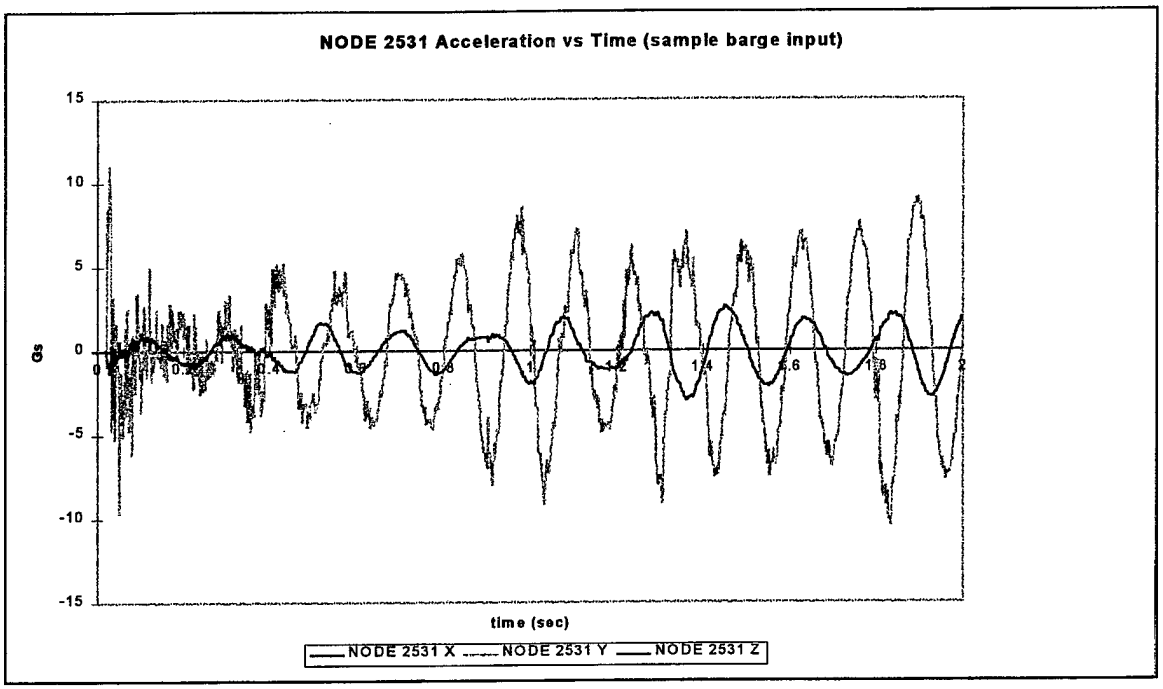

Figure 54: Acceleration Response to Sample Barge Test Input of NODE 2531 (Monitor).

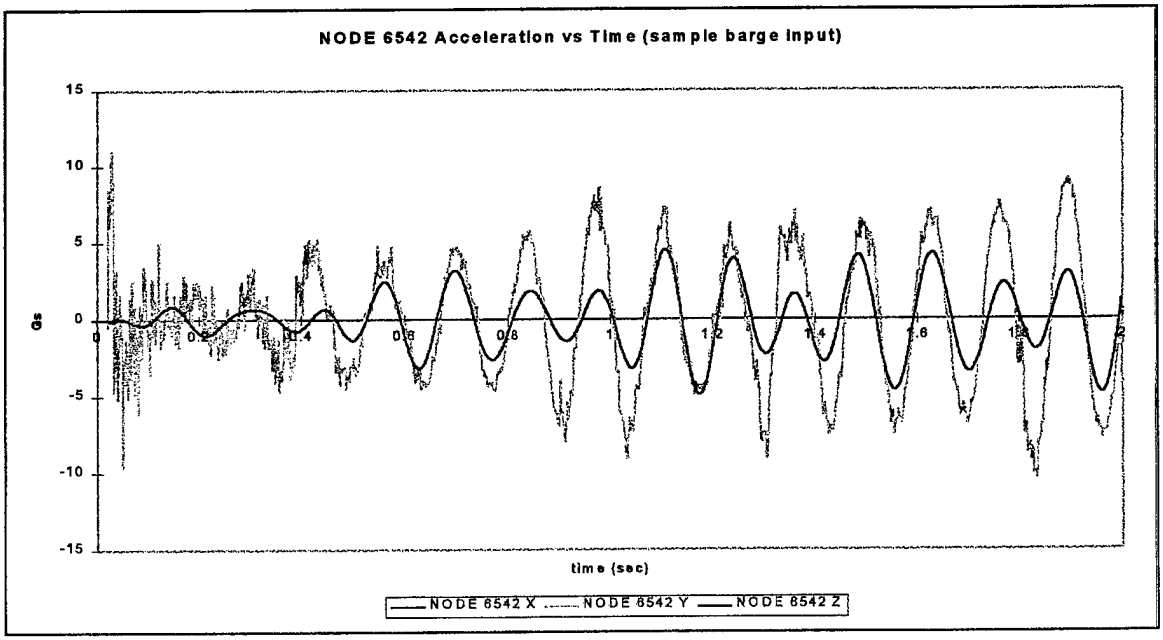

Figure 55: Acceleration Response to Sample Barge Test Input of NODE 6542 (Central Processing Unit).

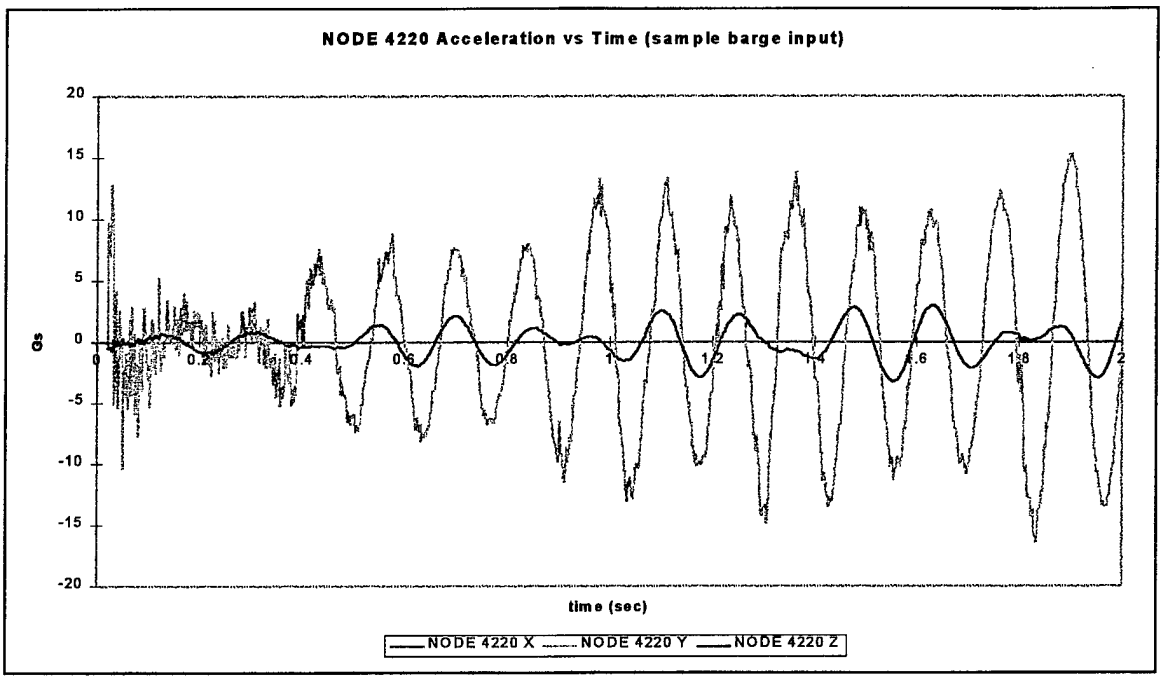

Figure 56: Acceleration Response to Sample Barge Test Input of NODE 4220 (Bullnose Tip).

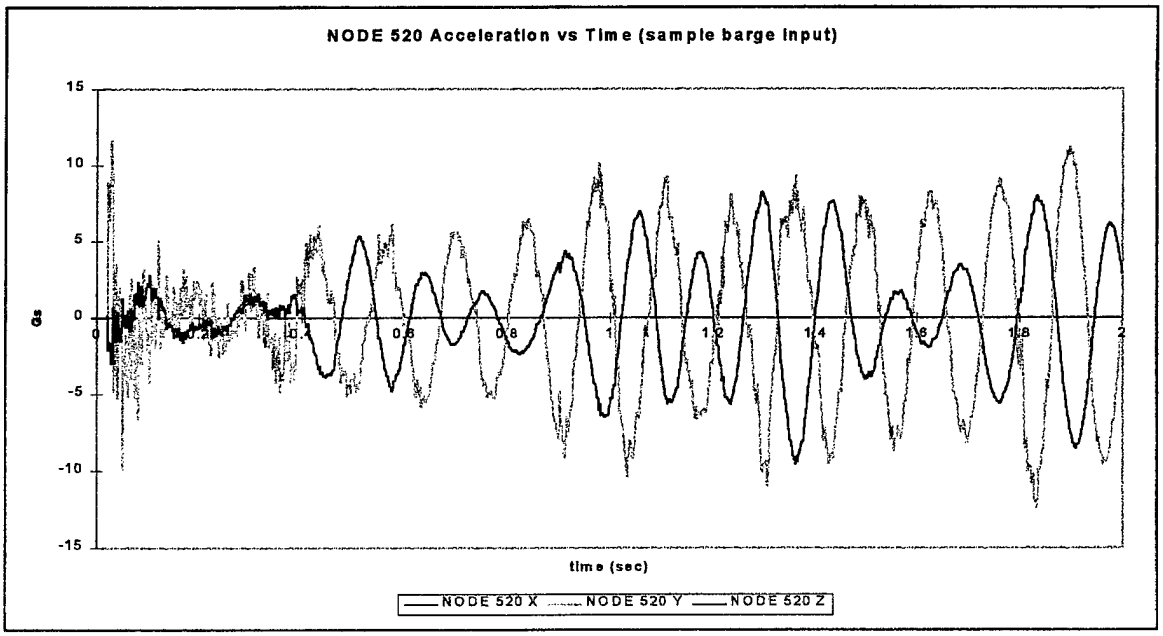

Figure 57: Acceleration Response to Sample Barge Test Input of NODE 520 (Top Front Left Cabinet Corner).

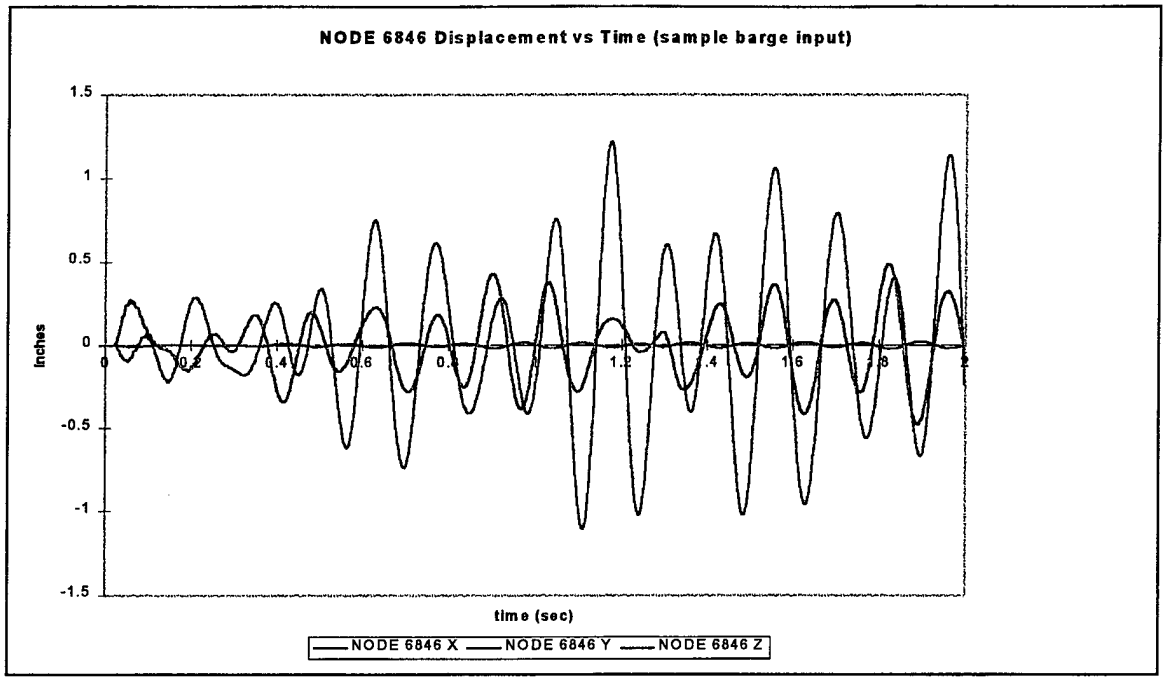

Figure 58: Displacement Response to Sample Barge Test Input of NODE 6846 (Bottom Left Front Isolation Mount).

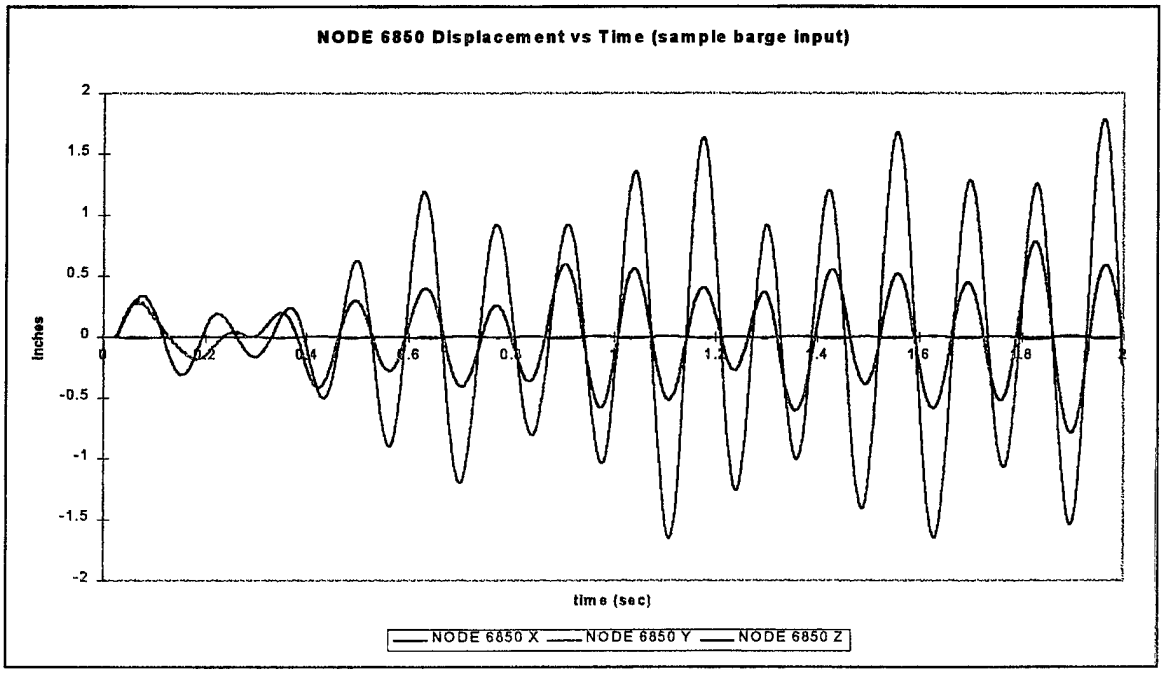

Figure 59: Displacement Response to Sample Barge Test Input of NODE 6850 (Bottom Rear Front Isolation Mount).

design specifications or bottom out for this shock input, this significant transference of energy will lead to mount failure in the Z direction first for larger shock inputs.

The peak acceleration values for all electronic equipment nodes were generally less than the combined magnitude of both shocks of about 17.7 G's. However, to ensure that these are the true peak values, longer input time histories are required. Responses for longer time periods were not calculated because a longer shock input time record was not available. Calculating the system free response following the 2 second input would not represent factual data results.

2. Dual Monitor Variant (CLIN 0001AA)

As noted in the Halfsine Input case, the general response characteristics for this Representative Barge Shock Input are similar between rack variants. Figures 60 and 61 show the acceleration at the tops of the left, bottom mounts, NODES 7369 and 7501 respectively. As with the single monitor variant, there is a rather violent motion of the rear mount, Figure 61, which is also more prevalent in the forward mount, Figure 60. The peak amplitude in the rear mount (18Gs) is about the same as the input acceleration peak only appearing much later in the time history. Again this shows a reinforcing of the motion over time.

Figures 62 through 66 show the acceleration response time histories for representative nodes of the electronic components mounted with the cabinet, corresponding to the Power Supply, Power Distribution Unit, Lower Monitor, Upper Monitor, and Central Processing Unit respectively. Figure 67 shows the acceleration response of bullnose tip. The response amplitudes for all of these electronic components generally increases once past the initial peak acceleration until about 1 second, then the peaks remain relatively steady. This is again due to the previously mentioned two factors, the addition of shock energy throughout the entire analysis period and the

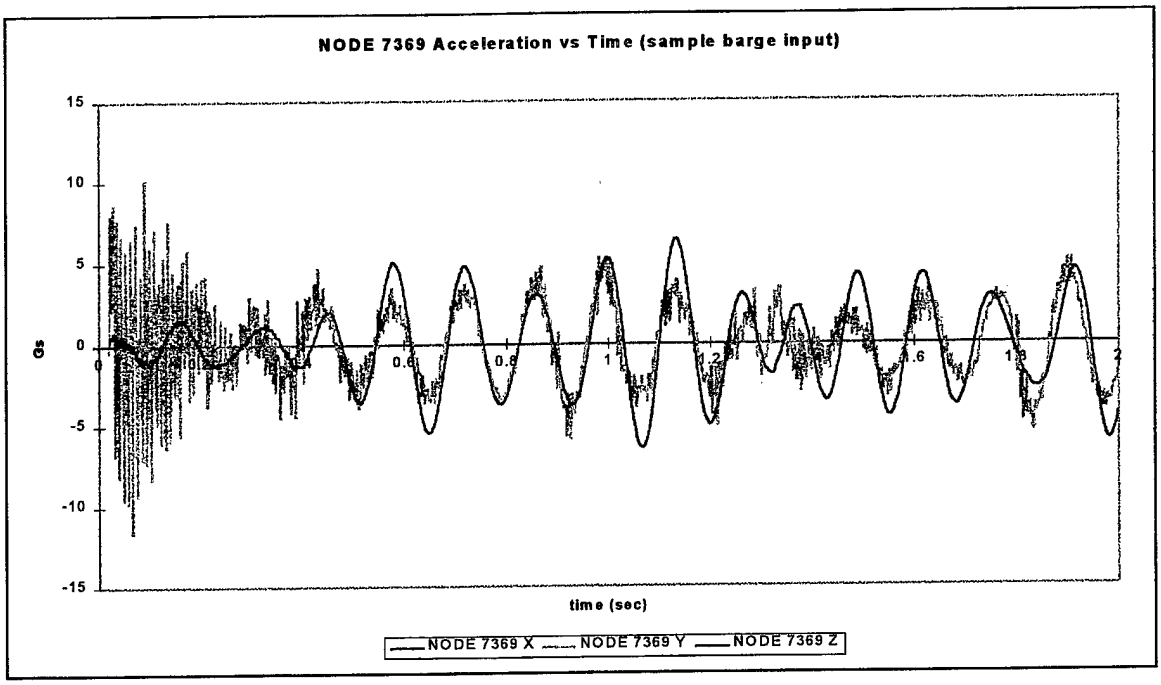

Figure 60: Acceleration Response to Sample Barge Test Input of NODE 7369 (Top of Front Left Bottom Isolation Mount).

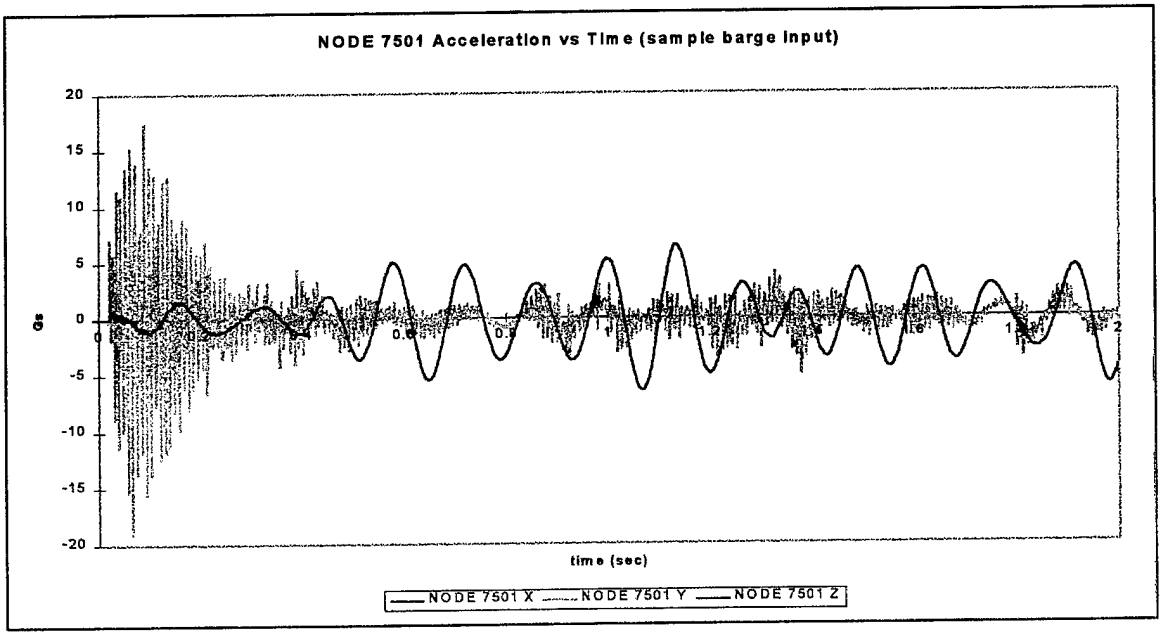

Figure 61: Acceleration Response to Sample Barge Test Input of NODE 7501 (Top of Rear Left Bottom Isolation Mount).

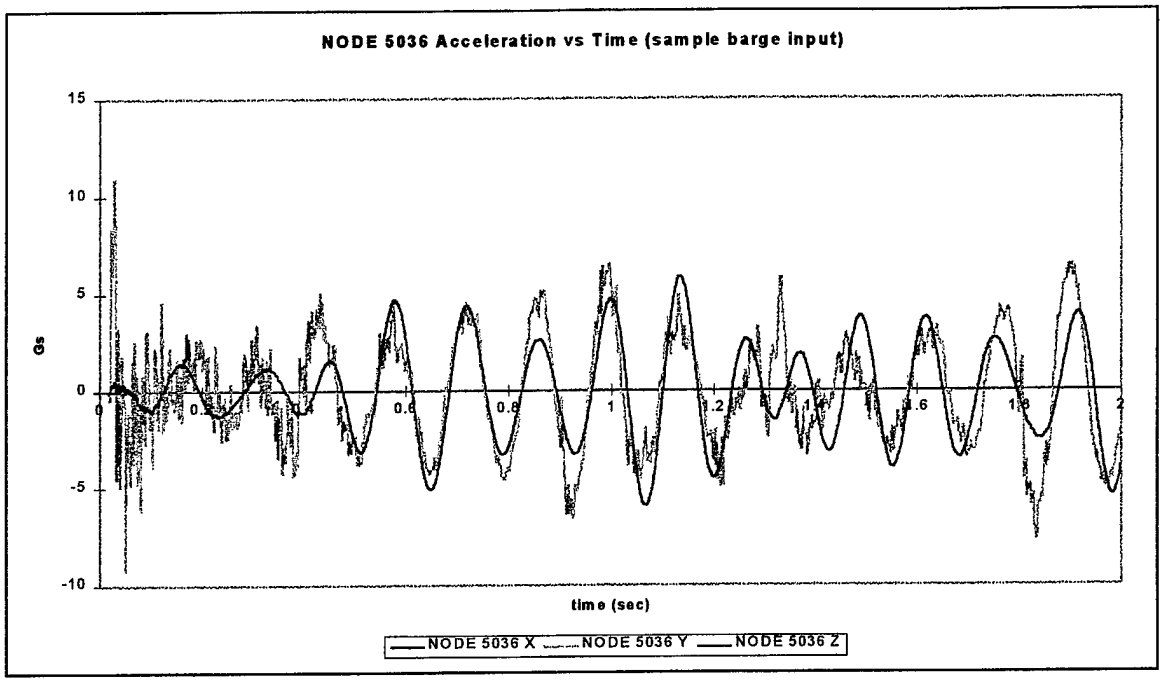

Figure 62: Acceleration Response to Sample Barge Test Input of NODE 5036 (Power Supply).

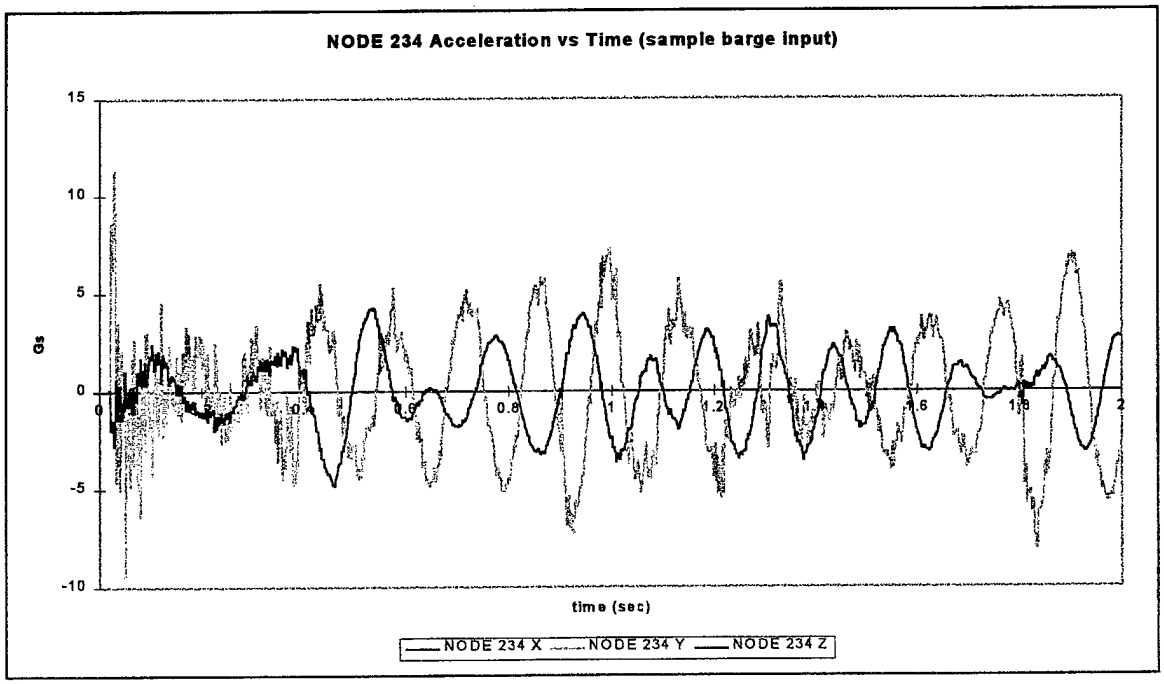

Figure 63: Acceleration Response to Sample Barge Test Input of NODE 234 (Power Distribution Unit).

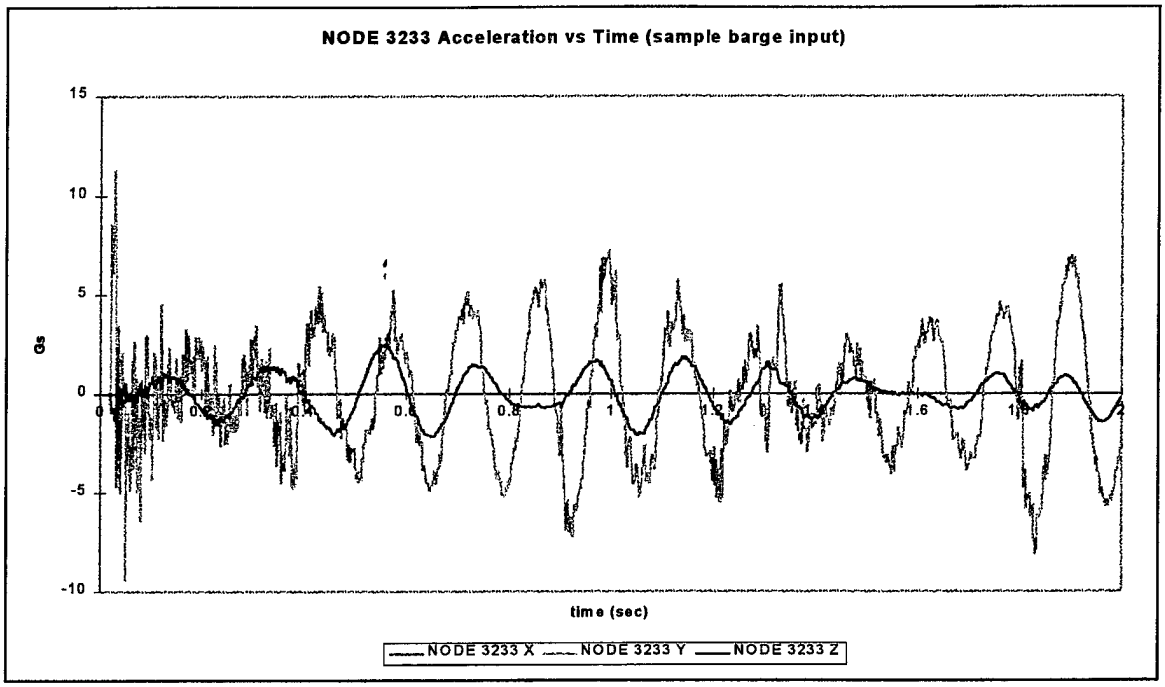

Figure 64: Acceleration Response to Sample Barge Test Input of NODE 3233 (Lower Monitor).

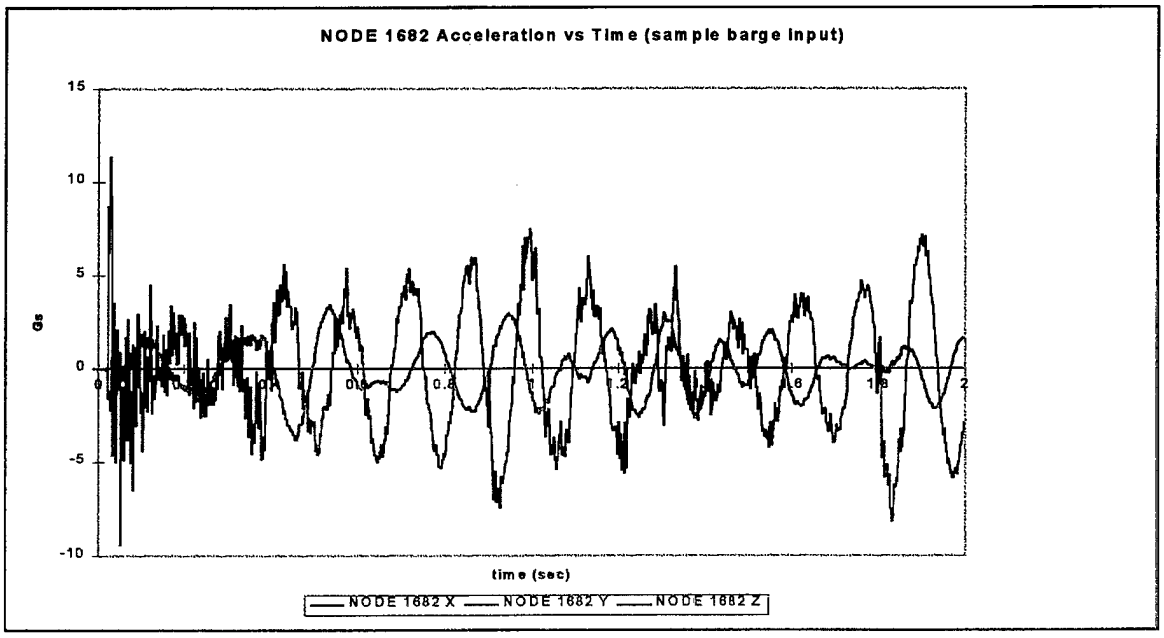

Figure 65: Acceleration Response to Sample Barge Test Input of NODE 1682 (Upper Monitor).

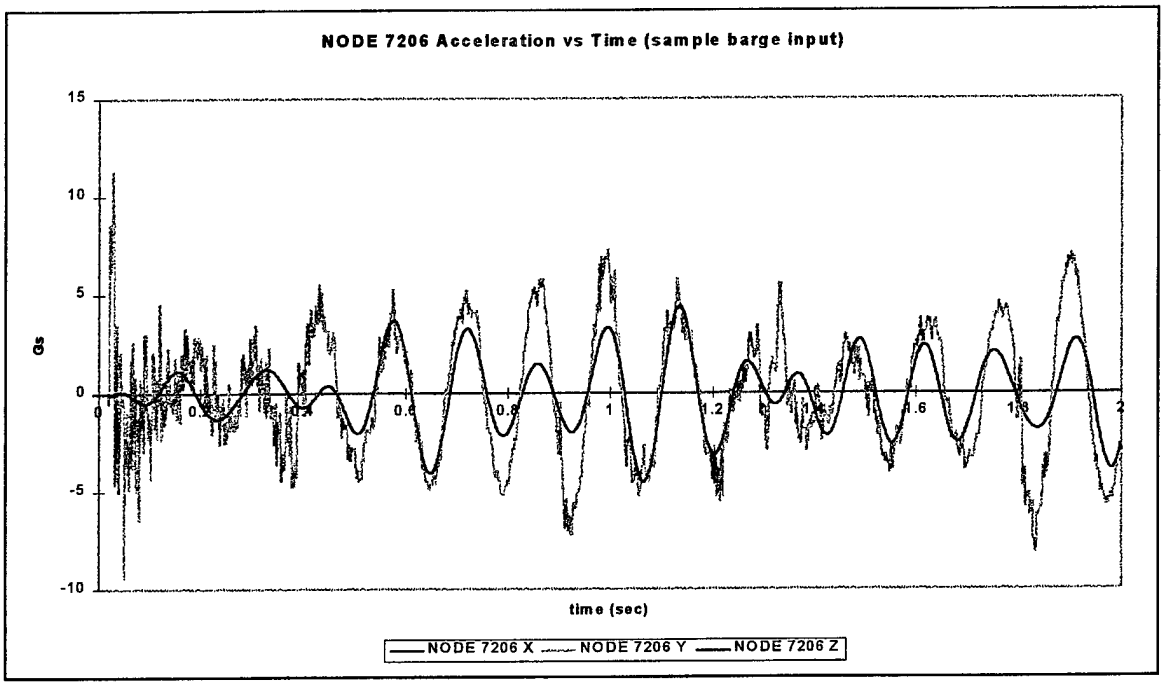

Figure 66: Acceleration Response to Sample Barge Test Input of NODE 7206 (Central Processing Unit).

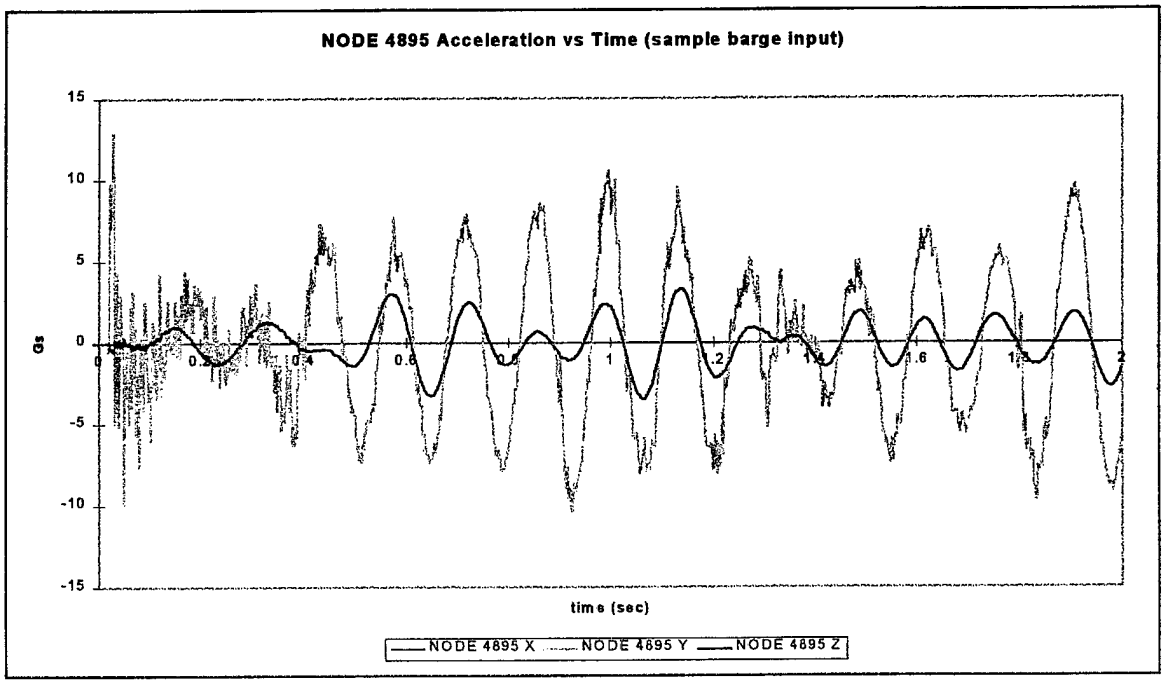

Figure 67: Acceleration Response to Sample Barge Test Input of NODE 4895 (Bullnose Tip).

compounding of the inertial response of the system. As before, the bullnose values are higher than the internally mounted components due to the cantilevered position of the bullnose.

Next, Figures 68 shows the acceleration response of the upper left corner of the cabinet (NODE 551). The response characteristics for this node are similar to the response characteristics of the electronic components. Again note that the maximum values here are generally, slightly larger than those seen in the electronic components themselves, indicating that the rack is mitigating the shock transmitted to the electronic components somewhat.

Figures 69 and 70 show the displacement time histories of the left bottom front and rear mounts (NODES 7515 and 7514, respectively). The large transference of energy from the Y to the Z direction is even larger here than in the single monitor variant. The Z deflection for these mounts is likely very close to their design limits.

The peak acceleration values for all electronic equipment nodes was generally less than the combined magnitude of both shocks of about 17.7 G's. However as with the single monitor variant, longer input time histories are required to ensure that these are the true peak values.

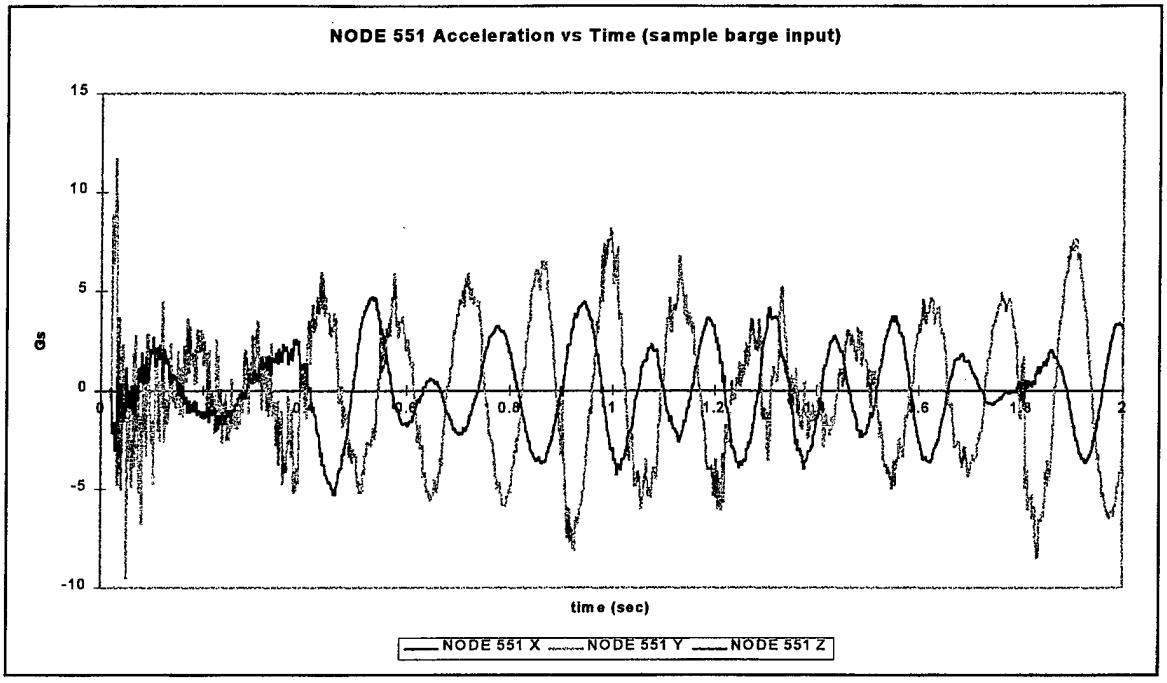

Figure 68: Acceleration Response to Sample Barge Test Input of NODE 551 (Top Front Left Cabinet Corner).

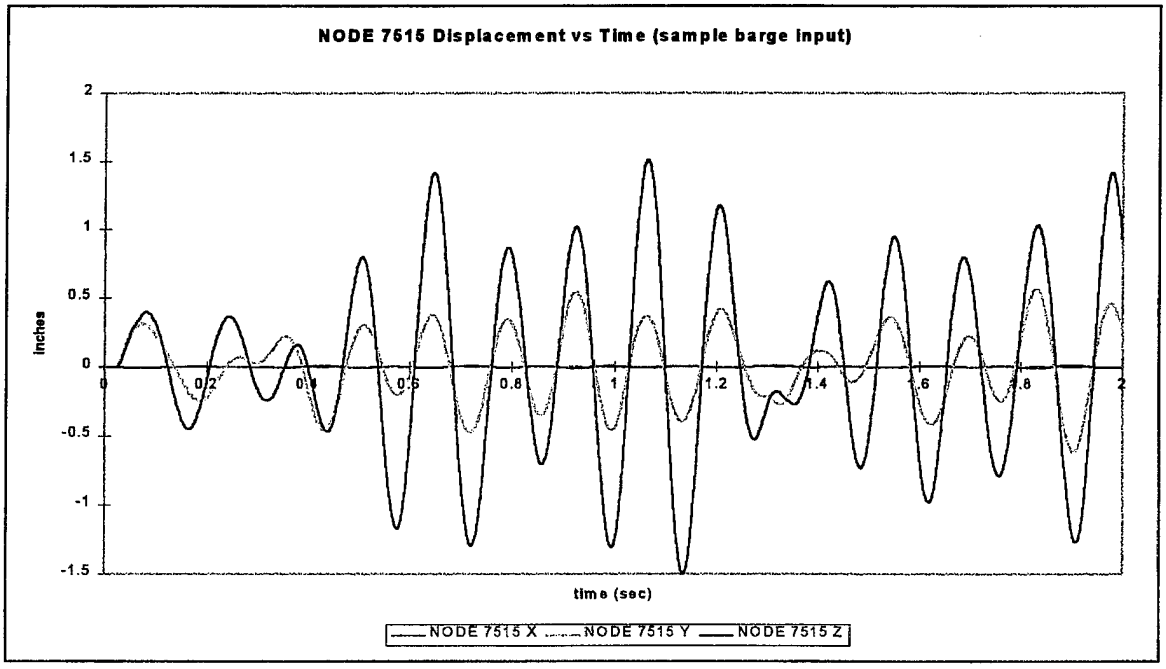

Figure 69: Displacement Response to Sample Barge Test Input of NODE 7515 (Bottom Left Front Isolation Mount).

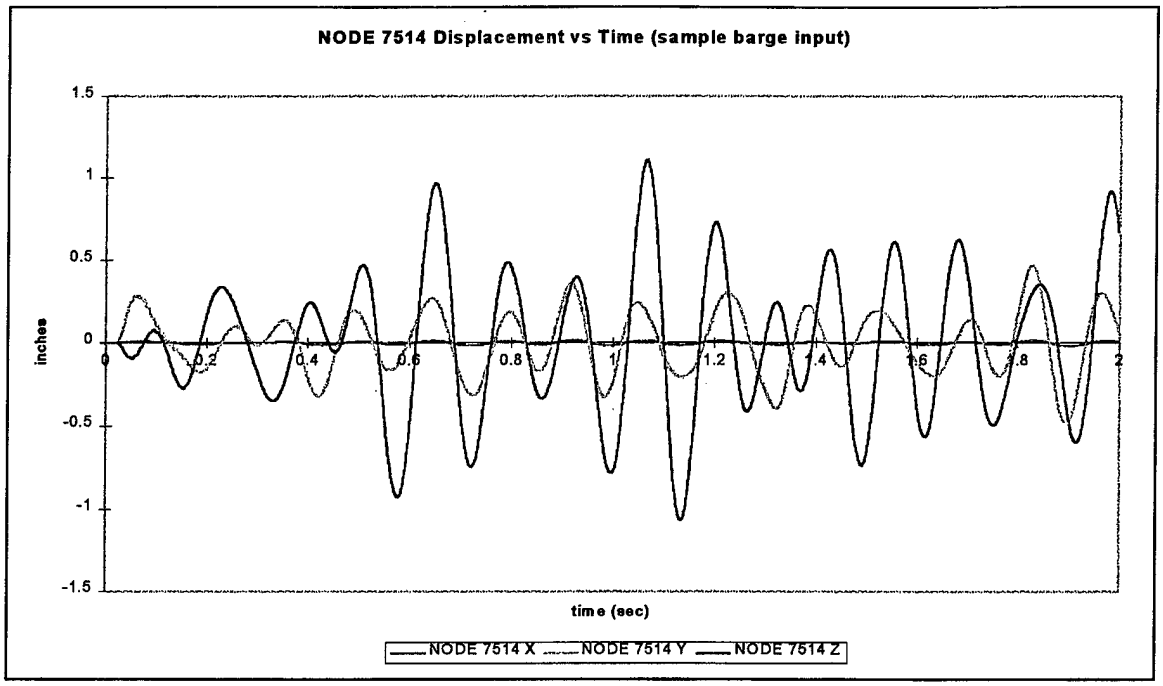

Figure 70: Displacement Response to Sample Barge Test Input of NODE 7514 (Bottom Rear Front Isolation Mount).

VI. MOUNT STIFFNESS SENSITIVITY ANALYSIS

The dynamic response characteristics of both models under the simulated barge test input do not necessarily show that the rack's isolation mounts are functioning as well as they could because the shock transmitted to the electronic components is still rather high late into the time histories. The easiest way to change the response characteristics of the rack system is to change the isolation mount characteristics, specifically the spring stiffness. Modifying the nominal design value of the mount stiffness and re-running the computer transient analysis will determine if this factor has a significant impact on the shock values transmitted to the electronic components.

Any change to a finite element model will affect, to varying degrees, the eigenvalues and eigenvectors of the system. For both models presented here, the effect of the change in the spring stiffness is manifest in the first six eigenpairs, or mode shapes. These first six modes, previously referred to as the system's gross modes, have the largest effect on the entire rack's dynamic response characteristics.

The Single Monitor Variant (CLIN 0003AA) was used for this analysis with the sample barge test input acceleration time history. The sensitivity analysis is based upon increasing and decreasing the nominal spring stiffness for each direction on each mount by 25 percent. NODE 241 from the Power Distribution Unit (mounted at the top of the rack) and NODE 6542 from the Central Processing Unit (mounted low in the rack) were chosen to show the general effect that the mount stiffness change has on the electronic components. NODE 6850 from the lower left rear mount was chosen to show the effect the change in stiffness has on the mount displacement response. For all of these nodes, only the Y and Z direction responses are presented because the X direction responses are not significant enough for a good comparison.

Figure 71 shows the Y acceleration responses of NODE 241 for the three different spring stiffness values: 75%, 100%, and 125% of nominal spring stiffness. Figure 72 shows the Z acceleration response of the same node. Figures 73 and 74 are the

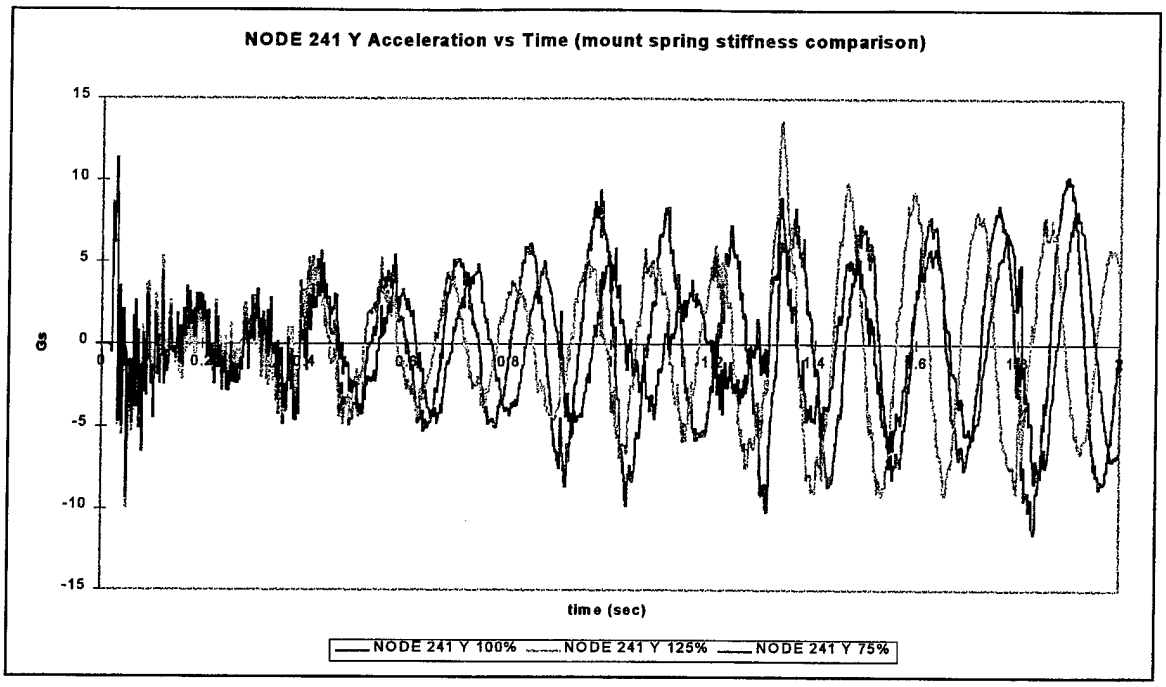

Figure 71: Y Acceleration Response to Sample Barge Test Input of NODE 241 (PDU), Comparing responses to Varying Spring Stiffnesses.

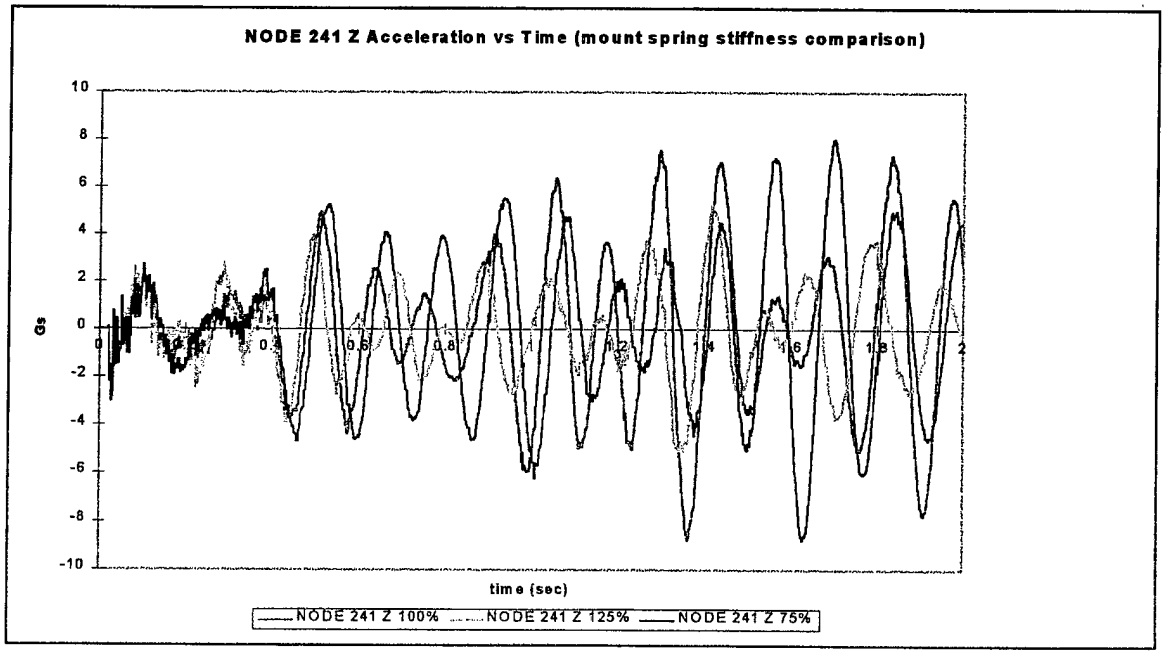

Figure 72: Z Acceleration Response to Sample Barge Test Input of NODE 241 (PDU), Comparing responses to Varying Spring Stiffnesses.

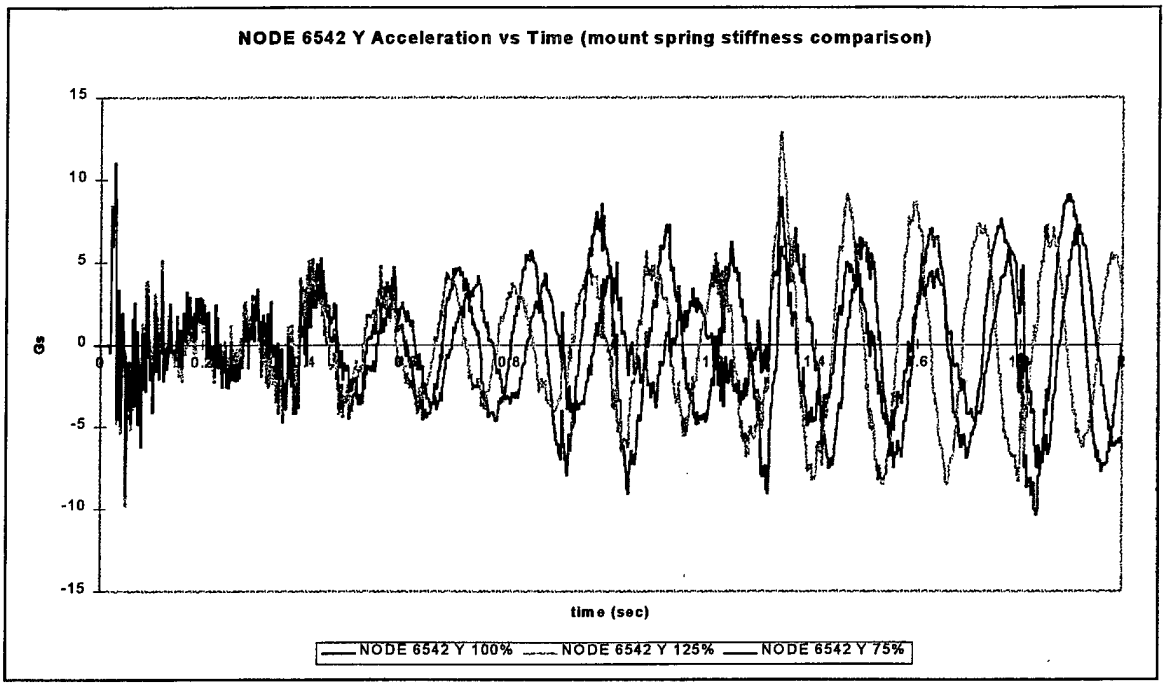

Figure 73: Y Acceleration Response to Sample Barge Test Input of NODE 6542 (CPU), Comparing responses to Varying Spring Stiffnesses.

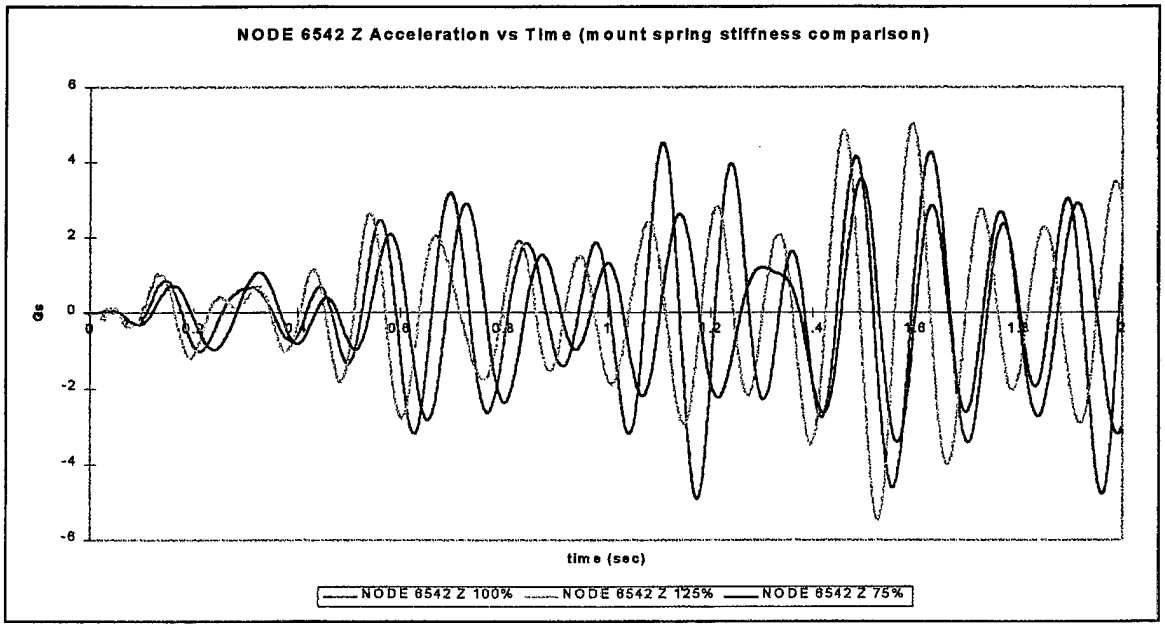

Figure 74: Z Acceleration Response to Sample Barge Test Input of NODE 6542 (CPU), Comparing responses to Varying Spring Stiffnesses.

Y and Z acceleration responses for NODE 6542 under the same conditions. The curves for other electronic components are very similar in nature. These figures show that varying the spring stiffness has little effect on the initial response of each node, up until about 0.6 seconds. Following this time, the responses histories vary greatly with respect to time, but generally have similar acceleration peaks. Other than this, no general trend is evident with respect to acceleration response versus spring stiffness. In this case, no particular spring stiffness is best in order to minimize shock transmission to electronic components.

The next logical place to check the effectiveness of changing the spring stiffness is in the mount deflection. Figures 75 and 76 are the Y and Z displacement response time histories for NODE 6850 for the three different values of spring stiffness. None of these displacements exceeds design specifications. These figures also show that there is no evident general trend of displacement magnitude versus spring stiffness. Again, no spring stiffness is best with respect to minimizing mount displacement.

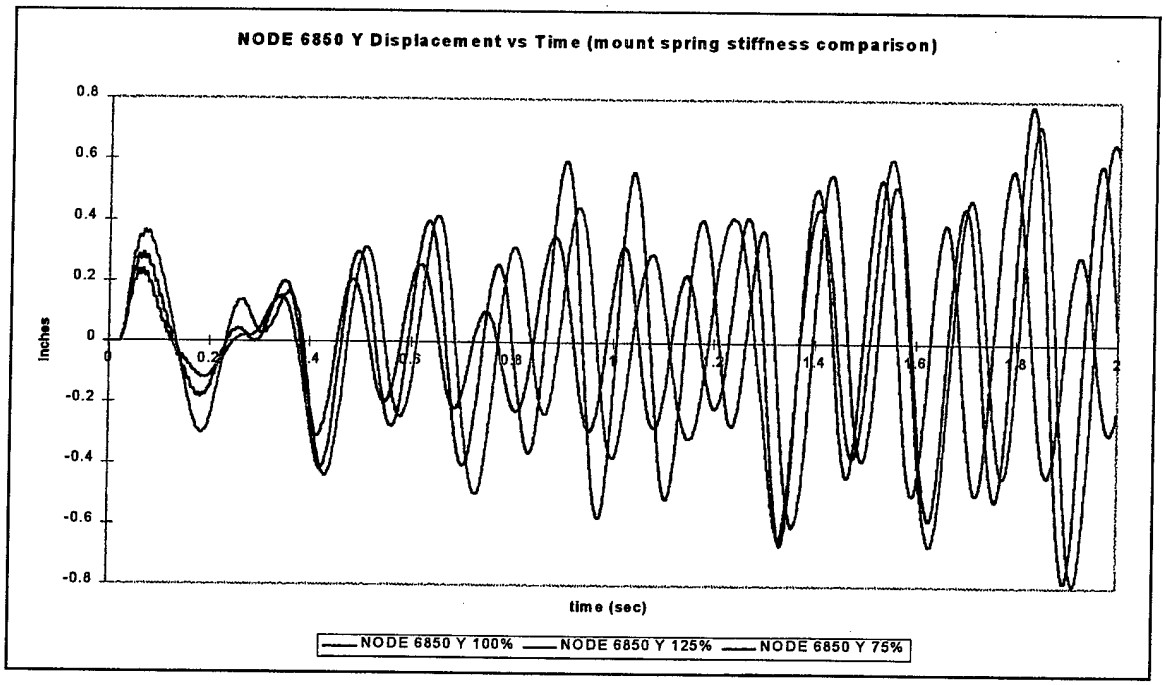

Figure 75: Y Displacement Response to Sample Barge Test Input of NODE 6850 (Right Rear Bottom Mount), Comparing responses to Varying Spring Stiffnesses.

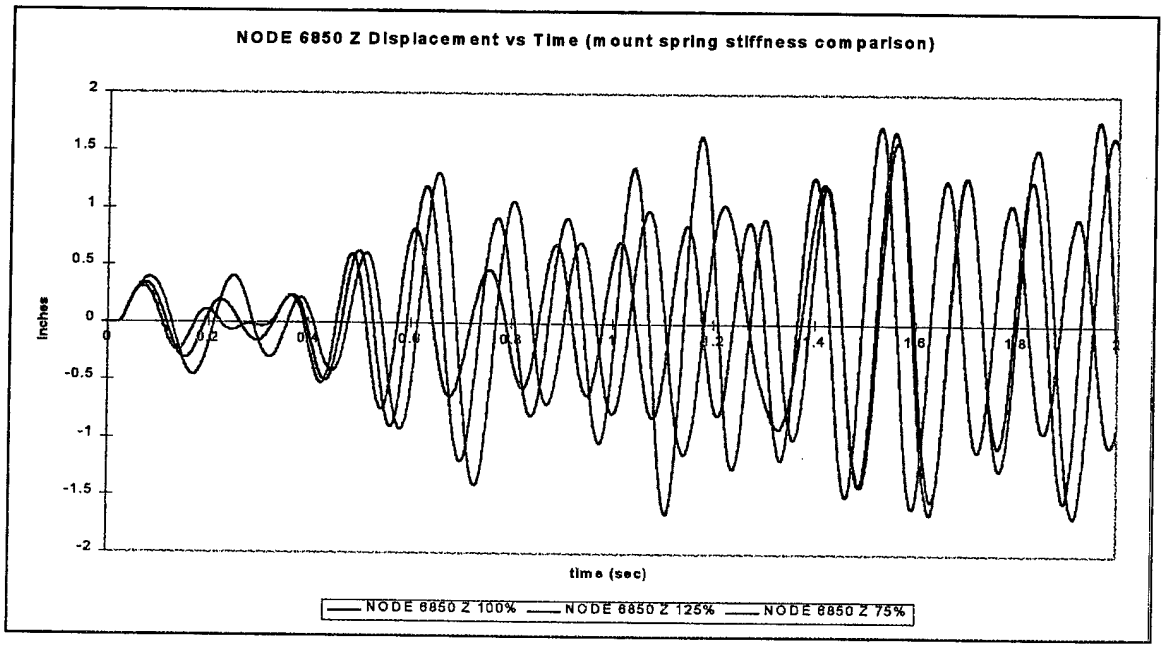

Figure 76: Z Displacement Response to Sample Barge Test Input of NODE 6850 (Right Rear Bottom Mount), Comparing responses to Varying Spring Stiffnesses.

VII. CONCLUSIONS

A. DISCUSSION OF RESULTS

The transient response characteristics of the model for the two simulated shock inputs show that the rack system works extremely well for limiting the transmitted shock to the electronic components for short duration shock inputs (halfsine input). The longer the duration of the input (sample barge test input), however, the less well the rack works. This is due to the reinforcing nature of these types of shock inputs. To improve the model's response in this area requires more than simply changing the isolation mount's stiffness characteristics. A computer model and simulation technique works well for this type of study.

The finite element modeling and subsequent computer simulation of the shock response of the TAC-4 72 Inch Rack provides an effective method to reduce the costs of shock qualification testing per MIL-STD-901D. This is accomplished by creating a computer model of a generic rack in the TAC-4 family and applying the simulated shock input. Next, the generic rack is physically shock tested to verify the computer results as a conservative estimate of the response. Now the generic rack can be modified as required for each particular application and shock tested through computer simulation only, eliminating the need for physical shock testing.

Although the time needed to construct the initial model of the Single Monitor Rack Variant (used as the generic rack) was lengthy, all modifications and the subsequent construction of the Dual Monitor Rack Variant went very quickly. Because the TAC-4 system is a family of similar racks, all of them can be constructed from the same base model rapidly. Also, changes in configuration (i.e., different electronic components in different locations) can be made quickly by simply modifying the base model. Each model can then have the simulated shock input applied to determine the model's dynamic response. Each shock transient analysis took slightly less than an hour of computer time

(using a single processor SGI OCTANE with 500MB memory and 9GB hard drive) with about a day used for results analysis. This computerized testing method provides an acceleration level seen by the electronic components. Coupling this with an industry specified acceptable acceleration level (for each particular electronic component) will then determine if the rack passed or failed the shock criteria.

This shock testing method would only require that one series of shock tests be performed on one rack variant for computer simulation verification purposes, instead of a series for each possible rack type and configuration. This would greatly reduce the developmental costs of the system by eliminating most of the expensive physical testing requirements. Because the backbone of the TAC-4 Rack family is based upon using COTS equipment, which changes very rapidly as technology progresses, the mandated shock testing is already prohibitively expensive and in all practicality is unachievable. Computer simulation is a viable option to achieve the required shock testing for all rack configurations while minimizing costs.

Computer modeling and simulation provides another benefit. The rack system construction can be optimized using currently available computer-based optimization codes. These codes can change the materials used, part dimensions, equipment location, etc., so that the shock transmitted to the electronic components is minimized. This provides for the most efficient design for each rack configuration and can be done without the lengthy and costly process of prototyping and physical testing.

B. RECOMMENDATIONS

The scope of this research was limited to the development of an effective computer model (which is easily modified into other configurations) and applying simulated shock histories to this model to determine its dynamic response characteristics. Unfortunately, the physical shock testing of the rack was not completed prior to publication. With this in mind, the following areas deserve more research:

⇒ Comparing the computer model results with actual UNDEX testing results in order to verify the model.

⇒ Insert non-linear shock mount characteristics instead of the linear approximation currently used.

⇒ Determine what an acceptable peak acceleration level is for commercial electronic components.

⇒ Perform a sensitivity analysis of the entire computer model. From this, optimize the current rack system to minimize shock transmission to the electronic components. This could serve as the basis for the next TAC generation.

⇒ Design a more effective shock mount for this type of application.

APPENDIX A: MODEL CHARACTERISTICS

SINGLE MONITOR VARIANT (CLIN 0003AA):

Height: 72 inches

Width: 24 inches

Depth: 36 inches (exclusive of bullnose)

Weights:

Overall:	703.25 lbf
CPU:	105 lbf
Monitor:	75 lbf
Power Distribution Unit:	15 lbf
Power Supply:	180 lbf
Bullnose:	20 lbf

Center of Gravity: (12.0 x, 24.8 y, 18.9 z) inches from left rear bottom corner of cabinet

Isolation Mount Characteristics:

Damping: 15%

Spring Stiffness: (using model coordinate system)

Front/Bottom	X	460 lbf/in
	Y	2500 lbf/in
	Z	460 lbf/in
Rear/Bottom	X	440 lbf/in
	Y	2000 lbf/in
	Z	440 lbf/in
Back/Upper	X	440 lbf/in
	Y	440 lbf/in
	Z	2000 lbf/in

Structural Damping: 2%

Modal Damping: 2%

DUAL MONITOR VARIANT (CLIN 0001AA):

Height: 72 inches

Width: 24 inches

Depth: 36 inches (exclusive of bullnose)

Weights:

Overall:	803.5 lbf
CPU:	105 lbf
Upper Monitor:	75 lbf
Lower Monitor:	75 lbf
Power Distribution Unit:	15 lbf
Power Supply:	180 lbf
Bullnose:	20 lbf

Center of Gravity: (12.0 x, 27.5 y, 19.8 z) inches from left rear bottom corner of cabinet

Isolation Mount Characteristics:

Damping: 15%

Spring Stiffness: (using model coordinate system)

Front/Bottom	X 460 lbf/in
	Y 2500 lbf/in
	Z 460 lbf/in
Rear/Bottom	X 440 lbf/in
	Y 2000 lbf/in
	Z 440 lbf/in
Back/Upper	X 440 lbf/in
	Y 440 lbf/in
	Z 2000 lbf/in

Structural Damping: 2%

Modal Damping: 2%

MATERIAL CHARACTERISTICS:

All metal parts: 18-8 STAINLESS STEEL

Density (ρ):	0.29 lbf/in^3
Young's Modulus (E):	2.76x10^7 lbf/in^2
Poisson's Ratio (ν):	0.305
Damping Coefficient (ξ):	0.02

Electronic Components:

Density (ρ):	various to match weight of component
Young's Modulus (E):	1.72x10^6 lbf/in^2
Poisson's Ratio (ν):	0.35
Damping Coefficient (ξ):	0.02

APPENDIX B: MODE SHAPES AND FREQUENCIES

A complete description of the first six modes of each model is contained in the chapter on Normal Mode Analysis. Only the 7th through the25th modes are described here. These correspond to the local bending modes. All of these modes are applicable to both models and are the same. The "MAX" parameter used in the table is not a physical dimensional value, but a mass normalized quantity intended to show relational displacements. The magnitude of this value shows which component of each particular vibration mode dominates in that particular mode.

MODE 7 FREQUENCY 23.98 Hz

PART	MAX	DESCRIPTION
Bottom Panel	18.12	1st Plate Bending Mode

MODE 8 FREQUENCY 24.65 Hz

PART	MAX	DESCRIPTION
Side Panels	7.03	1st Plate Bending Mode (out of phase)
Top Panel	0.94	1st Plate Bending Mode

MODE 9 FREQUENCY 25.08 Hz

PART	MAX	DESCRIPTION
Side Panels	7.22	1st Plate Bending Mode (in phase)

MODE 10 FREQUENCY 26.20 Hz

PART	MAX	DESCRIPTION
Top Rear Panel	25.44	1st Plate Bending Mode
2nd from Top, Rear Panel	3.39	1st Plate Bending Mode
3rd from Top, Rear Panel	5.09	1st Plate Bending Mode
Bottom Rear Panel	3.39	1st Plate Bending Mode

MODE 11 FREQUENCY 26.31 Hz

PART	MAX	DESCRIPTION
Top Rear Panel	4.15	1st Plate Bending Mode
2nd from Top, Rear Panel	2.77	1st Plate Bending Mode
3rd from Top, Rear Panel	2.77	1st Plate Bending Mode
Bottom Rear Panel	20.77	1st Plate Bending Mode
CPU Cover Panel	2.77	1st Plate Bending Mode

MODE 12 FREQUENCY 26.35 Hz

PART	MAX	DESCRIPTION
Top Rear Panel	3.52	1st Plate Bending Mode
2nd from Top, Rear Panel	5.86	1st Plate Bending Mode
3rd from Top, Rear Panel	17.57	1st Plate Bending Mode
Bottom Rear Panel	3.52	1st Plate Bending Mode

MODE 13 FREQUENCY 26.48 Hz

PART	MAX	DESCRIPTION
Front Panel above Monitor	2.07	1st Plate Bending Mode
CPU Cover Panel	3.45	1st Plate Bending Mode
Side Panels	3.45	2nd Plate Bending Mode (out of phase)
Top Panel	1.38	1st Plate Bending Mode
Top Rear Panel	3.45	1st Plate Bending Mode
2nd from Top, Rear Panel	7.58	1st Plate Bending Mode
3rd from Top, Rear Panel	2.07	1st Plate Bending Mode
4th from Top, Rear Panel	10.34	1st Plate Bending Mode
Bottom Rear Panel	2.07	1st Plate Bending Mode

MODE 14 FREQUENCY 26.54 Hz

PART	MAX	DESCRIPTION
Side Panels	5.19	2nd Plate Bending Mode (out of phase)
Front Panel above Monitor	2.17	1st Plate Bending Mode
CPU Cover Panel	4.76	1st Plate Bending Mode
Top Panel	2.17	1st Plate Bending Mode
Top Rear Panel	2.60	1st Plate Bending Mode
2nd from Top, Rear Panel	6.05	1st Plate Bending Mode
3rd from Top, Rear Panel	2.17	1st Plate Bending Mode
4th from Top, Rear Panel	6.49	1st Plate Bending Mode

MODE 15 FREQUENCY 26.55 Hz

PART	MAX	DESCRIPTION
Side Panels	4.33	2nd Plate Bending Mode (out of phase)
Front Panel above Monitor	3.61	1st Plate Bending Mode
CPU Cover Panel	4.33	1st Plate Bending Mode
Top Panel	1.45	1st Plate Bending Mode
Top Rear Panel	4.33	1st Plate Bending Mode
2nd from Top, Rear Panel	10.82	1st Plate Bending Mode
3rd from Top, Rear Panel	4.33	1st Plate Bending Mode
4th from Top, Rear Panel	1.45	1st Plate Bending Mode

MODE 16 FREQUENCY 26.77 Hz

PART	MAX	DESCRIPTION
Front Panel above Monitor	4.19	1st Plate Bending Mode
CPU Cover Panel	5.03	1st Plate Bending Mode
Top Rear Panel	1.68	1st Plate Bending Mode
2nd from Top, Rear Panel	3.36	1st Plate Bending Mode
3rd from Top, Rear Panel	3.36	1st Plate Bending Mode
4th from Top, Rear Panel	5.86	1st Plate Bending Mode
Bottom Rear Panel	3.36	1st Plate Bending Mode

MODE 17 FREQUENCY 26.87 Hz

PART	MAX	DESCRIPTION
Side Panels	7.36	2nd Plate Bending Mode (in phase)
Top Panel	0.49	2nd Plate Bending Mode

MODE 18 FREQUENCY 27.44 Hz

PART	MAX	DESCRIPTION
Front Panel above Monitor	14.87	1st Plate Bending Mode
CPU Cover Panel	2.97	1st Plate Bending Mode
Top Rear Panel	2.97	1st Plate Bending Mode
2nd from Top, Rear Panel	3.96	1st Plate Bending Mode
3rd from Top, Rear Panel	1.98	1st Plate Bending Mode
4th from Top, Rear Panel	1.98	1st Plate Bending Mode

MODE 19 FREQUENCY 27.94 Hz

PART	MAX	DESCRIPTION
Front Strip Panel Above Bullnose	26.42	1st Plate Bending Mode
CPU Cover Panel	7.05	1st Plate Bending Mode

MODE 20 FREQUENCY 29.52 Hz

PART	MAX	DESCRIPTION
2nd from Top, Rear Panel	3.96	2nd Plate Bending Mode

MODE 21 FREQUENCY 29.58 Hz

PART	MAX	DESCRIPTION
Side Panels	6.32	3rd Plate Bending Mode (out of phase)
2nd from Top, Rear Panel	2.87	2nd Plate Bending Mode
Top Panel	8.62	1st Plate Bending Mode

MODE 22 FREQUENCY 30.13 Hz

PART	MAX	DESCRIPTION
Side Panels	7.06	3rd Plate Bending Mode (out of phase)
Top Panel	1.41	2nd Plate Bending Mode

MODE 23 FREQUENCY 30.18 Hz

PART	MAX	DESCRIPTION
Front Strip Panel above PS	45.55	1st Plate Bending Mode

MODE 24 FREQUENCY 31.43 Hz

PART	MAX	DESCRIPTION
Side Panels	4.56	3rd Plate Bending Mode (in phase)
Top Panel	13.67	1st Plate Bending Mode

MODE 25 FREQUENCY 32.83 Hz

PART	MAX	DESCRIPTION
2nd from Top, Rear Panel	24.5	2nd Plate Bending Mode

LIST OF REFERENCES

1. MIL-S-901D, "Shock Tests, H.I. (High Impact) Shipboard Machinery, Equipment, and Systems, Requirements for," 17 March 1989.

2. Clements, E.W., "Shipboard Shock and Navy Devices for its Simulation," NRL Report 7369, 14 July, 1972.

3. Guide to Operations and Technical Information Manual for Standard Configuration TAC-4 Rugged Racks, SAIC-Computer Systems, San Diego, CA.

4. Craig, Roy R. Jr., "Structural Dynamics, An Introduction to Computer Methods," John Wiley & Sons, Inc.,1981.

5. Blakely, Ken, "MSC/NASTRAN Basic Dynamic Analysis (V68)," MacNeal-Schwendler Corp., Los Angeles, CA, 1993.

6. FAX Transmission from Eric Jansson of Aeroflex International to Mark Oesterreich of NPS Monterey, October 1997. Force Deflection Curves for CB1400 Series and CB61400 Series Wire Rope Isolators.

7. Caffrey, John P, and Lee, John M., "MSC/NASTRAN Linear Static Analysis (V68)," MacNeal-Schwendler Corp., Los Angeles, CA, 1994.

8. Komzsik, L. and Dilley, G., "Practical Experiences with the Lanczos Method," Proceedings of the MSC/NASTRAN Users Conference, Paper No. 13, March 1985.

9. Base Accelerometer Data from UERD SITE Phase 3, SHOT 9991, June 1996.

INITIAL DISTRIBUTION LIST

	No. of Copies
1. Defense Technical Information Center 8725 John J. Kingman Rd., STE 0944 Ft. Belvoir, Virginia 22060-6218	2
2. Dudley Knox Library Naval Postgraduate School 411 Dyer Rd. Monterey, California 93943-5101	2
3. Professor Y.S. Shin, Code ME/Sg Department of Mechanical Engineering Naval Postgraduate School Monterey, California 93943	1
4. Lieutenant Mark H. Oesterreich 17157 Cregier Ave South Holland, Illinois 60473	1
5. Naval/Mechanical Engineering Curricular Officer, Code ME 700 Dyer Rd Monterey, California 93943-5000	1
6. Larry Core, Code D4103 NCCOSC, RDT&E Division TAC Project Office 49184 Transmitter Road San Diego, California 92152-7346	2
7. Russ Eyres, Code D4103 NCCOSC, RDT&E Division TAC Project Office 49184 Transmitter Road San Diego, California 92152-7346	1
8. John Walker, Code D6625 Commanding Officer, NCCOSC, RDT&E Div 53560 Hull St San Diego, California 92152-5001	1

9. LCDR Joseph M Iacovetta, Code D3201 — 1
   Commanding Officer, NCCOSC, RDT&E Div
   53560 Hull St
   San Diego, California 92152-5001

10. Adam Simonoff, Code B325 — 1
    NSWC
    Dahlgren, Virginia 2248-5000

11. Wynne Davis — 1
    c/o CHET
    P.O. Box 280114
    Naval Station Mayport, Florida 32228

12. Mike Winnette — 1
    NSWCCDSSMDUERD
    1445 Crossways Blvd
    Cheasapeake, Virginia 23320